On the Modeling of Mobile Ad Hoc Networks

Name :	Arta Cika
College :	Oriel
Supervisor :	Justin P. Coon
Department :	Engineering Science

A thesis submitted to the University of Oxford in accordance with the requirements of the degree of Doctor of Philosophy in the Department of Engineering Science.

198 pages

On the Modeling of Mobile Ad Hoc Networks

Arta Cika

October, 2020

On the Modeling of Mobile Ad Hoc Networks

Name: Arta Cika

College: Oriel

Degree: Doctor of Philosophy

Term and Year of Submission: Trinity 2020

This thesis examines the effects of node mobility and signal fading on the performance of mobile ad hoc networks.

Chapter 3 presents novel expressions for the statistical properties of the received signal-to-noise ratio (SNR) and the separation distance in mobile ad hoc networks (MANETs). A full mathematical description of the squared distance process is provided, including its distribution and autocorrelation function. Next, the stochastic differential equation of the link SNR is derived. Closed-form expressions for the distribution and bivariate distribution of the link SNR are given in the absence and presence of signal fading. Finally, the connectivity probability is calculated for both scenarios.

Chapter 4 develops an entropy-based metric that quantifies link uncertainty and evaluates its stability by taking full advantage of the correlation between the link's current and future state. This formulation is based on a stationary Markov chain representation of link connectivity whose source of randomness is the separation distance between the nodes or the variations in the propagation channel. The simulation results demonstrate that the proposed metric thoroughly captures the link dynamics and accurately reflects changes in the state of a wireless connection.

Chapter 5 combines the theoretical modeling of the communication link developed in Chapter 3 with the topological uncertainty analysis carried out in Chapter 4 to conclude that the primary source of uncertainty on the link state is random mobility. It then proposes a new routing decision strategy for MANETs based on the entropy-based metric presented in Chapter 4. The key idea of this strategy is to identify and select the route with the longest lifetime between a source and a destination in an environment where different paths are available. Identifying the set of most stable paths, i.e., those that are expected to be active for a longer time, can potentially reduce the number of route discoveries and overhead throughout the network. The performance evaluation of the proposed approach is performed via simulation and analysis.

(< 300 words)

Acknowledgements

I would like to thank first and foremost my supervisor, Professor Justin Coon, for helping me formulate and solve my research problems. I truly enjoyed working in a research environment that stimulates original thinking and initiative, which he created. I also thank him for his invaluable advice, continuous support, and patience during my PhD study.

I would also like to thank Dr. Mihai-Alin Badiu for inspiring and guiding me during these years and contributing to many discussions that helped shape this project. He was always there for me, willing to help to resolve the most challenging modeling issues.

I would also like to thank Moogsoft, particularly the CEO Phil Tee, for believing in my abilities to carry this project to its conclusions and generously fund my DPhil.

I would also like to thank Professor Dominic O'Brien and Professor Ekaterina Shamonina for being on my first and third years' assessment committee and for the constructive feedback they provided.

These acknowledgments would not be complete without mentioning my office and group colleagues. It was a great pleasure working with them, and I appreciate their ideas, help, and good humor. A special thanks to the beautiful people I met in my Oriel college, who became close friends and made Oxford feel like home. In particular, I want to thank my dearest friend Tatjana Schulze for always being there

for me and for being the greatest friend anyone could ask for.

A special thanks to my family. Words cannot express how grateful I am to my mother, father, sisters, and brother for everything you have done for me. You have been there at every step, always guiding me throughout this journey. I would not be who I am today without your support.

Lastly, I would like to thank my husband Maurizio for his unconditional love, kindness, and support throughout the years. I love you so much.

Acronyms

MANET	Mobile Ad Hoc Network
SNR	Signal-to-Noise Ratio
DARPA	Defense Advanced Research Projects Agency
TI	Tactical Internet
RWP	Random Waypoint
RW	Random Walk
RD	Random Direction
pdf	Probability Density Function
cdf	Cumulative Distribution Function
OU	Ornstein-Uhlenbeck
IOU	Integrated Ornstein-Uhlenbeck process
SDE	Stochastic Differential Equation
DSDV	Destination-Sequenced Distance-Vector
OLSR	Optimized Link State Routing
DSR	Dynamic Source Routing
AODV	Ad hoc On-Demand Distance Vector
QoS	Quality of Service
UAV	Unmanned Aerial Vehicles
CIR	Cox-Ingersoll-Ross
RGG	Random Geometric Graph
Mbps	Megabits Per Second

IEEE	Institute of Electrical and Electronics Engineers
GHz	Gigahertz
WSS	Wide-Sense Stationary
2D	Two-Dimensional
BESQ	Bessel-Squared Process
Erfc	Complementary Error Function
MBd	Megaboud
LCR	Level Crossing Rate
D2D	Device-to-Device
OFDMA	Orthogonal Frequency Division Multiple Access
ETX	Expected Transmission Count
NC	Network Coding
AWGN	Additive White Gaussian Noise

Notation

Scalar random variables are represented using upper-case non-boldface letters, and their realization using lower case non-boldface letters. Random vectors are represented using upper-case boldface letters and their realization using lower-case boldface letters. Sets are generally represented using calligraphic notation. $\mathbb{N}$ is the set of positive integers and $\mathbb{R}$ is the set of reals.

Below, is a list of algebraic notation used in the thesis.

P_R	Received power
P_T	Transmitted power
A_T	Transmitting antenna gain
A_R	Receiving antenna gain
N	White Gaussian noise power
t	Continuous time
k	Discrete time
w	Wavelength
U_t	Channel envelope
G_t	Channel gain
$\mathcal{K}_X(\cdot)$	Normalized autocovariance function of stochastic process X
η	Path-loss exponent

$V_{i,t}$	Velocity of node i
N_t	SNR
R_t	Euclidean distance
Z_t	Squared distance
λ^2	Expected value of the channel gain
$\mathrm{J}_0(\cdot)$	Zero-order Bessel function of the first kind
ν	Maximum Doppler shift
f_c	Carrier frequency
c	Speed of light
$H(X)$	Entropy of the random variable X
$H(X\|Y)$	Conditional entropy
$H(\mathcal{X})$	Entropy rate of the stochastic process X
$p(x)$	Probability mass function of X
$f_X(x)$	Probability density function of random variable X
$F_X(x)$	Cumulative distribution of random variable X
$\mathbb{E}[\cdot]$	Expectation operator
ρ_{th}	SNR threshold
$A_{i,t}$	Location of node i
$X_{i,t}$	$x-$coordinate of node i
$Y_{i,t}$	$y-$coordinate of node i
μ	Desired position in the OU process
W_t	Standard Brownian motion
$\mathcal{N}(m,\alpha)$	Normal distribution with mean m and variance α
τ	Relaxation time
D	Diffusion coefficient
Δt	Sampling interval
ξ_t	White Gaussian noise

χ^2	Chi-square distribution
θ	Expectation of the squared pair distance
$\Gamma(\cdot)$	Gamma function
$\gamma(a,x)=\int_x^{\infty} v^{a-1}e^{-v}\mathrm{d}v$	Incomplete gamma function
$G_{s,t}^{m,n}(z\vert\ {}^{u_1,\ldots,u_s}_{v_1,\ldots,v_t})$	Meijer-G function
$L_{ij,k}$	Link state random variable
r_0	Typical connection range
$\mathcal{V}$	Set of nodes
$\mathcal{G}_k$	Sequence of graphs

Manuscripts Since Beginning of DPhil

Below is a complete list in reverse chronological order of manuscripts that have been published.

Published **Arta Cika**, Mihai-Alin Badiu, and Justin P. Coon, "Statistical Properties of Transmissions Subject to Rayleigh Fading and Ornstein-Uhlenbeck Mobility", in IEEE Transactions on Mobile Computing, 2020.

Published **Arta Cika**, Mihai-Alin Badiu, and Justin P. Coon, "Quantifying Link Stability in Ad Hoc Wireless Networks Subject to Ornstein-Uhlenbeck Mobility", in IEEE International Conference on Communications (ICC), 2019.

Published **Arta Cika**, Mihai-Alin Badiu, Justin P. Coon, and Shahriar E. Tajbakhsh, "Entropy rate of time-varying wireless networks", in IEEE Global Communications Conference (GLOBECOM), 2018.

Published **Arta Cika**, Justin P. Coon, and Sunwoo Kim, "Effects of Directivity on Wireless Network Complexity", in IEEE International Symposium Modeling and Optimization in Mobile, Ad Hoc, and Wireless Networks (WiOpt), 2017.

List of Figures

List of Tables

Contents

Chapter 1

Introduction

A mobile ad hoc network (MANET) is an autonomous wireless networking system consisting of a collection of mobile nodes that create a network in a decentralized manner, without the need for a fixed infrastructure. These networks can be formed in a self-organizing ad hoc fashion, anywhere, at any time, as long as two or more nodes are connected and communicate with one another [1]. Wireless technologies such as Bluetooth or 802.11 standards enable mobile devices to establish a connection when they come within the transmission range of each other. Such networks may operate in a standalone fashion or may be connected to broader networks through gateways. The main characteristics of these systems are energy-constrained operation, mobility, flexibility, scalability, unreliable channel and dynamic topology [2].

The lack of a centralized structure within these systems requires mobile nodes to perform both the roles of a host and a router. Throughout this thesis, the terms "host", "node", and "device" will be used interchangeably. As a router, the mobile device represents an intermediate node that forwards packets on behalf of other devices that may not be within direct communication range to the destination node. Very often, routes between nodes may include multiple hops; hence we also

refer to these networks as multi-hop mobile ad hoc networks. Routing protocols allow source hosts to discover multi-hop paths through the network to destination hosts. Several routing protocols for MANETs have been developed in the literature [3]; each protocol tries to maximize network performance while at the same time addressing the special constraints imposed by the unique characteristics of MANETs.

MANETs find interesting applications in various areas. Since there is no fixed infrastructure, a wireless ad hoc network can be quickly deployed independently from the underlying territory or pre-existing networking capabilities. In comparison to traditional wireless networks, MANETs offer several advantages in terms of resistance to failures and cost-effectiveness. An ad hoc network is naturally resilient toward the departure of a number of nodes and targeted attacks because of its lack of a central organizational entity. Moreover, given the dynamically changing network topology due to node mobility, they have an inherent capability to resolve connectivity issues such as isolation/disconnection from the network [4].

Among real-world applications of mobile ad hoc networks, it is of particular interest their application in emergency search-and-rescue operations in a post-disaster environment. Other civil applications include machine-to-machine communications, delay-tolerant networking, peer-to-peer computing, and file sharing. A primary use of MANETs in a military environment is real-time tactical communication in unknown territories or difficult terrains [1].

1.1 Challenges in MANETs

The dynamic nature of MANETs poses several design issues to networking protocols able to provide efficient end-to-end communication. Many factors affect the networking and application protocol performances of ad hoc wireless networks. Node mobility, in particular, plays a significant role [5]. A good mobility model should

mimic the movement pattern of real mobile devices, describing how their locations change over time. Real-life mobility patterns can be very complicated, and the more complex the mobility pattern is, the more challenging it is to model it effectively [6, 7]. Thus, when modeling mobile ad hoc networks, it is necessary to choose the most appropriate underlying mobility model for the application under consideration.

In addition to node mobility, links change over time due to the error-prone propagation channel. A communication link between two nodes is established if their received signal power is greater than a system-dependent threshold. Consequently, connections between nodes are established and broken intermittently, leading to highly dynamic, frequently changing, random, multi-hop network topologies. Because any node can behave as a router or a host, any changes in states of its links can affect every communication going through that node. For these reasons, the topology of any real-world MANET is not fixed but exhibits a time-dependent evolution, i.e., a network snapshot represents a particular network state at a specific time. Understanding the evolution of the links and quantifying the topological uncertainty is beneficial for network synchronization [8], routing protocols [9], evaluation of route stability [10] and fault localization [11].

Particularly, routing in these systems faces strong challenges [12]. For instance, the protocol must be able to efficiently use limited resources to update its routes rapidly to maintain connectivity. At the same time, it may need to provide different levels of quality of service to different types of applications and users. In parallel with this, multi-path routing requires the availability of alternative paths between start and destination to prevent node failures from affecting the communication. However, available alternative paths are inherently unreliable, leading to an increase in overhead throughout the network due to frequent route discoveries

control packets [13]. One of the main techniques to reduce the number of route discoveries is based on the identification of a set of most stable paths, i.e., those paths that are expected to be active for a longer time. The selection of routes with longest expected lifetime guarantees a stable connection between nodes, which also satisfies the quality of service requirements for the different applications.

Therefore, it is imperative to take into account the random movements of nodes and the variations in the wireless medium when designing and implementing these networks. These are the main factors impacting the network stability and connectivity, and consequently, the performance of MANETs' protocols [14, 15]. Equally important is to measure the topological uncertainty of the wireless network and quantify how quickly the underlying topology is varying over time. Entropy-based tools have been widely used to better understand the properties of dynamic systems. Entropy gives a measure, in unit of bits, that describes the uncertainty in the link state evolution from one time step to the next one. This powerful tool, which is deeply rooted in statistical physics and information theory, allows one to quantitatively characterize the complexity, uncertainty, or inherent information content of dynamic networks.

The primary goals of the thesis are:

- To advance the theoretical modeling of the communication link between nodes in MANETs, by taking into account the effects of the mobility pattern and physical characteristics of the underlying wireless channel.

- To exploit this modeling in designing an entropy-based metric that quantifies link uncertainty and evaluates its stability, by taking full advantage of the correlation between the link current and future state.

- To analyze the main causes that impact the state of the communication link,

such as node mobility and wireless channel randomness.

- To propose a routing decision strategy that relies on the entropy-based metric, which can identify the route with the longest expected lifetime between a source and a destination wherever multiple routes are available.

1.2 Thesis Outline and Contributions

The thesis is composed of three research chapters, preceded by a literature review of wireless mobile ad hoc networks and followed by a conclusion and potential future works. The detailed outline of the thesis is as follows

- In chapter 2, we briefly summarize the history of mobile ad hoc networks. We then present the necessary background on the mobility and communication technology for MANETs highlighting the existing literature's challenges and gaps.

- In chapter 3, we determine novel expressions for the statistical properties of the received signal-to-noise ratio (SNR) and the separation distance in MANETs. Characterizing and managing the SNR variations users would see across a MANET is a challenging but essential problem towards understanding network stability and connectivity. These SNR variations and the low reliability of communications in MANETs are due to changes in the radio channel and users' mobility. Our contribution contrasts with those previously presented in the literature, where they mainly focus on the ergodic properties of the link SNR. In more detail, we start our analysis by first considering the case when there is no small-scale fading affecting the link between nodes. In this scenario, the statistical properties of the link SNR are entirely determined by the distance between the two nodes. As main contributions, we provide

a full mathematical description of the squared distance process, including its distribution and autocorrelation function, and show that it forms a stationary Markov process. We also derive closed-form expressions for the distribution and the bivariate distribution of the link SNR. We then proceed by taking into account variations in the propagation channel (e.g., Rayleigh fading), and deriving the distribution of the link SNR for rational path loss exponents. Crucially, this chapter provides a fundamental study of the temporal evolution of the SNR and distance processes in networks subject to Rayleigh fading and random mobility; as it is the most complete such study, it forms the starting point for further work.

This research has been published in the journal IEEE Transactions on Mobile Computing, 2020, [16].

- In chapter 4, we propose an entropy-based metric that quantifies link uncertainty by taking full advantage of the correlation between the link current and future state. In this regard, we take into account both the temporal and spatial properties of the wireless system. The motivations behind this work arise from the intrinsic location uncertainty of wireless networks and the ability of entropy to capture this randomness. Our formulation is based on a stationary Markov chain representation of link connectivity whose source of uncertainty is the separation distance between the nodes and the variations in the propagation channel. We then make progress by showing that the stochastic process describing the state of the dynamic system is stationary. This result then enables us to derive simple bounds on the network complexity. The simulation results demonstrate that the proposed metric thoroughly captures the link dynamics and accurately reflects changes in the state of a wireless connection. Thus, it

can be considered a valuable performance metric for quantifying topological uncertainty and connectivity in these networks.

This research has been published in IEEE Global Communications Conference (GLOBECOM), 2018, [17] and in IEEE International Conference on Communications (ICC), 2019, [18].

- Chapter 5 constitutes our final research chapter. In it, we combine the theoretical modeling of the communication link developed in chapter 3 with the topological uncertainty analysis carried out in chapter 4. Using these two tools, we investigate the main source of uncertainty in the link state in MANETs, concluding that random mobility is the primary cause. Finally, we provide an operational interpretation of the entropy-based metrics and propose a new routing decision strategy for MANETs. The key idea of this strategy is to identify and select the route with the longest lifetime between a source and a destination in an environment where different paths are available. The performance evaluation of the strategy is performed via simulation and analysis.

- Chapter 6 discusses the conclusions and potential future work.

Chapter 2

Communication and Mobility Modeling for MANETs

In this chapter, we start by describing the evolution of mobile ad hoc networks. We then provide the mathematical modeling of the wireless propagation channel that will be crucial for the rest of this thesis. Next, we present and examine different mobility models proposed in the recent research literature for MANETs. We then discuss the entropy-based methods that have been widely used to understand the properties of wireless networks better. Finally, we present a review of routing protocols for mobile ad hoc networks. In each of these sections, we highlight the challenges and gaps in the existing literature on MANETs and point out the research contribution of this thesis.

2.1 A Brief History of Mobile Ad Hoc Networks

Historically, mobile ad hoc networks have primarily been used in military applications to improve battlefield communications/survivability. The dynamic nature of these operations means that the military cannot rely on access to fixed infrastruc-

ture communication on the battlefield. The infrastructure-less nature of MANET, together with other advantages, such as flexibility, mobility, and resilience, drew immediate attention among military, police, and rescue agencies to use such networks under hostile environments.

The original mobile ad hoc networking application can be traced back to the Defense Advanced Research Projects Agency (DARPA) Packet Radio Network project in 1972, which was inspired by the efficiency of the packet switching technology, such as bandwidth sharing and store-and-forward routing, and its possible application in a mobile wireless environment. Tactical Internet (TI) implemented by the US Army in 1997 is by far the largest-scale implementation of mobile wireless multi-hop packet radio network. In 1999, another MANET deployment was carried out by the Marine Corps consisting of approximately 20 nodes. This network successfully proved the possibility to use aerial relays to connect users that are not in line-of-sight with each other [14].

For a long time, ad hoc network research stayed in the realm of the military. In the middle of the 90s, with the advent of commercial radio technologies such as IEEE 802.11 and the proliferation of mobile computing devices, the research community became aware of the tremendous commercial potential and advantages of mobile ad hoc networks outside the military domain.

2.1.1 Enabling Technologies

The primary technologies adopted in ad hoc wireless networks are the IEEE 802.11 standard for wireless local area network and Bluetooth standard for short-range wireless communications [14]. Due to their extreme simplicity, the IEEE 802.11 protocols are the world's most widely used standard to implement a wireless local area ad hoc network. Furthermore, this technology potentially allows covering

vast areas of several square kilometers by building a multi-hop wireless network, known as wide or metropolitan area network. In 1997, the IEEE released the first wireless local area network standard, IEEE 802.11. Several amendments (designated by letters) have been created to extend the IEEE 802.11 original version. Among the most widely used ones we find 802.11b standard, operating in the 2.4 GHz band and capable of transferring up to 11 Mbps of data, and the IEEE 802.11a, using the relatively unused 5 GHz band and capable of data rates up to 54 Mbps. On the other hand, Bluetooth technology is the leading standard for low-cost, short-range wireless links between mobile units. Bluetooth specifications can be used to build ad hoc wireless body networks, i.e., networks that connect devices on a person, or personal area networks where the devices are placed in closed proximity around the person [19].

Most of the existing ad hoc networks applications outside the military arena have been developed in the academic environment. Over the last years, some commercially oriented solutions are starting to appear, i.e., MeshNetworks[1] and SPANworks[2] [12]. Mobile ad hoc network research is a very vibrant and active field. The efforts of the research community, together with current and future MANET enabling radio technologies, will undoubtedly pave the way for a greater number of commercially viable solutions.

2.2 Wireless Propagation Channel: Modeling and Characterization

In real-world communication systems, the environment can cause the creation of several reflected, diffracted, and scattered copies of a transmitted signal due to ob-

[1]https://www.meshnetworks.com
[2]https://www.spanworks.com

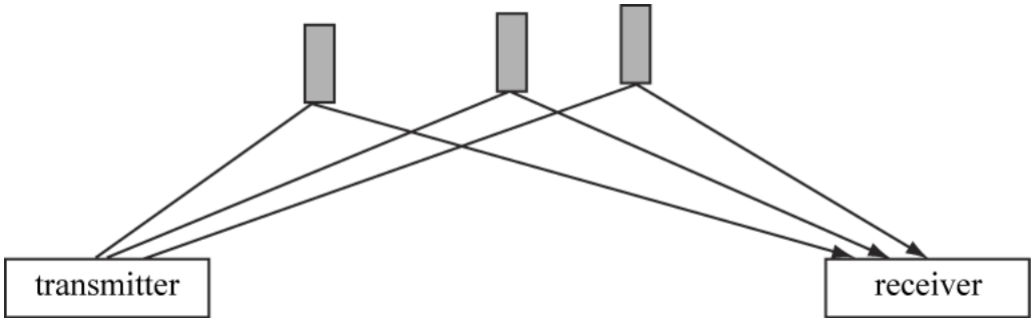

Figure 2.1: A visualization of multi-path propagation.

stacles present in the propagation channel between the transmitter and the receiver. The receiving antenna picks up a superposition of a series of attenuated and delayed versions of the original signal. The strength of the wave components decreases as the distance between the transmitter and receiver increases. Substantial variations, therefore, occur in the signal amplitude from the constructive and destructive addition of the different components. We use the terminology signal fading to describe this phenomenon [20].

Two types of signal fading are inherent to mobile radio systems:

- *Large-scale fading*, due to path-loss and shadowing by large objects such as buildings or hills. This can cause a random deviation of the received signal power from an average value.

- *Small-scale fading*, due to multi-path propagation, i.e., the fact that a transmit signal can reach the receiver via different paths. This occurs at the spatial scale of the order of the signal wavelength. The statistical properties of small-scale fading are of vital importance to the design of reliable and efficient communication systems.

In addition to fading, the Doppler effect also strongly impacts the transmission characteristics of mobile ad hoc networks. The movement of the transmitter and

receiver causes a shift in the received frequency of the multi-path components, called the Doppler shift.

The properties of the radio propagation channel, the transmission medium linking the transmitter and the receiver, determine the ultimate performance limit of the communication systems. It is thus fundamental to fully understand the behavior of the wireless medium and apply this knowledge to system design.

2.2.1 Path-Loss Propagation Model

This is the simplest model. It is the ideal propagation condition in which there is a clear line-of-sight between the transmitter and receiver and there are no obstacles nearby to cause reflection or diffraction. In this perfect environment, denoted as free-space, the attenuation of an electromagnetic waves is caused only by the wavelength of the signal and the distance between the transmitter and the receiver. The Friis transmission equation is one of the most fundamental equations in antenna theory. It is used in telecommunications engineering to calculate the received power under such ideal conditions. It is given by [21]

$$\frac{P_R}{P_T} = A_T A_R \left(\frac{w}{4\pi r}\right)^2, \tag{2.1}$$

where P_R is the received and P_T is the transmitted power, A_T and A_R are the gains of the transmitting and receiving antennas respectively, w is the wavelength, and r is the distance between the two stations. The ratio between the radiated and received power by isotropic antennas, i.e. $A_R = A_T = 1$, is known as the free-space path-loss

$$PL_{free}(r) = \frac{P_T}{P_R} = \left(\frac{4\pi r}{w}\right)^2. \tag{2.2}$$

In real-world scenarios, ideal conditions are hardly achievable, due to obstructions and reflections from the environment. In many scenarios a clear line-of-sight is often not available, and there are strong multi-path effects. In the literature, the most common way to deal with these effects is by using a path-loss exponent η to approximate the attenuation. The overall path-loss is given by [22]

$$PL(r) = r^{\eta} \left(\frac{4\pi}{w}\right)^2, \quad \eta \geq 2. \tag{2.3}$$

Then, the empirical variant of Friis transmission formula is equal to

$$\frac{P_R}{P_T} = A_T A_R \left(\frac{w}{4\pi}\right)^2 r^{-\eta}, \tag{2.4}$$

The parameter $\eta > 0$ is typically an experimentally determined number that indicates how quickly a transmission is attenuated as it propagates through the wireless medium. It is usually taken to be $\eta = 2$ in free space and $\eta > 2$ in cluttered urban environments.

2.2.2 Rayleigh Fading Channel Model

MANET applications are most likely to be deployed in urban areas. In such environments, a simplistic propagation model does not represent the real wireless channel effects caused by reflection, diffraction, and scattering phenomena. A well-accepted model to simulate an environment that has multiple scatterers and no line-of-sight path between a transmitter and a receiver is Rayleigh distribution. In the following, we consider a narrowband flat-fading channel, i.e., the coherence bandwidth of the channel is larger than the bandwidth of the signal. Therefore, all frequency components of the transmitted signal experience the same magnitude of fading. Additionally, we assume that that the Rayleigh fading channel is slow

enough that the received power remains at a certain level for the time duration of a channel symbol. In this regime, the channel is considered to be time-invariant during the symbol interval, but it varies spatially due to scattering (small-scale fading).

We refer to Jakes' model for effectively representing the mobile radio channel [23]. This model assumes that the electromagnetic waves travel horizontally and that the angle of arrival of waves is uniformly distributed from 0 to 2π. Consequently, the in-phase and quadrature components of the channel response tend towards a zero-mean Gaussian distribution with variance λ^2. It follows that the channel's envelope, $\{U_t, t \geq 0\}$, is a Rayleigh process with first-order probability density function (pdf) equal to [20]

$$f_{U_t}(u) = \frac{2u}{\lambda^2} e^{-u^2/\lambda^2}, \quad u \geq 0, \tag{2.5}$$

where $\lambda^2 = \mathbb{E}[U_t^2]$. Equation (2.5) indicates that the received signal envelope U_t is a first-order stationary process, since its pdf does not depend on time t. In a fading channel, the parameter of highest interest is the squared envelope or the channel gain, $G_t = U_t^2$, as it determines the received power at any time instance. By a simple transformation of random variables it is easy to show $G_t \sim \text{Exp}(\lambda^2)$ for all t, i.e., the channel gain is exponentially distributed with time-invariant mean λ^2. Its pdf is given by

$$f_{G_t}(g) = \frac{1}{\lambda^2} e^{-g/\lambda^2}. \tag{2.6}$$

In Fig. 2.2, as an example, is shown the pdf of the channel gain in the scenario when the channel exhibits Rayleigh fading with unit power. The normalized auto-covariance function best describes the temporal variability of the channel gain. In

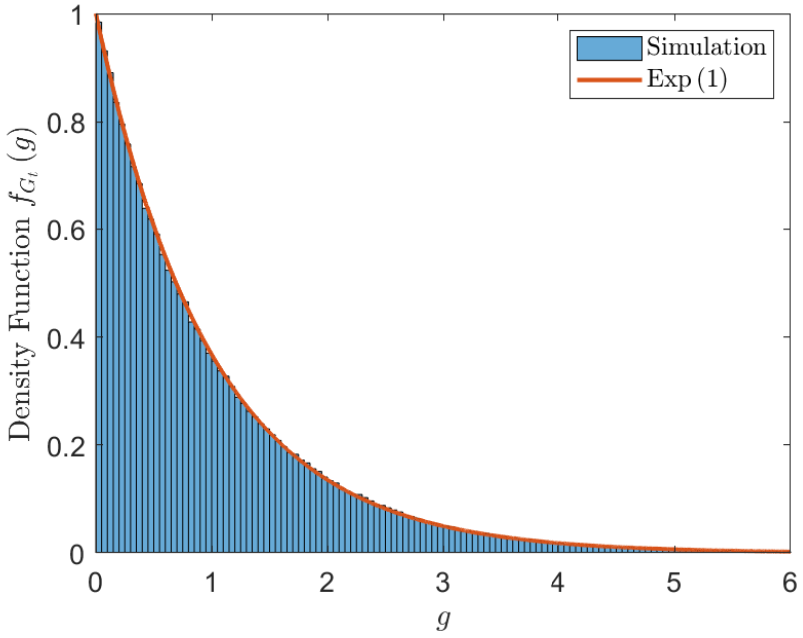

Figure 2.2: The probability density of the channel gain G_t.

Jakes' channel model, it is shown to be [24]

$$\frac{\mathcal{K}_G(\Delta t)}{\mathbb{E}[G]^2} = \frac{\mathbb{E}\{[G_{t+\Delta t}][G_t]\} - \mathbb{E}[G]^2}{\mathbb{E}[G]^2} = \mathrm{J}_0^2(2\pi\nu\Delta t), \tag{2.7}$$

where $\mathrm{J}_0(\cdot)$ is the zero-order Bessel function of the first kind, and ν is the maximum Doppler shift, a measure for the rate of change of the fading channel. It follows that the channel gain $\{G_t, t \geq 0\}$ is a wide-sense stationary (WSS) process since its mean and variance are time-invariant, and its autocovariance function depends only on the time shift Δt. In Fig. 2.3, we plot the correlation of the channel gain as a function of the product between the maximum Doppler shift ν and the time lag Δt.

The Rayleigh distribution is widely used in wireless communications to model fading statistics for several reasons [20]:

- Extensive experiments have confirmed that it is an excellent approximation of

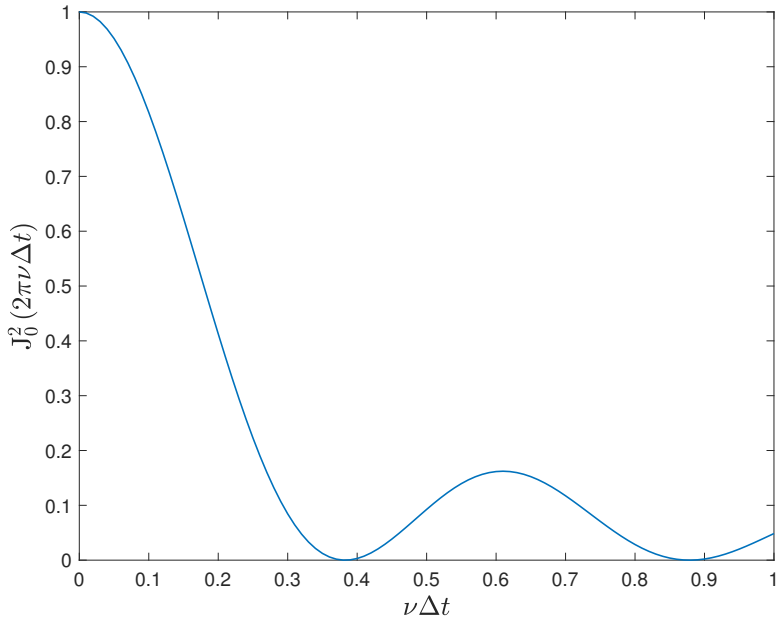

Figure 2.3: The normalized autocovariance function of the channel gain G_t.

practical scenarios.

- It describes a worst-case scenario in the sense that there is no direct line-of-sight path between the receiver and the transmitter.

- It depends only on a single parameter; the mean received power $\mathbb{E}[G_t]$. Once this parameter is known, the full signal statistics are known.

2.2.3 Rician Fading Channel Model

The model behind Rician fading is similar to that for Rayleigh fading, except that in Rician fading a line-of-sight component is present. In such a situation, random multi-path components arriving at different angles are superimposed on a stationary dominant signal. The Rician distribution is given by [20]

$$f(x \mid \nu, \lambda) = \frac{x}{\lambda^2} \exp\left(\frac{-(x^2+\nu^2)}{2\lambda^2}\right) I_0\left(\frac{x\nu}{\lambda^2}\right), \quad x \geq 0, \tag{2.8}$$

where $I_0(\cdot)$ is the modified Bessel function of the first kind and zero-order, ν denotes the peak amplitude of the dominant signal, λ^2 is the time-averaged power of the scattering components. The Rician distribution is often described in terms of a parameter K, which is defined as the ratio between the deterministic signal power and the variance of the multipath

$$K = \frac{\nu^2}{2\lambda^2}. \tag{2.9}$$

The parameter K is known as the Rician factor and completely specifies the Rician distribution. As $\nu \to 0$, $K \to 0$, and as the dominant path decreases in amplitude, the Rician distribution degenerates to a Rayleigh distribution.

2.2.4 Mitigating the effects of Fading

Fading can cause poor performance in a wireless communication system. In the event of a deep fade caused by destructive interference, there is no signal power received at the receiver causing a communication failure. In the literature, various diversity techniques have been proposed that mitigate the effects of Rayleigh fading [20]. Diversity is a powerful communication technique that is used to improve the performance over a fading radio channel at a relatively low cost. The principle of diversity is to ensure that the same information reaches the receiver on statistically independent channels. It exploits the random nature of radio propagation by finding independent signal paths for communication. As there is more than one path to select from, both the instantaneous and average SNRs at the receiver are improved. There are different diversity methods that can be used to combat small-scale fading [20]:

- *Spatial diversity:* several antenna elements, usually with the same characteristics, separated in space. It is the most used form of diversity, employing

multiple antennas to improve a wireless link's quality and reliability. Antenna diversity is effective at mitigating the effects of multi-path propagation. The reason is that several observations of the same signal will be available at the receiver, and each antenna will experience a different interference environment. Thus, while one antenna is experiencing a deep fade, it is probable that another has a sufficient signal. Collectively such a system can provide a strong link.

- *Temporal diversity:* the original signal is transmitted at different times over different channels. Intervals between the transmitted symbols should be at least equal to the coherence time to ensure that different copies of the same symbol undergo independent fading.

- *Frequency diversity:* transmission of the signal on different frequencies over different channels. For the received signals to be statistically independent or at least uncorrelated, the carrier frequencies must have a separation that is greater than the coherence bandwidth of the radio channel. Consequently, their fading is approximately independent, and the probability is low that the signal is in a deep fade at all frequencies simultaneously. However, we want to point out that it is not common to repeat the same information at several different frequencies, as this would significantly decrease spectral efficiency. Rather, information is spread over a large bandwidth, so that small parts of the data are conveyed by different frequency components to enhance the robustness against fading. The receiver can then sum over the different frequencies to recover the original information. This spreading can be done by deploying orthogonal frequency division multiplexing access (OFDMA). In OFDMA, multiple access is achieved by assigning different OFDM sub-

channels to different users.The sub-channels must be orthogonal to each other to avoid interference among overlapping sidebands of the individual carriers. The main advantage of OFDM over single-carrier schemes is its ability to converts a high-rate data stream affected by frequency selective fading into a number of low-rate streams that are transmitted over parallel, narrowband channels that can be easily equalized.

- *Angular diversity:* multiple antennas (with or without spatial separation) with different antenna patterns. Angular diversity is usually used in conjunction with spatial diversity; it enhances the decorrelation of signals at closely spaced antennas. Different antenna patterns can be achieved very easily. Of course, different types of antennas have different patterns. But even identical antennas can have different patterns when mounted close to each other.

- *Polarization diversity:* multiple antennas with different polarizations (e.g., vertical and horizontal). Horizontally and vertically polarized multi-path components propagate differently in a wireless channel, as the reflection and diffraction processes depend on polarization. The fading of signals with different polarizations is statistically independent. Thus, receiving both polarizations using a dual-polarized antenna, and processing the signals separately, offers diversity. This diversity can be obtained without any requirement for a minimum distance between antenna elements.

2.2.5 Maximum Doppler Frequency

In a multi-path propagation channel, the emitted wave is subject to the Doppler effect, i.e., a shift in the received frequency due to the movements of the transmitter and the receiver. The maximum Doppler shift, ν, is a measure for the rate of change of the channel [20].

Let $V_{i,t}$ and $V_{j,t}$ be the velocity of nodes i and j at time t, respectively. Then, the maximum Doppler shift is given by

$$\nu = f_c \frac{\Delta V}{c}, \tag{2.10}$$

where f_c is the carrier frequency, c is the speed of light, and $\Delta V = |V_{i,t} - V_{j,t}|$ is the change in velocities. This relationship is based on several assumptions such as static interfering objects, no double reflections on moving objects, and that the direction of the movement is aligned with the direction of wave propagation.

MANETs are formed in a self-organizing ad hoc fashion, anywhere, at any time, as long as two or more nodes are connected and communicate with one another via direct wireless links or multi-hop wireless links through a sequence of intermediate nodes. In the following, we assume that nodes rely on the 802.11a wireless technology to establish a connection when they come within the transmission range of each other. In modeling the mobile radio channel, we will refer to this section throughout the thesis. Finally, we assume that the wireless devices are identical, have the same design parameters and that these devices are present throughout the system's lifetime.

2.3 Mobility Models for Wireless Ad Hoc Networks

Taking into account the nature of mobile ad hoc networks, the mobility model plays a very important role in determining their performance. Several mobility models have been proposed in the literature, modeling both individual and group movement in ad hoc networks. The most commonly used models are [6, 7, 25]:

- *Random Waypoint Model (RWP)*: The RWP model is considered a "benchmark" mobility model to evaluate the MANET routing protocols. By far, it is

the most used model in simulation studies because of its simplicity and availability [26–28]. In this model, each mobile node travels to a random destination with a random speed that is uniformly distributed between a minimum and a maximum value. Once at the destination, it pauses for a random time before starting another movement [29]. The maximum node speed and pause time are the two key parameters that determine the mobility behavior of nodes. By varying these two parameters, we can generate different mobility patterns. But, the relationship between the maximum speed and the pause time is complex. For instance, a scenario with fast nodes and long pause times generates a more stable topology than a scenario with slower nodes and shorter pause times. Hence, before using this model for performance evaluation of MANET, appropriate parameters need to be estimated.

- *Random Walk Model (RW)*: The random walk model, also referred to as the Brownian motion, was initially proposed to mimic the unpredictable movement of particles in physics. Since there are practical scenarios where mobile nodes can move unexpectedly, this model is widely used in simulation studies to emulate this erratic pattern [30, 31]. We can consider the random walk as a specific random waypoint model with pause time set to zero. However, in this model, nodes change their speed and direction at each time interval. Each movement in the RW mobility model occurs in either a constant time interval or a constant distance traveled, at the end of which a new direction and speed are calculated.

- *Random Direction Model (RD)*: Several studies [32, 33] pointed out that the spatial node distribution of the RWP model is transformed from uniform to non-uniform distribution after the simulation starts. As the simulation time

elapses, this phenomenon becomes even worse. RD was proposed by Royer et al. in [34] to overcome the non-uniform spatial node distribution phenomenon that is inherent to the random waypoint model. Instead of picking a random destination within the simulation area, nodes choose a random direction in which to travel until they reach the simulation boundary. Once the boundary is reached, nodes stop for a specific time, choose another direction to travel, and continue the process. This process guarantees that nodes are uniformly distributed within the simulation area.

- *Gauss-Markov Model*: In RWP and its variant, the velocity of the mobile node is a memoryless random process, i.e., the current status is independent with its previous status. However, in many real-life scenarios, this is not the case. Hence, these mobility models may generate unrealistic movements. The Gauss-Markov model was first introduced by Liang and Haas in [35]. In this model, nodes move randomly according to a Gauss-Markov process using one tuning parameter to obtain different levels of randomness in the mobility pattern. The Gauss-Markov model represents a wide range of patterns with varying degrees of memory, including, as the two extreme cases, the random walk and the constant mobility model. For ad hoc environments where networks may change randomly and quickly, this mobility model is a good approach for the performance evaluation of these networks. For these reasons, we will use this model throughout this thesis, and in chapter 3, we will provide the mathematical formulation and the stochastic proprieties of this mobility model.

2.4 Signal-to-Noise Ratio

In a Rayleigh fading channel the end-to-end instantaneous signal-to-noise ratio (SNR) of a communication link with additive white Gaussian noise at any time t is equal to

$$N_t = \rho_0 G_t, \tag{2.11}$$

where G_t is the channel gain. The channel gain is exponentially distributed with mean λ^2, i.e., $G_t \sim \text{Exp}(\lambda^2)$ for all t. For the remainder of the thesis, we enforce the normalization $\lambda = 1$, i.e., $\mathbb{E}[G_t] = 1$. Under this assumption, ρ_0 represents the average SNR, i.e., $\rho_0 = \mathbb{E}[N_t]$.

Now, the average signal-to-noise-ratio ρ_0, measured at the receiver before detection, is defined as the ratio between the average received power and the white Gaussian noise power. Further, the transmit power P_T is designed for an average received power $\overline{P_R}$, which is computed based on path-loss alone. We combine these definitions with the Friis transmission formula (2.4) to obtain the following relation

$$\rho_0 = \frac{\overline{P_R}}{N} = \frac{P_T A_T A_R R_t^{-\eta}}{N} \left(\frac{w}{4\pi}\right)^2, \tag{2.12}$$

where η is the path-loss exponent (typically $2 \leq \eta \leq 6$), P_T is the transmitted power, $\overline{P_R}$ is the average received power, R_t is the distance between nodes, N is the white Gaussian noise power, w is the signal wavelength, and A_T and A_R are the antenna gains of the transmitter and the receiver, respectively. Then, the end-to-end instantaneous SNR can be succinctly written as

$$N_t = \psi R_t^{-\eta} G_t, \quad \psi = \frac{P_T A_T A_R}{N} \left(\frac{w}{4\pi}\right)^2. \tag{2.13}$$

In (2.13) the distance between nodes R_t and the channel gain G_t are random processes. The other design parameters, which we represent with ψ, are considered as system constants. By a simple transformation of random variables, it is straightforward to derive the distribution of the instantaneous SNR for static wireless networks, i.e., for networks where $R_t = R$. In this scenario, the received instantaneous SNR N_t has an exponential distribution with probability density function

$$f_{N_t}(\rho) = \frac{1}{\rho_0} e^{-\rho/\rho_0}, \quad \rho \geq 0, \tag{2.14}$$

where $\rho_0 = \psi R^{-\eta}$. Equation (2.14) indicates that the received signal-to-noise ratio N_t is a first-order stationary process, since its pdf does not depend on time t. Hence, in static wireless networks subject to Rayleigh fading, the received instantaneous SNR follows an exponential distribution with time-invariant mean ρ_0.

The instantaneous SNR has been extensively analyzed in the literature as it directly impacts the quality of the communication link. Authors in [36] used the link SNR to evaluate the mean proportion of time that two mobile devices are connected for five different types of mobility. In [37], the link SNR was proposed as a quality measure to predict links' state evolution in mesh networks. In [38], the authors characterized variations in the SNR process to study the coverage and outage durations experienced by mobile users, while in [39] they studied the time variations of the SNR in the absence of fading experienced when a mobile user moves across a Poisson cellular network. The connectivity achievable in mobile ad hoc networks with the RWP mobility was addressed in [40–42].

The statistics of the received signal power are well understood for static wireless networks. The probability distribution of the received power in a static ad hoc network subject to log-normal shadowing and distance-dependent path-loss model

is derived in [43]. Closed-form expressions for the outage probability and the average probability of error based on the SNR of dual-hop wireless systems subject to Rayleigh fading were presented in [44]. The distribution of the received signal strength for an indoor WLAN is derived in [45]. Jakes et al. in [23] showed that the received power follows as a Rayleigh distribution for the nodes moving with a constant speed.

In the field of MANET, not much exploration has been done on the statistical analysis of the end-to-end instantaneous SNR, especially when the moving pattern is random. Authors in [27] obtained the pdf of the received SNR for two different mobility models, RWP and RD, in a Rayleigh fading channel. In [28], the outage probability and average bit error rate in a Nakagami-m fading environment with the RWP mobility model were derived, whereas in [46] the authors calculated the same quantities for the RD mobility model. In [47] the pdf of received power is obtained by combining the Pareto distribution due to unknown locations with log-normal shadowing. Statistics of the received signal power at the central base station in a cellular direct sequence code division multiple access system with Rayleigh fading is analyzed in [48]. However, the works above only describe the ergodic properties of the link SNR. To the best of the author's knowledge no attempt has been made to characterize the temporal evolution of the SNR and distance processes in networks subject to Rayleigh fading and random mobility. This will be the main focus of chapter 3. In the following, we outline some of the major contributions of this chapter:

- The stochastic differential equation of the link SNR N_t in mobile networks where nodes experience an OU mobility model in (3.26). This is a significant result because we can directly simulate samples of the SNR by implementing this equation as, shown in Fig. 3.10. It is the first time in the literature that

the stochastic differential equation of the link SNR in any scenario for any mobility or wireless channel model is reported.

- The bivariate density function of the link SNR in (3.30). This result is significant for stability issues because it tells us how links change over time. To derive this result, we used the Taylor expansion of the Bessel function and we solved the resulting integral.

- Distribution of the SNR in (3.32). It is the most complete mathematical analysis of the distribution of the link SNR reported in the literature for a system subject to Rayleigh fading and OU Mobility accounting for rational path loss exponent.

2.5 Shannon (Ergodic) Capacity

For a memoryless time-invariant channel with random input X and random output Y the capacity, C bits/channel use, of a channel is defined to be the mutual information (to be described in (2.25)) between input X and random output Y, maximized over all input signal distributions [21], i.e.,

$$C = \max_{p(x)} I(X;Y). \tag{2.15}$$

The cornerstone of modern information theory, the channel coding theory, provides an operational interpretation for C. Specifically, it tells us that C is the maximum rate at which information can be transmitted over the channel with arbitrarily small probability of bit error.

Now, consider an additive white Gaussian noise (AWGN) channel with bandwidth B. For this channel, the maximizing input distribution is Gaussian, which

results in the capacity formula

$$C(\rho) = B \log_2(1 + \rho), \tag{2.16}$$

where ρ is the instantaneous signal-to-noise ratio.

The AWGN channel is used as a building block to study the capacity of wireless fading channels. In a fading channel, the ergodic capacity is the expected value of the capacity, taken over all realizations of the channel. Formally,

$$\mathbb{E}\left[C(\rho)\right] = \int_0^\infty B \log_2(1 + \rho) f(\rho) \mathrm{d}\rho, \tag{2.17}$$

Shannon capacity of a fading channel is equal to the capacity of a AWGN with SNR ρ averaged over the distribution of ρ. That is why the Shannon capacity is called the ergodic capacity. Each channel realization can be associated with a capacity value, which is a random variable with an associated cumulative distribution function [20]. This function can used to calculate the capacity that can be guaranteed for $x\%$ of all channel realizations. The latter quantity is also known as outage capacity.

Unlike the AWGN channel, there is no single definition of capacity for fading channels that is applicable in all scenarios. For a slow fading environment, it is impossible to drive the probability of error to zero. This happens because deep fades will cause the SNR of the link to drop dramatically. In the strict sense, the capacity of a slow fading channel is zero, and we must take into account the probability that the channel has dropped into a deep fade and is unable to support the desired rate, C_{th}, of the link. The probability of outage characterizes the probability of deep fading, and is defined as [49]

$$\mathbb{P}_o = \mathbb{P}\left(C \leq C_{th}\right). \tag{2.18}$$

As capacity is monotonically increasing function of SNR, this equation is often expressed as

$$\mathbb{P}_o = \mathbb{P}\left(\rho \leq \rho_{th}\right), \tag{2.19}$$

where ρ_{th} is the SNR threshold. For a gaussian channel, the relationship between ρ_{th} and C_{th} is given by $C_{th} = \log_2\left(1 + \rho_{th}\right)$. If the received instantaneous SNR is below ρ_{th} then the bits received over that transmission burst cannot be decoded correctly, and the receiver declares an outage. The threshold ρ_{th} is determined by the communication hardware and the modulation and coding scheme of the wireless system. Hence, to calculate the achievable capacity and the outage probability, the signal-to-noise ratio distribution is critical. The distribution presented in chapter 3 in (3.32) is the most complete mathematical analysis of the distribution of the link SNR reported in the literature for a system subject to Rayleigh fading and OU Mobility accounting for rational path loss exponent. We then define the connection probability as the complement of the outage probability, and derive this probability in mobile networks in (3.36) using (3.32). This is a significant result because it provides some insight into the relationship between the link connectivity probability, mobility parameters, and the SNR threshold ρ_{th}.

2.6 Shannon Entropy

Information theory is the mathematical framework used to study communication and was introduced by Claude E. Shannon in 1948 in his groundbreaking paper "A Mathematical Theory of Communication", [50]. A fundamental concept from information theory is the quantification of the amount of information associated with any random variable. Entropy gives a measure, in units of bits or nats, of the average amount of uncertainty or information intrinsic in the variable's possible outcomes. It is often used as a tool to quantify disorder in a dynamic system.

2.6.1 Definitions

The entropy of a discrete random variable X with a probability mass function $p(x) = \mathbb{P}(X = x)$ is defined by [51]

$$H(X) = -\mathbb{E}\left[\log p(x)\right] = -\sum_{x} p(x) \log p(x). \tag{2.20}$$

The units for entropy are "nats" when the natural logarithm is used and "bits" for base 2 logarithms. The natural logarithms are usually more convenient for mathematics while the base 2 logarithms provide more intuitive descriptions. We will use logarithms to base 2. From an information-theoretic perspective, the entropy measures the average number of bits required to describe the random variable X. As an example, let us consider a Bernoulli random variable X with 2 possible outcomes

$$X = \begin{cases} 1, & \text{with probability } p \\ 0, & \text{with probability } 1-p. \end{cases} \tag{2.21}$$

In this particular case, the entropy is equal to

$$H(X) = -p \log p - (1-p) \log(1-p) \overset{\text{def}}{=} H(p). \tag{2.22}$$

In Fig. 2.4 we plot the graph of the function $H(p)$. This figures illustrates some of the basic properties of the entropy such as: $H(X) \geq 0$, entropy is a concave function of the distribution, it reaches its highest value $H(X) = 1$ bit when $p = 1/2$, and equals 0 when $p = 0$ or 1. This makes sense because the uncertainty is maximum for $p = 1/2$, and there is no uncertainty when $p = 0$ or 1.

Now, consider a pair of discrete random variables X and Y with joint probability

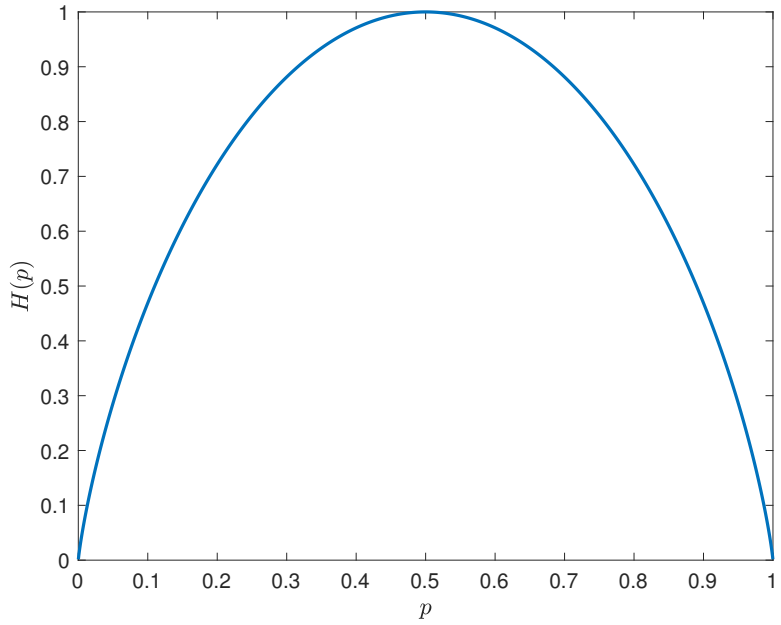

Figure 2.4: $H(p)$ versus p.

distribution $p(x, y)$. The joint entropy $H(X, Y)$ is defined as

$$H(X, Y) = -\sum_{x}\sum_{y} p(x, y) \log p(x, y). \tag{2.23}$$

We also define the conditional entropy, $H(X|Y)$, which quantifies the amount of bits needed to describe the outcome of X, given that the outcome of Y is known. It is equal to

$$H(X|Y) = -\sum_{y} p(y) H(X|Y = y) = -\sum_{y} p(y) \sum_{x} p(x|y) \log p(x|y). \tag{2.24}$$

The conditional entropy $H(X|Y) = H(X)$ if and only if the random variables X and Y are independent.

Finally, we introduce mutual information, which is a measure of the amount of information that one random variable contains about another random variable. It

is defined as

$$I(X;Y) = \sum_x \sum_y p(x,y) \log \frac{p(x,y)}{p(x)p(y)}. \tag{2.25}$$

The relationship between entropy and mutual information is given by

$$I(X;Y) = H(X) - H(X,Y). \tag{2.26}$$

Thus, the mutual information is the reduction in the uncertainty of one random variable due to the knowledge of the other.

2.6.2 Entropy Rate of a Markov Process

A discrete stochastic process $\{X_n, n \in \mathbb{N}\}$ is said to be a stationary Markov process if, for all time-steps n

$$\mathbb{P}\left(X_{n+1} = x_{n+1} | X_n = x_n, \ldots, X_1 = x_1\right) = \mathbb{P}\left(X_{n+1} | X_n\right) = \mathbb{P}\left(X_2 | X_1\right), \tag{2.27}$$

where $x_1, \ldots, x_n, x_{n+1} \in \mathcal{X}$. The first equality follows from the Markov property, i.e., the conditional distribution of X_n depends only on X_{n-1} and is independent of any other previous state. The second equality follows from the stationary property, i.e., the conditional probability does not depend on the time-step n.

The entropy rate of a stationary stochastic process $\{X_n, n \in \mathbb{N}\}$ is defined by [51]

$$H\left(\mathcal{X}\right) = \lim_{n\to\infty} \frac{H\left(X_1, X_2, \ldots, X_n\right)}{n} = \lim_{n\to\infty} H\left(X_n | X_{n-1}, \ldots, X_1\right). \tag{2.28}$$

For a stationary Markov chain, the entropy rate simplifies to

$$H\left(\mathcal{X}\right) = H\left(X_2 | X_1\right), \tag{2.29}$$

where the conditional entropy $H(X_2|X_1)$ is calculated using the stationary distribution of the Markov process. We can interpret the entropy rate as a measure of the uncertainty of the future status of the random variable X_n given its past behavior. Given that $\{X_n, n \in \mathbb{N}\}$ is a Markov process, then the future status of X_n depends only on the current status.

2.6.3 Entropy-Based Metrics

Entropy-based methods have been widely used to better understand the properties of dynamic networks. Dehmer et al. [52] introduced an information functional on each of the vertices of a graph in order to associate an entropic quantity with the network. More precisely, an information functional quantifies structural information of a graph based on a derived probability distribution. Such a probability distribution leads directly to an entropy of a graph. Studies in [53–56] used Shannon entropy to quantify the topological uncertainty of wireless networks embedded within a spatial domain, while in [57] different lower bounds on the Shannon entropy of random geometric graphs were derived by using the notion of conditional entropy. Rate-distortion theory was used in [58] to characterize the minimum cost of tracking the motion state information of nodes in dynamic networks. Rate-distortion theory was introduced in 1948 by Shannon [50]. It is the branch of information theory that addresses data compression problems. Specifically, it provides an analytical expression for the minimal number of bits per symbol that should be communicated over a channel, so that the source (input signal) can be approximately reconstructed at the receiver (output signal) without exceeding an expected distortion.

In the field of mobile ad hoc networks, a probabilistic method to assess the quality of the link in terms of link duration was proposed in [59]. Specifically, the proposed stability estimation scheme is able to estimate the link stability in both stationary

and non-stationary scenarios, and the proposed routing method enhances packet delivery rate effectively in ad-hoc networks. In [60], authors studied three mobility metrics and evaluated their ability to predict the routing protocol performance. These metrics do not require global network knowledge and are feasible to compute. In the field of temporal networks, entropy rates of random walks have been used to characterize the temporal network structure [61,62]. The authors in [10] introduced an entropy-based model for evaluating route stability, [63] derived an entropy-based mobility metric to describe scaling properties of mobile ad hoc networks under the random walk mobility model, and [64] proposed the entropy of the link change as a mobility metric.

However, we believe entropy rate can represent a more accurate metric of topological uncertainty in dynamic networks, considering its ability to measure the uncertainty of the future state of the link given its current state. The entropy rate gives a measure (in bits) of the uncertainty in the link state evolution from one time step to the next one. If we consider one communication link, the entropy rate can reach its maximum value of one bit when the link state at time step k is independent from the link state at time step $k-1$. In chapter 4, we will show how the value the entropy rate can actually take is much less than its maximum theoretical one because of the correlation in the link state from one time step to the next one induced by the node mobility and Rayleigh fading channel.

2.7 Routing Protocols in MANETs

MANETs are composed of mobile nodes that communicate via direct wireless links or multi-hop wireless links through a sequence of intermediate nodes. The lack of a centralized structure within mobile ad hoc networks requires mobile nodes to behave as a host and as a router. As a router, the mobile device represents an

intermediate node that forwards packets on behalf of other devices that may not be within direct communication range to the destination node. Routing protocols allow source hosts to communicate through multi-hop paths with destination hosts when a direct link can not be established.

The challenges and complexities of MANETs described in section 1.1 pose real challenges to the routing problem. Most of the main functionalities of networking protocols (e.g., routing protocols) need to be re-designed to cope with the dynamic peer-to-peer unreliable communication environment in MANETs [14]. The classical routing protocols in MANETs are typically subdivided into two main categories: proactive and reactive routing protocols [65,66]. These routing strategies aim to find a path between two communicating nodes without taking into account the quality of the intermediary links. In proactive routing protocols, each node maintains routing information to every other node in the network by propagating, proactively, route updates at fixed time intervals. The routing information is usually stored in several different tables. These tables are updated and maintained through both periodic and event-driven (e.g., triggered by links breakages) control messages. The most representative proactive protocols are: Destination-Sequenced Distance-Vector (DSDV) [67], and Optimized Link State Routing (OLSR) [68].

On the other hand, reactive on-demand routing protocols establish the path to a destination only when there is a request for it. The source node, through the route discovery process, usually initiates the route requested. Once a path has been established, it is maintained until either the destination becomes inaccessible, or until the path is no longer used. Dynamic Source Routing (DSR) is a loop-free, source-based, on-demand protocol [69]. The route discovery process is only initiated when a source node does not already have a valid route to the destination in its routing table; entries are periodically updated as new routes are discovered. Ad

hoc On-Demand Distance Vector (AODV) is a reactive improvement of the DSDV protocol. AODV minimizes the number of route broadcasts by creating routes on-demand [70], as opposed to maintaining a complete list of routes as in the DSDV algorithm.

In the classical routing in MANETs, paths are generally established according to the minimum hop-count metric. These protocols do not guarantee, in most cases, the Quality of Service (QoS) requirements for multimedia applications [71]. Another class of the routing protocols called QoS routing protocols has emerged to accommodate these requirements [72]. In this class, instead of using the hop-count metric, the QoS requirements (e.g., delay, bandwidth, jitter, etc.) are the key metrics to establish the paths. However, this class of routing protocols does not take into account the stability and longevity of the selected paths. Several factors influence the stability of the routes, such as the nodes' mobility and wireless channel quality.

A new class of routing protocols that take into account the stability of links in MANETs was proposed in the literature [13]. In this class, the route selection process considers the link stability criterion, i.e., links' longevity [73]. Here, the routing decision is based on two metrics: the distance and the mobility of the nodes. Distance-based metric strategies try to minimize the distance between two nodes; hence a longer route in terms of hop-count might be chosen if the total distance would be shorter. Generally, the signal strength or a localization system is used for calculating this metric. In [74], authors propose a route stability routing protocol with a distance-based metric calculated from received signal strengths. On the other hand, strategies based on the mobility of the nodes use the mobility parameters such as the speed of nodes and the connectivity probability, to estimate the link stability value. For instance, authors in [71] use a stability function as the

routing decision criterion based on the calculation of the mobility degree of a node relative to its neighbor. Authors in [75] proposed a method for measuring the route stability based on the information entropy which utilized the degree of uncertainty as the standard for stable route selection. In chapter 5, we will propose a new routing decision strategy for MANETs based on the entropy-based metric presented in chapter 4, which takes into account path longevity. The key idea of this strategy is to identify and select the route with the longest expected lifetime between a source and a destination in an environment where different paths are available.

Chapter 3

Statistical Properties of Transmissions in MANETs

In this chapter, we derive closed-form expressions for significant statistical properties of the end-to-end instantaneous signal-to-noise ratio (SNR) and the separation distance in mobile ad hoc networks subject to Gauss-Markov mobility, and Rayleigh fading. SNR is a critical measure that gives clear indications on the quality of a node's connectivity with its neighbors. One of the fundamental characteristics of mobile ad hoc networks is the time-varying nature of the received signal power, which is attributed to node mobility and variations in the propagation channel. Characterizing and managing the SNR variations users would see across MANET is a challenging but essential problem towards understanding network stability and connectivity. The focus of this chapter is to provide such a study. To that end, we first present the random mobility model adopted in this work, highlighting why it is a good approach for the performance evaluation of ad hoc environments. We then derive the statistics of the distance process and the SNR process, both in fading and non-fading scenarios.

3.1 Introduction

Transmission between two nodes is successful (the communication link is active) if the end-to-end instantaneous SNR is higher than a system-dependent threshold. In mobile networks, the received signal power changes over time due to node mobility, multi-path fading, and path-loss via distance attenuation. Therefore, connections between nodes are established and broken intermittently, leading to dynamically changing network topology. Node mobility and channel randomness are thus the main factors impacting the distribution of the link SNR, and consequently, the performance of MANET.

As discussed in section 2.4, the current state-of-the-art only describes the ergodic properties of the link SNR. To the best of the author's knowledge, no attempt has been made to characterize the temporal evolution of the SNR and distance processes in networks subject to Rayleigh fading and random mobility. Hence, this chapter goes much further by giving full information about the SNR distribution rather than just ergodic properties. We begin by deriving a complete statistical description of the squared distance process, including its distribution and autocorrelation function, and show that it forms a stationary Markov process. Next, we compute the stochastic differential equation of the link SNR. In the absence of signal fading, we derive closed-form expressions for the probability density function (pdf), the cumulative distribution function (cdf), the bivariate pdf, and the bivariate cdf of the link SNR. We then introduce signal fading in our model and evaluate the link SNR distribution for rational path-loss exponents. Following this, we calculate the connectivity probability for both fading and non-fading scenarios. Finally, we analyze the distribution of the received signal power in the low SNR regime. The validity of our theoretical analysis is verified by extensive simulation studies.

3.2 System Model

Consider two arbitrary nodes i and j (mobile wireless devices) moving randomly over a two-dimensional plane using the radio channel to communicate with each other. Each device movement is assumed to be independent from the other. The locations of the nodes at time $t \geq 0$ are given by $A_{i,t} = (X_{i,t}, Y_{i,t})$ and $A_{j,t} = (X_{j,t}, Y_{j,t})$, respectively. We denote by R_t the Euclidean distance between two nodes, $R_t = \|A_{j,t} - A_{i,t}\|$, and by Z_t the squared distance, $Z_t = R_t^2$. In modeling the mobile radio channel, we refer to section 2.2. In the following, we assume that large-scale fading is only caused by the path-loss, neglecting the shadowing effect, and there is either no small-scale fading or the small-scale fading is Rayleigh.

3.2.1 Signal-to-Noise Ratio

From section 2.4 we have that in a Rayleigh fading channel the end-to-end instantaneous SNR is given by

$$N_t = \psi Z_t^{-\eta/2} G_t, \quad \psi = \frac{P_T A_T A_R}{N} \left(\frac{w}{4\pi}\right)^2, \tag{3.1}$$

where η is the path-loss exponent (typically $2 \leq \eta \leq 6$), G_t is the channel gain with $\mathbb{E}[G_t] = 1$, P_T is the transmitted power, $\overline{P_R}$ is the average received power, Z_t is the squared distance between nodes, N is the white Gaussian noise power, w is the signal wavelength, and A_T and A_R are the antenna gains of the transmitter and the receiver, respectively. It is evident from (3.1) that the instantaneous SNR N_t depends on the distance between nodes Z_t, which, in turn, is governed by the mobility model and the environmental factors controlling the propagation channel, which are captured by G_t. These two factors are the main sources of uncertainty in the link state. The other design parameters, which we represent with ψ, are

considered as system constants.

All mobile nodes within the network require some minimum received SNR for acceptable performance. A transmission between nodes at any time t is successful if the instantaneous SNR of the link is higher than a certain threshold ρ_{th}, determined by the communication hardware, as well as the modulation and coding scheme of the wireless system. We define the connection probability as the complement of the outage probability. For a single-input single-output transmission in a Rayleigh fading channel, this probability is given by

$$\mathbb{P}\left(N_t \geq \rho_{th}\right). \tag{3.2}$$

If the received instantaneous SNR is below ρ_{th} then the bits received over that transmission burst cannot be decoded correctly, and the receiver declares an outage.

3.2.2 Mobility Model

In our analysis, nodes move according to an Ornstein-Uhlenbeck (OU) process, a continuous-time Gaussian Markov process [76]. This mean-reverting process is particularly suitable for describing the movement of a group of elements having the same destination suffering from random deviations around the projected trajectory. An example would be Unmanned Aerial Vehicles (UAV) moving toward the same target. Moreover, the OU process represents a wide range of patterns with varying degrees of memory, including, as the two extreme cases, the random walk and the constant mobility model [6]. The main advantage of this model with respect to the ones described in section 2.3 is that it fully captures the temporal dependency of the movement of a node over time, i.e., how the current position of a mobile node depends on its previous position. By choosing appropriate parameters we can generate movement patterns that one might expect in the real world. For these

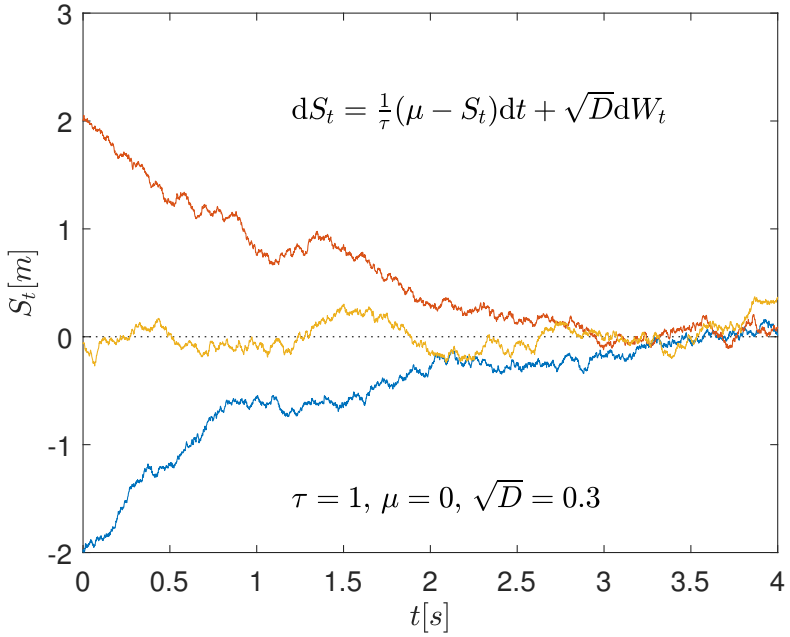

Figure 3.1: Three sample paths of OU processes with the same parameters: $\tau = 1$ s, $\mu = 0$ and $\sqrt{D} = 0.3$ m^2/s, but different initial positions S_0.

reasons, the OU mobility model is a good approach for the performance evaluation of ad hoc environments.

In the following, we model the node displacements along the x and y coordinates, $\{(X_{i,t}, Y_{i,t}), (X_{j,t}, Y_{j,t})\}$, by independent identical OU processes. Specifically, each coordinate $X_{i,t}, Y_{i,t}, X_{j,t}, Y_{j,t}$ is equal in distribution with S_t. The continuous-time stochastic process $\{S_t, t \geq 0\}$ is an OU process which takes real values. Such process S_t is defined as the solution to the stochastic differential equation (SDE) [77, 78]

$$\mathrm{d}S_t = \frac{1}{\tau}(\mu - S_t)\mathrm{d}t + \sqrt{D}\mathrm{d}W_t, \quad S_0 = s_0 \in \mathbb{R}, \tag{3.3}$$

where μ is the desired position, $\{W_t, t \geq 0\}$ is the standard Brownian motion, $W_t \sim \mathcal{N}(0, t)$, and $\mathrm{d}W_t$ is a temporally uncorrelated normal random variable with mean 0 and variance $\mathrm{d}t$. The solution to this SDE exists, and is unique [79]. It is

equal to

$$S_t = (s_0 - \mu)\, e^{-t/\tau} + \mu + \sqrt{D} \int_0^t e^{(u-t)/\tau} \mathrm{d}W_u. \tag{3.4}$$

The parameters τ and D are positive constants called the *relaxation time* and the *diffusion coefficient*, respectively; $\sqrt{D}$ controls the fluctuation in the position of the devices along each coordinate axis, and $1/\tau$ controls the rate of reversion of the device to the desired position μ. Given the starting point $\{S_0 = s_0, t = 0\}$, the expectation m and variance α of the process are equal to:

$$\begin{aligned} m &= \mu + (s_0 - \mu) e^{-t/\tau}, \\ \alpha &= \frac{D\tau}{2} \left(1 - e^{-2t/\tau}\right). \end{aligned} \tag{3.5}$$

Note that $\alpha \to \frac{D\tau}{2}$ and $m \to \mu$ as $t \to \infty$. If the initial condition of the process, S_0, is drawn according to the steady-state distribution, then the process is stationary. In Fig. 3.1 are shown three sample paths of OU processes with the same parameters, $\tau = 1$, $\mu = 0$ and $\sqrt{D} = 0.3$, but different initial positions. In the long term, all paths approach the steady-state. A 2D simulation of nodes' trajectories is plotted in Fig. 3.2.

3.2.2.1 Parameter Values

The Gauss Markov Mobility Model was initially proposed to simulate a Personal Communications Service (PCS) [80]. While PCS boasts more extended mobility than that of cellular, it essentially is a phone service with additional features such as caller id and paging. The key differences between PCS and cellular services are the frequencies in which they operate, coverage areas of their different cell architectures, and the power levels each uses to transmit signals.

To better understand the coefficients of the OU process, we refer to (3.4). Clearly, as $\tau \to 0$, the process represents a drifting random walk mobility pattern with mean

μ and variance $D\tau/2$. We can consider the random walk as a specific random waypoint model with pause time set to zero. The random waypoint model is used in several simulation studies of ad hoc network protocols. For instance, it appears to create realistic mobility patterns for the way people might move in a conference setting or museum [6].

On the other hand, when $\tau \to \infty$, (3.4) degenerates into a constant mobility pattern with $S_t = s_0$ for all t. This pattern is used to model nodes' mobility in a Vehicular Ad hoc Network (VANET) in a highway where nodes move following a certain path in a certain direction. In this model, nodes' velocity is dependent on the three lanes (slow, medium, and fast lane). Vehicles can change lanes as they do in real-life situations, i.e., from slow to medium lane but not to the fast lane directly [81].

For all other values of τ, the process in (3.4) represents the case where the nodes are tethered to a desired location. Hence, they drift randomly with a control mechanism that tends to push the device back to the target location. This mean-reverting process is particularly suited for modeling node mobility in robotic swarms or D2D UAV networks subject to positional perturbations [82]. These types of networks are widely utilized in various rescues, disaster management and military operations [83].

Therefore, not only does the Gauss-Markov model represent a wide spectrum of mobility patterns with various degree of memory, it also includes the random walk and constant mobility model as its two extreme cases.

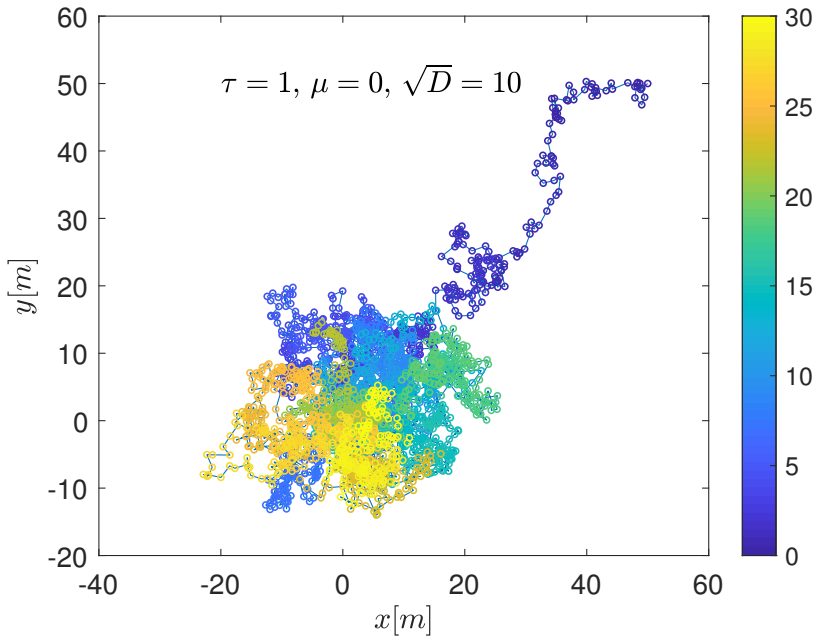

Figure 3.2: A 2D simulation of nodes' trajectories along the x and y coordinates.

3.2.2.2 Autocovariance Function

Another quantity of interest is the autocovariance function of the OU process. It is given by [76]

$$K_S(t,u) = \mathbb{E}\left\{[S_t - m]\,[S_u - m]\right\} = \alpha e^{-\Delta t/\tau}, \tag{3.6}$$

where $\Delta t = |t-u|$ is the lag time. The stationary autocovariance function is obtained by allowing the system to approach its steady-state. That is,

$$K_S(\Delta t) = \lim_{t\to\infty} K_S(t,u) = \frac{D\tau}{2} e^{-\Delta t/\tau}. \tag{3.7}$$

In the steady-state, the random variables S_t and S_{tu} are only significantly correlated if $|t-u| \approx \tau$, also known as the *correlation time*. Under the model described above, the random variables $X_{i,t}, Y_{i,t}, X_{j,t}, Y_{j,t} \sim \mathcal{N}(m,\alpha)$ are independent, and the squared

pair distance, at any time t, is given by

$$Z_t = X_t^2 + Y_t^2, \tag{3.8}$$

where $X_t = X_{j,t} - X_{i,t} \sim \mathcal{N}(0, 2\alpha)$ and $Y_t = Y_{j,t} - Y_{i,t} \sim \mathcal{N}(0, 2\alpha)$ are independent random variables.

3.2.2.3 Distribution of the Velocity

Next, we are interested in the distribution of the velocity. Let $V_{i,t} = \{V_{i,t}^x, V_{i,t}^y\}$ be the velocity (vector) of node i (the same applies to node j, as their velocities are independent and identically distributed) along the x or y coordinates at time t. Velocity is defined as the rate of change of displacement with respect to time, i.e.,

$$V_{i,t}^x = \frac{\mathrm{d}X_{i,t}}{\mathrm{d}t} \tag{3.9}$$

Then, we can write

$$V_{i,t}^x = \frac{1}{\tau}(\mu - X_{i,t}) + \sqrt{D}\frac{\mathrm{d}W_t}{\mathrm{d}t} = \frac{1}{\tau}(\mu - X_{i,t}) + \sqrt{D}\xi_t, \tag{3.10}$$

where W_t is the standard Brownian motion, and $\mathrm{d}W_t$ is a temporally uncorrelated normal random variable with mean 0 and variance $\mathrm{d}t$. The process ξ_t is the white Gaussian noise and it can be described as the generalized time derivative of Brownian motion [79]. Specifically, we can define it as the $\mathrm{d}t \to 0$ limit of the temporally uncorrelated normal random variable with mean 0, with variance $1/\mathrm{d}t$, and autocorrelation function $\mathbb{E}[\xi_t \xi_u] = \delta(t-u)$, where δ denotes the Dirac delta function [84]. It is evident from (3.10) that the variance of the velocity $V_{i,t}^x$ tends to infinity as $\mathrm{d}t$ goes to zero. To overcome this issue, we approximate the velocity as the change of

the position divided by a fixed time interval Δt. That is,

$$V_{i,t}^{x} = \frac{X_{i,t+\Delta t} - X_{i,t}}{\Delta t}. \tag{3.11}$$

Now, $X_{i,t+\Delta t}, X_{i,t} \sim \mathcal{N}(m, \alpha)$, hence, $X_{i,t+\Delta t} - X_{i,t} \sim \mathcal{N}(0, 2\alpha)$. It follows that, for a fixed time interval Δt, the velocity $V_{i,t}^{x}$ is approximately normally distributed with fixed variance $2\alpha/(\Delta t)^2$, i.e., $V_{i,t}^{x} \sim \mathcal{N}\left(0, 2\alpha/(\Delta t)^2\right)$. The node displacements $X_{i,t}$ and $Y_{i,t}$ are independent normal random variables, consequently, so are the velocity components $V_{i,t}^{x}$ and $V_{i,t}^{y}$. Applying the change-of-variables formula, the random variable $V_{i,t} = \sqrt{\left(V_{i,t}^{x}\right)^2 + \left(V_{i,t}^{y}\right)^2}$ follows a Rayleigh distribution with parameter $\sqrt{2\alpha}/\Delta t$, i.e., $V_{i,t} \sim \text{Rayleigh}\left(\sqrt{2\alpha}/\Delta t\right)$.

3.2.3 Modeling the Position of the Nodes versus Modeling their Velocity

Another way to overcome the issue of the node velocity having an infinite variance is to model the node velocity directly by an OU process. In this scenario, the velocity components $V_{i,t}^{x}$ and $V_{i,t}^{y}$ are independent identical OU processes. The integrated Ornstein-Uhlenbeck process (IOU) will then describe the position of the node. If $X_{i,t}$ is the $x-$coordinate of node i at time t, it follows that

$$X_{i,t} = X_{i,0} + \int_0^t V_{i,s}^{x} \mathrm{d}s. \tag{3.12}$$

Fixing the initial condition $X_{i,0} = 0$, it follows that the distribution of $X_{i,t}$ is Gaussian with mean 0. Its variance is equal to

$$\mathbb{E}\left[X_{i,t}^2\right] = \int_0^t \int_0^t K_{X_i}(s,v)\,\mathrm{d}s\mathrm{d}v = \alpha \int_0^t \int_0^t e^{-|s-v|/\tau}\mathrm{d}s\mathrm{d}v = 2\alpha\tau^2\left(\frac{t}{\tau} + e^{-t/\tau} - 1\right). \quad (3.13)$$

It is straightforward from (3.13) that the variance of displacement $X_{i,t}$ depends on time t, and, as $t \to \infty$ the variance will go to infinity. Furthermore, the OU process $V_{i,t}$ posses the Markov property, whereas, the integrated OU process, $X_{i,t}$, does not [84]. For these reasons, and given that the instantaneous SNR directly depends on the distance between nodes (Eq. (3.1)), in the following, we choose to model the node displacements along the x and y coordinates by independent identical OU processes.

3.3 Statistical Properties of Mobile Networks Without Rayleigh Fading

In this Section, we derive the statistical properties of the link SNR when there is no small-scale fading affecting the link between nodes, i.e., $G_t = 1$ for $t \geq 0$. Neglecting the fading effects of the underlying wireless channel, the SNR simplifies to

$$N_t = \psi Z_t^{-\eta/2}. \quad (3.14)$$

Consequently, the connectivity probability can be written as $\mathbb{P}(Z_t \leq r_0^2)$, where $r_0 = (\psi/\rho_{th})^{\frac{1}{\eta}}$ defines the typical connection range and depends, through ψ, on several system parameters, such as the transmit power, wavelength, bandwidth,

and the noise power spectral density. Unless specified otherwise, we set $\psi = 1$ for analysis simplification. It will become apparent that the omission of this detail does not hinder the development of important results.

This model is also known as the hard connection model of link connectivity [85]. It states that nodes can communicate whenever they lie within some critical distance of each other. Hence, in this scenario, the statistical properties of the link SNR are completely determined by the squared distance between the two nodes.

3.3.1 Squared Distance Process

From the mobility model described in section 3.2.2, it follows that $\{X_t, t \geq 0\}$ and $\{Y_t, t \geq 0\}$ are two identical independent OU processes that satisfy the SDEs

$$\mathrm{d}X_t = -\frac{1}{\tau} X_t \mathrm{d}t + \sqrt{2D}\mathrm{d}W_t^x, \tag{3.15}$$

$$\mathrm{d}Y_t = -\frac{1}{\tau} Y_t \mathrm{d}t + \sqrt{2D}\mathrm{d}W_t^y, \tag{3.16}$$

where $\{W_t^x, t \geq 0\}$ and $\{W_t^y, t \geq 0\}$ are two independent standard Brownian motions. Using Itô's formula, (Theorem 4.1.2 in [79]), we can compute the SDEs of the squared stochastic processes as follows

$$\mathrm{d}X_t^2 = \left(2D - \frac{2}{\tau} X_t^2\right) \mathrm{d}t + 2\sqrt{2D} X_t \mathrm{d}W_t^x, \tag{3.17}$$

$$\mathrm{d}Y_t^2 = \left(2D - \frac{2}{\tau} Y_t^2\right) \mathrm{d}t + 2\sqrt{2D} Y_t \mathrm{d}W_t^y. \tag{3.18}$$

Then, we derive the SDE of the squared distance Z_t stated in the following proposition.

Proposition 1. *The stochastic differential equation of the squared distance Z_t between two nodes moving randomly in a two-dimensional plane according to indepen-*

dent identical OU processes with mobility parameters τ and D is

$$\mathrm{d}Z_t = p\left(\theta - Z_t\right)\mathrm{d}t + \sigma\sqrt{Z_t}\mathrm{d}W_t, \quad Z_0 = z_0, \tag{3.19}$$

where $p = 2/\tau$, $\theta = 2D\tau$, $\sigma = 2\sqrt{2D}$, W_t is a standard Brownian motion, and $z_0 \geq 0$ is the starting point of the process. The solution to this SDE exists, and is unique if $k, \theta > 0$. It is given by

$$Z_t = z_0 e^{-pt} + \theta\left(1 - e^{-pt}\right) + \sigma\int_0^t \sqrt{Z_u}e^{p(u-t)}\mathrm{d}W_u. \tag{3.20}$$

Proof See Appendix A.1. ■

The stochastic process Z_t solving (3.19) belongs to the Cox-Ingersoll-Ross (CIR) family of diffusions. They were first introduced in finance to model short-term interest rates [86]. By performing particular space-time changes, Z_t can be represented as a Bessel-squared process, $BESQ^{\delta}_{z_0}$, with dimension $\delta = 2$. The transition densities of Bessel-squared processes are known explicitly [87]; therefore, the transition density of Z_t can be determined precisely as follows.

Corollary 1. *The squared distance at time s, conditioned on its value at the current time t, follows a non-central chi-square distribution, $\chi^2\left[2z_s c; 2, 2z_t u\right]$, with 2 degrees of freedom and parameter of non-centrality $2z_t u$. Its transition pdf can be expressed as*

$$f_{Z_s|Z_t}\left(z_s|z_t\right) = ce^{-(z_s c + z_t u)}\mathrm{I}_0\left(2\sqrt{z_t u z_s c}\right), \tag{3.21}$$

where $c = \frac{1}{\theta\left(1-e^{-p(s-t)}\right)}$, $u = ce^{-p(s-t)}$, and I_0 is the modified Bessel function of the first kind with order zero.

Proof The result follows from a time-space transformation of the transition density

of the corresponding Bessel-squared process [87]. ■

The parameters p and θ influence the behavior of the process Z_t in several ways [88]. First, if $p, \theta > 0$, then (3.19) admits a unique solution. Second, if $2p\theta \geq \sigma^2$, the stochastic process Z_t is strictly positive for $t > 0$, and never hits zero [86, 89]. These conditions are always verified in our model for every value of τ and D. Therefore, Z_t is a mean-reverting diffusion process with speed of adjustment p and long-term average θ. Next, we make two remarks.

Remark 1. *If $p, \theta > 0$, then as $s \to \infty$ the conditional density will approach an exponential distribution, $f_{Z_\infty|Z_t}(z) \sim \text{Exp}(\theta)$, with mean and variance equal to θ and θ^2, respectively. The result follows by taking the limit for $s \to \infty$ of* (3.21).

Remark 2. *The stochastic process Z_t possesses the Markov property. The result follows from the fact that Z_t is a Bessel-squared process, and Bessel (squared) processes are Markov processes [87].*

We verify the validity of our theoretical analysis by running different simulations. In Fig. 3.3 we plot the conditional probability density of the squared distance $f_{Z_t|Z_0}(z_t|z_0)$ at time $t = 0.2$ s, whereas, in Fig. 3.4 we plot the same function but at time $t = 10$ s. To generate these plots, we fix the starting point of the squared distance process, Z_0, and then perform Monte Carlo simulations to estimate the conditional distribution function empirically. At the beginning of the simulations, $t = 0.2$ s, we observe that the conditional distribution follows a non-central chi-square distribution. Eventually, as time goes by, it approaches the limiting distribution.

Now, if the initial condition of the process, Z_0, is drawn according to the limiting distribution, then the process $\{Z_t, t \geq 0\}$ is stationary. Beginning with (3.21) and

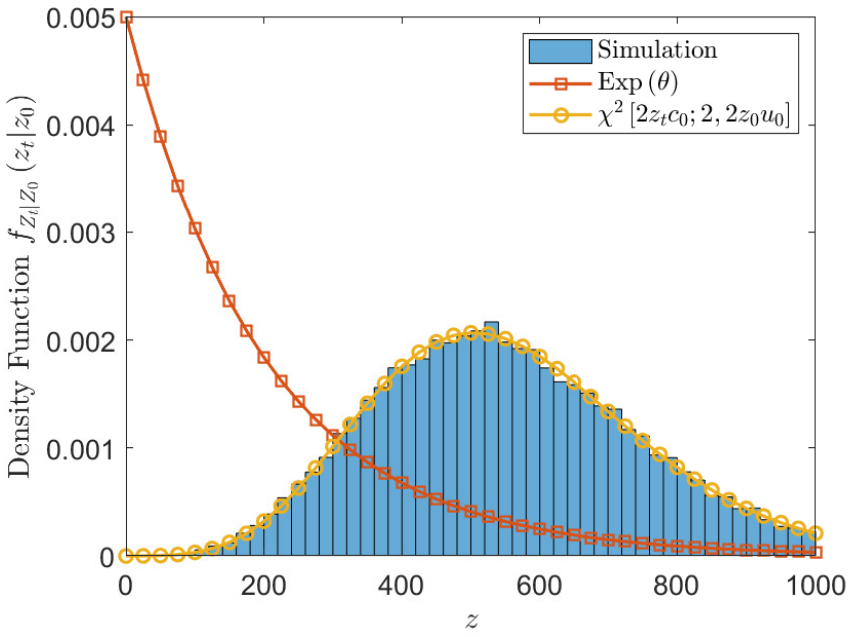

Figure 3.3: The conditional probability density of the squared distance $f_{Z_t|Z_0}(z_t|z_0)$ at time $t = 0.2$ s; mobility parameters $\tau = 1$ s and $D = 100$ m^2/s.

averaging over Z_0, the density function of the squared distance can be evaluated to yield the result stated in the following proposition.

Proposition 2. *At every time t, when the initial condition of the process Z_0 is drawn according to the limiting distribution, the squared pair distance, Z_t, is exponentially distributed. Its pdf can be written as*

$$f_{Z_t}(z) = \frac{1}{\theta} e^{-z/\theta}, \tag{3.22}$$

where $\theta = 2D\tau$.

Proof See Appendix A.2. ■

Equation (3.22) shows that $\{Z_t, t \geq 0\}$ is a stationary stochastic process, since its distribution does not depend on time t. Therefore, we can conclude that the squared

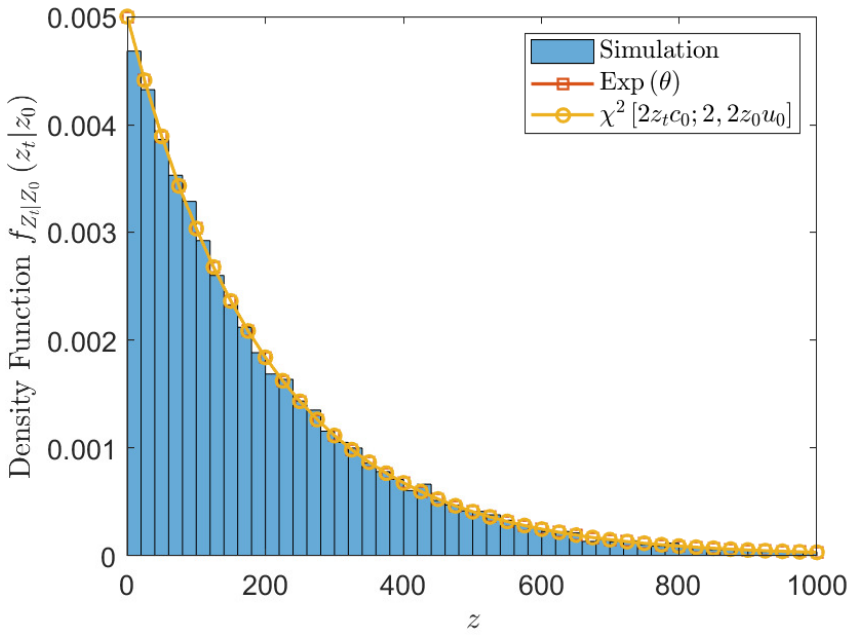

Figure 3.4: The conditional probability density of the squared distance $f_{Z_t|Z_0}(z_t|z_0)$ at time $t = 10$ s; mobility parameters $\tau = 1$s and $D = 100$ m^2/s.

pair distance forms a stationary Markov process with transition probability density given by (3.21), and steady-state pdf given by (3.22). The fact that the distribution of the squared distance converges to an exponential distribution comes from the properties of the OU model. Since the position coordinates are Gaussian, the squared distance will inevitably follow an exponential distribution. This property allows us to derive the pdf of the link SNR in (3.27) and the SDE of the link SNR in section 3.3.4. It is the first time in the literature that the stochastic differential equation of the link SNR in any scenario for any mobility or wireless channel model is reported. This is the most complete mathematical analysis reported in the literature proving that the distance process inherits the stationary and Markov properties of the OU process modeling node displacements along the x and y coordinates. As an example, in Fig. 3.5, we plot the pdf (3.22). It should be noted that in this figure the starting point of the process, Z_0, is drawn independently from the limiting distribution in

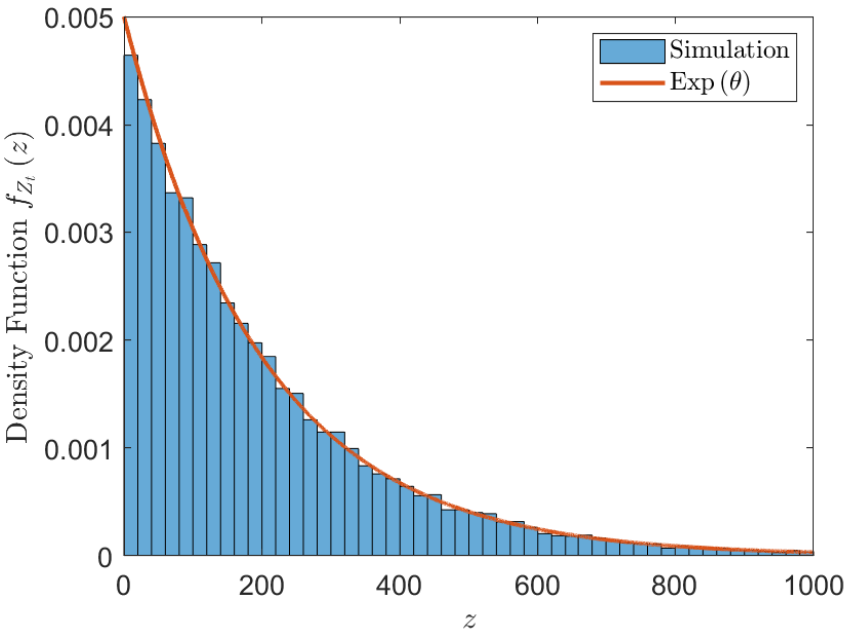

Figure 3.5: The probability density, $f_{Z_t}(z)$, of the squared distance at any time t; mobility parameters $\tau = 1$ s and $D = 100$ m^2/s.

each simulation trial. We observe an excellent agreement between the theoretical result and the Monte Carlo estimate.

3.3.2 Autocovariance Function

Another statistical property of interest is the stationary autocovariance function of the process $\{Z_t, t \geq 0\}$. It gives a measure of dependency of the random process to its delayed version, as a function of the time-lag, in the steady-state. Given that Z_t is stationary, this function depends only on the time shift $s - t = \Delta t$.

Proposition 3. *The stationary autocovariance function of the process* $\{Z_t, t \geq 0\}$ *is given by*

$$K_Z(\Delta t) = \theta^2 e^{-p\Delta t}, \tag{3.23}$$

where $p = 2/\tau$, *and* $\theta = 2D\tau$.

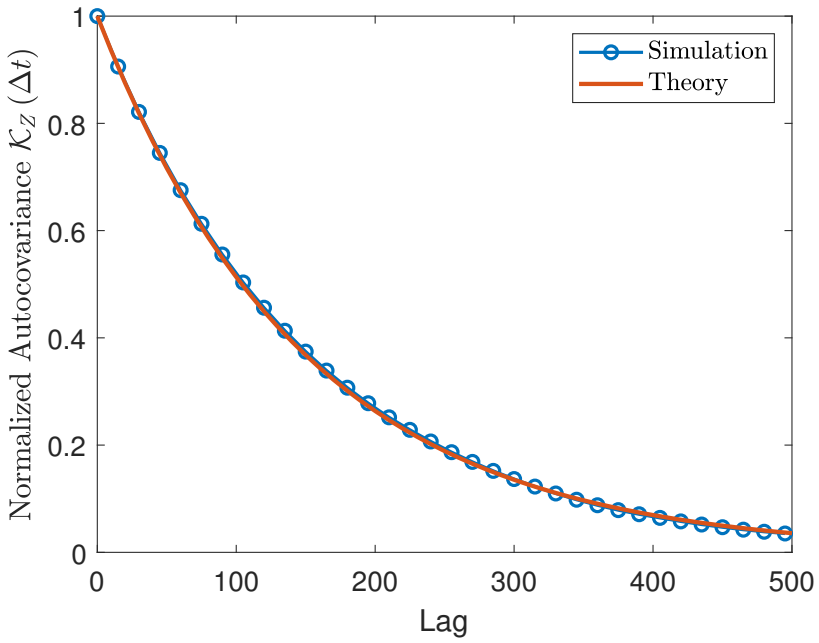

Figure 3.6: The normalized autocovariance function $\mathcal{K}_Z(\Delta t)$; $\Delta t = 0.0003$ s; Lag = number of time shifts Δt; mobility parameters $\tau = 0.1$ s and $D = 100$ m^2/s.

Proof See Appendix A.3. ■

This result implies that the autocovariance function tends toward zero as the time-lag increases. This is perfectly intuitive since an increase in time-lag would yield a decrease in the correlation of the random variables Z_s and Z_t. In Fig. 3.6 we plot the normalized autocovariance function $K_Z(\Delta t)$ versus the time-lag, and we observe how the autocovariance function decays exponentially with the time-lag.

Remark 3. *The stationary autocovariance function $K_Z(\Delta t)$ is proportional to the autocovariance function of the OU process $K_S(\Delta t)$ in* (3.7).

3.3.3 Distance Process

Here, we analyze the distance between nodes, $R_t = \sqrt{Z_t}$. From the theory of Bessel processes [87], the square root of $BESQ^{\delta}_{z_0}$ is also a Bessel process of dimension δ and starting point $r_0 = \sqrt{z_0}$.

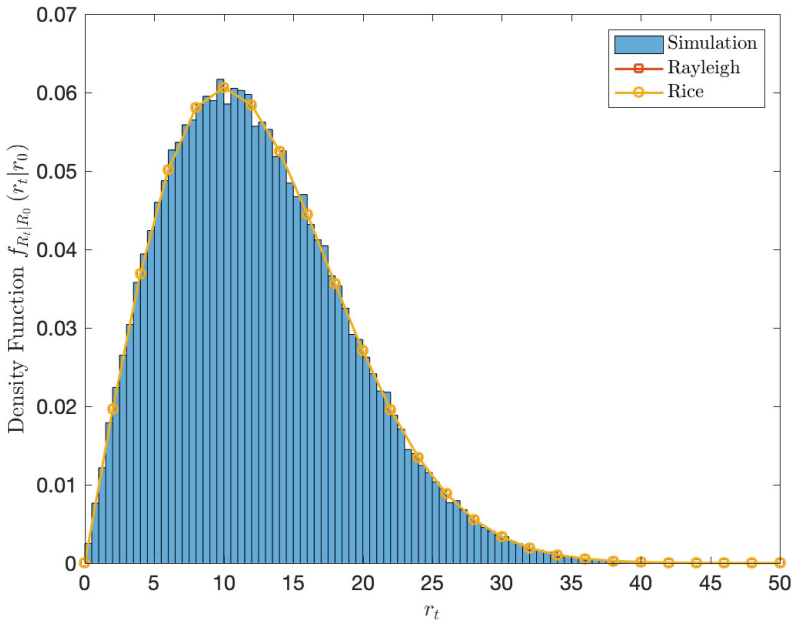

Figure 3.7: The conditional probability density of the distance $f_{R_t|R_0}(r_t|r_0)$ at time $t = 10$ s; mobility parameters $\tau = 1$ s and $D = 100$ m^2/s.

Corollary 2. *The transition probability density of the distance process R_t follows a Rice distribution, while its steady-state is Rayleigh distributed, i.e.,*

$$f_{R_s|R_t}(r_s|r_t) = \frac{r_s}{b^2} e^{\frac{-\left(r_s^2+r_t^2a^2\right)}{2b^2}} \mathrm{I}_0\left(\frac{r_s r_t a}{b^2}\right), \tag{3.24}$$

and

$$f_{R_t}(r) = \frac{2r}{\theta} e^{-r^2/\theta}, \tag{3.25}$$

respectively, with $\theta = 2D\tau$, $a^2 = u/c$, and $b^2 = 1/2c$.

Proof Apply the transformation of random variables $R_t = \sqrt{Z_t}$ and the result follows. ■

In Fig. 3.7 we plot the conditional probability density of the distance $f_{R_t|R_0}(r_t|r_0)$ for the particular time instance $t = 10$ s. In a similar fashion as for the squared distance,

we fix the starting point R_0 and then perform Monte Carlo simulations to estimate the conditional distribution function empirically. As expected, we observe the same behavior, i.e., at the beginning of the simulations, the conditional distribution follows a Rice distribution. Eventually, as time goes by, it approaches the steady-state which is Rayleigh distributed. To conclude, in a system where nodes move randomly in a two-dimensional plane according to an OU process, both the distance R_t and the squared distance Z_t form stationary Markov processes.

3.3.4 SNR Process

In the field of MANET, not much exploration has been done on the statistical analysis of the SNR, especially when the moving pattern is random. Authors in [27] obtained the pdf of the received SNR for two different mobility models, RWP and RD, in a Rayleigh fading channel. In [28], the outage probability and average bit error rate in a Nakagami-m fading environment with the RWP mobility model were derived, whereas in [46] the authors calculated the same quantities for the RD mobility model. In [47] the pdf of received power is obtained by combining the Pareto distribution due to unknown locations with log-normal shadowing. Statistics of the received signal power at the central base station in a cellular direct sequence code division multiple access system with Rayleigh fading is analyzed in [48]. However, the works above only describe the ergodic properties of the link SNR. To the best of the author's knowledge no attempt has been made to characterize the temporal evolution of the SNR and distance processes in networks subject to Rayleigh fading and random mobility. This will be the main focus of this section. In the following, we outline some of the major contributions:

- The stochastic differential equation of the link SNR N_t in mobile networks where nodes experience an OU mobility model in (3.26). This is a significant

result because we can directly simulate samples of the SNR by implementing this equation as, shown in Fig. 3.10. It is the first time in the literature that the stochastic differential equation of the link SNR in any scenario for any mobility or wireless channel model is reported.

- The bivariate density function of the link SNR in (3.30). This result is significant for stability issues because it tells us how links change over time. To derive this result, we used the Taylor expansion of the Bessel function and we solved the resulting integral.

Now, starting from the SDE of Z_t in (3.19) we will derive the SDE of N_t by applying Itô's formula, which enables us to find the differential of a scalar function of a stochastic process [79]. This formula is valid when the function is $\mathcal{C}^2$, i.e., it is twice differentiable. The SNR N_t is not $\mathcal{C}^2$ at the origin; but, in our system, Z_t never reaches zero for $t > 0$, and Z_0 is drawn according to the limiting distribution, i.e., $Z_0 \sim \text{Exp}(\theta)$. Therefore, since Z_t never hits the origin for $t \geq 0$, we can still apply Itô's formula and obtain the following result.

Proposition 4. *The stochastic differential equation of the link SNR N_t in mobile networks where nodes experience an OU mobility model is*

$$\mathrm{d}N_t = \left[\frac{p\eta}{2}N_t - \frac{p\theta\eta}{2}N_t^{1+2/\eta} + \frac{\sigma^2}{2}\frac{\eta}{2}\left(1+\frac{\eta}{2}\right)N_t^{1+2/\eta}\right]\mathrm{d}t - \frac{\sigma\eta}{2}N_t^{1+1/\eta}\mathrm{d}W_t, \quad (3.26)$$

where $N_0 = Z_0^{-\eta/2}$, $p = 2/\tau$, $\theta = 2D\tau$, $\sigma = 2\sqrt{2D}$, and W_t is a standard Brownian motion.

Proof See Appendix A.4. ■

Furthermore, starting from the distribution of the squared distance in (3.22), the pdf and the cdf of the SNR N_t at any time t can be determined precisely as follows.

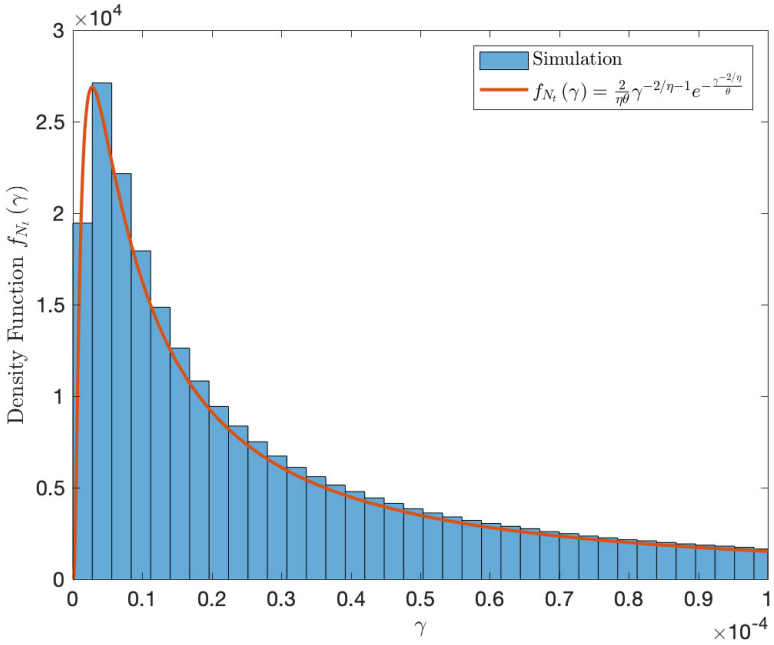

Figure 3.8: The probability density of the link SNR N_t for $\eta = 4$; mobility parameters $\tau = 1$ s and $D = 100$ m^2/s.

Corollary 3. *The density function of the link SNR is*

$$f_{N_t}(\rho) = \frac{2}{\eta\theta}\rho^{-2/\eta-1}e^{-\frac{\rho^{-2/\eta}}{\theta}}, \quad \rho > 0, \tag{3.27}$$

and its cumulative distribution is

$$F_{N_t}(\rho) = e^{-\frac{\rho^{-2/\eta}}{\theta}}, \tag{3.28}$$

where $\theta = 2D\tau$.

Proof To obtain the pdf, apply the principle of random variable transformation to (3.14) using (3.22) and the result follows. The cdf, instead, is obtained by integrating the pdf in (3.27). ■

To check the accuracy of the derived pdf in (3.27), in Fig. 3.8 we plot the pdf

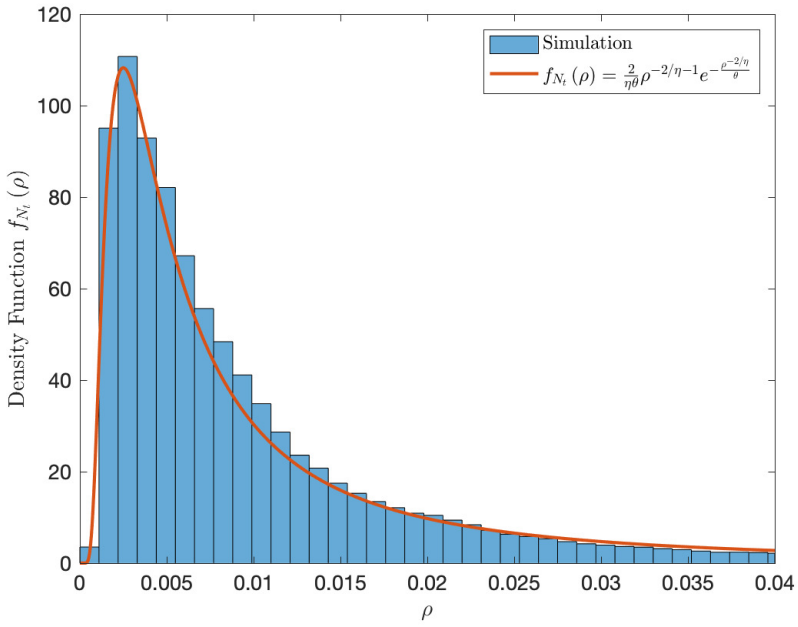

Figure 3.9: The probability density of the link SNR N_t for $\eta = 2$; mobility parameters $\tau = 1$s and $D = 100$ m^2/s.

of the link SNR for $\eta = 4$. We observe an excellent match between the theoretical result and the Monte Carlo simulation. It is important to note that the mean and the variance of the link SNR are undefined because the integral does not converge.

Eq. (3.26) provide a useful way to simulate values of the SNR N_t. In particular, we can simulate a discretized process $\{N_k, k \in \mathbb{N}\}$ for any time step $k = t_0 + k\Delta t$, $k \in \mathbb{N}$ and $\Delta t > 0$. The smaller the value of Δt, the closer our discretized path will be to the continuous-time path of (3.26). We perform numerical simulations to check the accuracy of the derived SDE. While there are a number of discretization schemes available to simulate the SDE in (3.26), we used the simplest and most common scheme, the Euler scheme [90]. In Fig. 3.9, we plot the density of the discretized path of the link SNR and the pdf in (3.27) when $\eta = 2$.

Understanding whenever the link SNR N_t is greater than some certain threshold is very important for connectivity issues. It determines if a successful communication

can be established between the two nodes. From (3.28), the probability that two nodes i and j are connected is given by

$$\mathbb{P}\left(N_t \geq \rho_{th}\right) = 1 - e^{-\frac{\rho_{th}^{-2/\eta}}{\theta}}. \tag{3.29}$$

From a system design perspective, this is a very important result, because it provides an explicit relation between the connectivity probability and various system parameters, such as the transmit power, wavelength, bandwidth, and the noise spectral density.

3.3.5 Bivariate Distribution of the Link SNR

In many situations, we may be interested in the future states of the link SNR. For instance, we may ask what is the probability that the link SNR is lower than some certain threshold for two different time instances. To that end, we derive the joint pdf and cdf of the link SNR random variables N_s and N_t, with $s > t$, as follows.

Proposition 5. *The bivariate cumulative distribution of the link SNR random variables N_s and N_t, $s > t$, is*

$$F_{N_s,N_t}\left(\rho_s, \rho_t\right) = \frac{1}{\theta} \sum_{j=0}^{\infty} \frac{u^j \gamma\left(j+1, c\rho_s^{-2/\eta}\right) \gamma\left(j+1, c\rho_t^{-2/\eta}\right)}{c^{j+1} j! \Gamma\left(j+1\right)}, \tag{3.30}$$

where $c = \frac{1}{\theta\left(1-e^{-p(s-t)}\right)}$, $u = ce^{-p(s-t)}$, $\Gamma\left(\cdot\right)$ is the gamma function, and $\gamma\left(a,x\right) = \int_x^{\infty} v^{a-1}e^{-v}\mathrm{d}v$ is the incomplete gamma function.

Proof See Appendix A.5. ■

Corollary 4. *The bivariate density function of the link SNR random variables N_s*

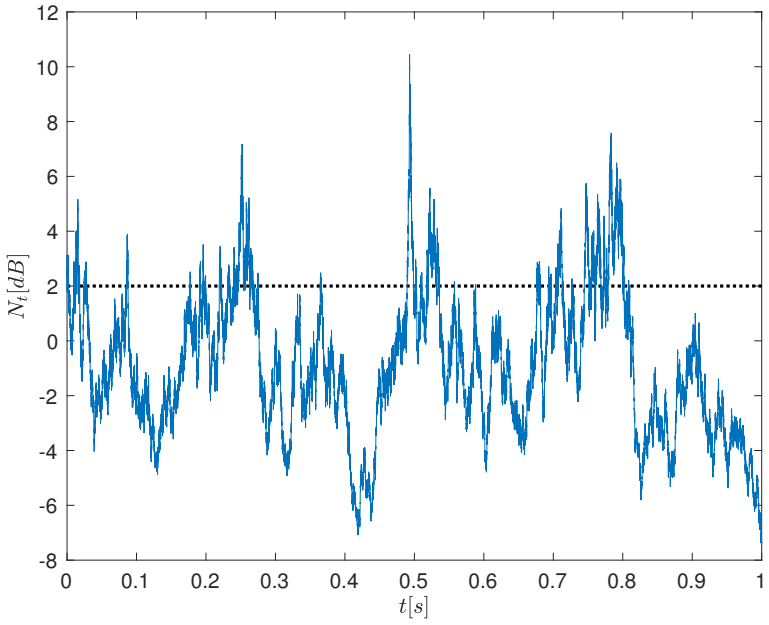

Figure 3.10: Simulation of a SNR path for $\eta = 2$ in mobile networks without fading; $\rho_{th} = 2$ dB; mobility parameters $\tau = 0.6$ s and $D = 4$ m^2/s.

and N_t, $s > t$, *is*

$$f_{N_s,N_t}(\rho_s,\rho_t) = \frac{4(\rho_s\rho_t)^{(-2-\eta)/\eta}}{\eta^2\theta}\sum_{j=0}^{\infty}\frac{u^j c^{j+1}}{j!\Gamma(j+1)}(\rho_s\rho_t)^{-2j/\eta}\, e^{-c\left(\rho_s^{-2/\eta}+\rho_t^{-2/\eta}\right)}, \quad (3.31)$$

where $c = \frac{1}{\theta\left(1-e^{-p(s-t)}\right)}$, $u = ce^{-p(s-t)}$, *and* $\Gamma(\cdot)$ *is the gamma function.*

Proof The result follows from differentiating the joint cumulative distribution function (3.30) with respect to ρ_s and ρ_t, i.e., $f_{N_s,N_t}(\rho_s,\rho_t) = \frac{\delta^2 F_{N_s,N_t}(\rho_s,\rho_t)}{\delta\rho_s\delta\rho_t}$. ■

Characterizing and managing the SNR variations users would see across mobile ad hoc networks is a challenging but important problem towards understanding network stability and connectivity. Therefore, the results derived in this section could be helpful to quantify the coverage and outage durations that each user will experience in the network. For instance, given an SNR threshold, as shown in Fig. 3.10, one

can characterize the temporal characteristics of the on/off level crossing process associated with the SNR being above and below a certain threshold, simply by simulating the discretized path of the link SNR in (3.26).

3.4 Statistical Properties of Mobile Networks subject to Rayleigh Fading

The diverse nature of radio channel causes a fundamental limitation on the performance of the mobile ad hoc networks. In this section, we generalize our analysis to take into account small-scale fading modeled by a Rayleigh random variable. Through this extension, the distribution of the link SNR depends both on the squared distance Z_t, which is governed by the mobility model, and the environmental factors controlling the channel between devices captured by G_t.

3.4.1 Distribution of the Link SNR for Rational path-loss Exponents

It is clear from (3.1) that the link SNR has a compound probability distribution, i.e., $N_t \sim \mathrm{Exp}\left(\Upsilon_t\right)$, where $\Upsilon_t = Z_t^{\eta/2}$. On that account, the unconditional density function of the link SNR can be evaluated to yield the result stated in the following proposition.

Proposition 6. *In a system where nodes move randomly according to an OU process and Rayleigh fading affects their connections, the pdf of the link SNR at any time t for rational path-loss exponents η is given by*

$$f_{N_t}\left(\rho\right) = \frac{2q}{p\theta} \frac{p^{\frac{3}{2}+\frac{p}{2q}}}{\sqrt{2q}} \left(2\pi\right)^{1-q-\frac{p}{2}} \theta^{1+\frac{p}{2q}} \times G_{p,2q}^{2q,p}\left(\left(\frac{\rho}{2q}\right)^{2q} (p\theta)^p \middle| \begin{matrix} \frac{2pq-2q-p}{2pq},\ldots,\frac{-p}{2pq} \\ 0,\ldots,\frac{2q-1}{2q} \end{matrix} \right), \quad \rho \geq 0, \quad (3.32)$$

where $G_{s,t}^{m,n}(z|\ {}^{u_1,\ldots,u_s}_{v_1,\ldots,v_t})$ *is the Meijer-G function,* $\theta = 2D\tau$*,* $p, q \in \mathbb{Z}^+$ *so that* $\eta = p/q$ *is a positive rational number.*

Proof See Appendix A.6. ■

Eq. (3.32) provides an explicit relation between the pdf of the link SNR, mobility parameters τ, D, and path-loss exponent η. A number of interesting points can be noted from this expression. First, it indicates that the link SNR $\{N_t, t \geq 0\}$ is a first-order stationary stochastic process, since its distribution does not depend on time t. Second, this is the most complete mathematical analysis of the distribution of the link SNR reported in the literature for a system subject to Rayleigh fading and OU Mobility accounting for rational path-loss exponent. Indeed, since the path-loss exponent is an experimentally estimated parameter, it is, by definition, rational in practice due to finite precision measurement equipment. Although the link SNR distribution is given in terms of the Meijer G function, it can be easily evaluated using numerical software such as Mathematica for any given inputs. It should be noted that (3.32) reduces to the following expressions for the special cases $\eta = 2$

$$f_{N_t}(\rho) = \frac{1}{\theta\left(\rho + 1/\theta\right)^2}, \quad \rho \geq 0, \tag{3.33}$$

and $\eta = 4$

$$f_{N_t}(\rho) = \frac{\sqrt{\pi} e^{1/4\rho\theta^2}\left(1 + 2\theta^2\rho\right)\mathrm{Erfc}\left(\frac{1}{2\theta\sqrt{\rho}}\right) - 2\theta\sqrt{\rho}}{4\theta^2\rho^{5/2}}, \tag{3.34}$$

where $\rho \geq 0$, and $\mathrm{Erfc}(x) = \frac{2}{\sqrt{\pi}}\int_x^\infty e^{-t^2}\mathrm{d}t$ is the complementary error function. However, for any other value of η, the expression given in proposition 6 is the most compact, accessible form. Eq. (3.33) corresponds to a shifted Pareto distribution with shape parameter 1 and scale parameter $1/\theta$. This is a heavy-tail distribution, with undefined mean and variance given that the shape parameter is equal to one.

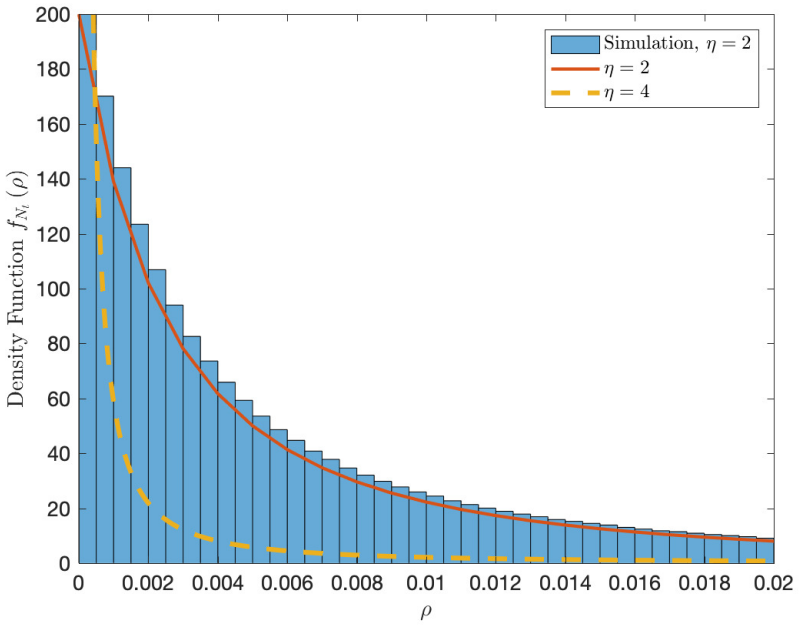

Figure 3.11: The probability density of the link SNR N_t for $\eta = 2$ and $\eta = 4$; Numerical simulation for $\eta = 2$; $\Delta t = 1$ s; mobility parameters $\tau = 1$ s and $D = 100$ m^2/s; channel parameter $\nu = 100$ Hz.

We perform numerical simulations to check the accuracy of the derived distribution formulae in (3.33) and in (3.34). In Fig. 3.11, we plot the pdf of the link SNR when $\eta = 2$. We observe an excellent agreement between the Monte Carlo result and the corresponding one from the mathematical analysis. In the same figure we also plot the pdf of the link SNR for $\eta = 4$, and we observe, as expected, a deterioration in the link SNR as η increases. The path-loss exponent η is an empirical parameter whose value is usually in the range of 2 to 6, where 2 is for the propagation in free space and $\eta > 2$ is for propagation in urban and suburban areas.

For the particular case $\eta = 2$, the cumulative distribution of the link SNR can be evaluated in closed-form by integrating (3.33)

$$F_{N_t}(\rho) = \frac{\rho\theta}{1 + \rho\theta}. \tag{3.35}$$

Then, the connectivity probability is given by

$$\mathbb{P}\left(N_t \geq \rho_{th}\right) = \frac{1}{1+\rho_{th}\theta}, \tag{3.36}$$

with $\theta = 2D\tau$. This is a significant result because it provides some insight to the relationship between the link connectivity probability, mobility parameters τ and D, and the SNR threshold ρ_{th}, which depends on the communication hardware, as well as the modulation and coding scheme of the wireless system.

3.4.2 Low SNR Regime

It is interesting to study the distribution of the received signal-noise-ratio in the low SNR regime, i.e., as the available SNR goes to 0. In this regime, either the transmission power is small or the bandwidth is large, leading to $\psi \to 0$. This can frequently happen when, for example, mobile nodes lie on the edge of the transmission range r_0. In such conditions, the system performance evaluation at low SNR is important to the system designers. On the other hand, there are scenarios where a low SNR regime might be desirable. For instance, low SNRs operations decrease the probability of intercept, as it is more difficult for an eavesdropper to detect signals [91].

In this regime, the link SNR also has a compound probability distribution, i.e., $N_t \sim \mathrm{Exp}\left(\Upsilon_t\right)$, with $\Upsilon_t = Z_t^{\eta/2}/\psi$. By the change-of-variables formula, the density function of parameter Υ_t is given by

$$f_{\Upsilon}\left(\upsilon\right) = \frac{2\psi^{2/\eta}}{\eta\theta}\upsilon^{2/\eta-1}e^{-\frac{\upsilon^{2/\eta}\psi^{2/\eta}}{\theta}}. \tag{3.37}$$

Considering the case when $\psi \to 0$, and retaining only the leading term, (3.37)

simplifies to

$$f_{\Upsilon}(\upsilon) = \frac{2\psi^{2/\eta}}{\eta\theta}\upsilon^{2/\eta-1} + O\left(\psi^{4/\eta}\right). \tag{3.38}$$

From this expression, we can develop the following lemma that gives the pdf of the link SNR at any time t in a low SNR regime.

Lemma 1. *As $\psi \to 0$, the probability density of the link SNR in ad hoc networks subject to OU mobility and Rayleigh fading in a low SNR regime, for any value of the path-loss exponents η, is equal to*

$$f_{N_t}(\rho) = \frac{2\psi^{2/\eta}}{\eta\theta}\Gamma\left(\frac{2+\eta}{\eta}\right)\rho^{-\frac{2+\eta}{\eta}} + O\left(\psi^{4/\eta}\right), \tag{3.39}$$

where $\Gamma(\cdot)$ is the gamma function, and $\theta = 2D\tau$.

Proof The result follows from solving the integral $f_{N_t}(\rho) = \int_0^\infty f_{N_t|\Upsilon_t}(\rho|\upsilon)\, f_{\Upsilon_t}(\upsilon)\, \mathrm{d}\upsilon$, where $f_{\Upsilon}(\upsilon)$ is given in (3.38) and $f_{N_t|\Upsilon_t}(\rho|\upsilon) = \upsilon e^{-\rho\upsilon}$. ■

It is straightforward from (3.39) to see that the distribution of the received signal-to-noise ratio in the low SNR regime follows a power law with undefined mean and variance. This behavior is also shown in Fig. 3.12, where we plot the density (3.39) in a log-log scale in the low SNR regime, $\psi = 0.01$, for different values of the path-loss exponent η. We observe a deterioration in the link SNR as η increases. On the other hand, in Fig. 3.13, we compare the distribution of the link SNR N_t in the normal regime, $\psi = 1$, versus the low SNR regime, $\psi = 0.01$, for $\eta = 4$.

Finally, the connectivity probability, in the low SNR regime, is given by

$$\mathbb{P}(N_t \geq \rho_{th}) = \frac{\psi^{2/\eta}}{\theta}\Gamma\left(\frac{2+\eta}{\eta}\right)\rho_{th}^{-2/\eta}. \tag{3.40}$$

This is an important result because it provides insights to the relationship between

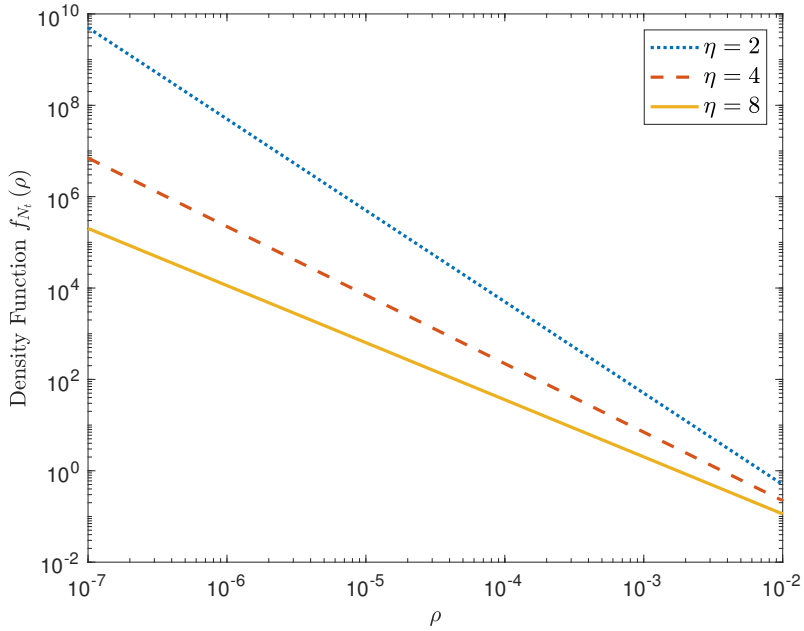

Figure 3.12: Log-Log scale plot of the probability density of the link SNR N_t in the low SNR regime, $\psi = 0.01$, for different values of the path-loss exponent η.

the link connectivity probability, mobility parameters τ and D, the SNR threshold ρ_{th}, and the path-loss exponent η in the low SNR regime. The macroscopic path-loss behavior has a direct impact on the link quality between the transmitter and receiver. The power of electromagnetic waves propagating in a wireless medium decreases according to the power law function of the distance between two nodes. In this function, the decaying rate is equal to the path-loss exponent η.

3.5 Summary

In this chapter, we derived closed-form expressions for the statistical properties of the link SNR and the separation distance in systems subject to Rayleigh Fading and Ornstein-Uhlenbeck Mobility. We started our analysis by first considering the case when there is no signal fading affecting the link between nodes. In this scenario, the statistical properties of the link SNR are entirely determined by the squared

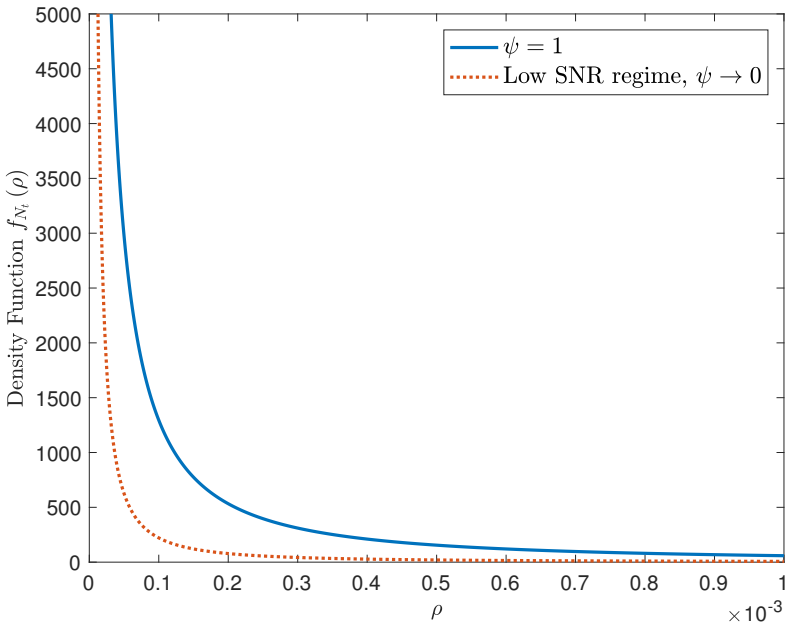

Figure 3.13: The comparison of the distribution of N_t in the normal regime, $\psi = 1$, versus the low SNR regime, $\psi = 0.01$, for $\eta = 4$.

distance between the two nodes. We provided a full statistical description of the squared distance process, including its distribution and autocorrelation function, and showed that it forms a stationary Markov process. Then, we derived closed-form expressions for the pdf, the cdf, the bivariate pdf, and the bivariate cdf of the link SNR. Next, we extended our analysis to take into account variations in the propagation channel (e.g., fading), and calculated the pdf of the link SNR for rational path-loss exponents η. To the best of our knowledge, this is the most complete mathematical analysis reported in the literature for the distribution of the link SNR in mobile wireless systems. Finally, we performed extensive simulations to check the accuracy of the proposed mathematical analysis. Our results provide useful insight and analytical tools that will be used to develop a framework to analyze link and network connectivity in systems subject to Rayleigh fading and Ornstein-Uhlenbeck mobility in chapter 4.

Appendix A

Chapter 3 Proofs

A.1 Proof of the stochastic differential equation of the squared distance process

From the mobility model described in section 3.2.2, We can write the SDE of the squared distance process Z_t as

$$\mathrm{d}Z_t = \mathrm{d}X_t^2 + \mathrm{d}Y_t^2, \tag{A.1}$$

where

$$\mathrm{d}X_t^2 = \left(2D - \frac{2}{\tau}X_t^2\right)\mathrm{d}t + 2\sqrt{2D}X_t\mathrm{d}W_t^x, \tag{A.2}$$

$$\mathrm{d}Y_t^2 = \left(2D - \frac{2}{\tau}Y_t^2\right)\mathrm{d}t + 2\sqrt{2D}Y_t\mathrm{d}W_t^y, \tag{A.3}$$

where $\{W_t^x, t \geq 0\}$ and $\{W_t^y, t \geq 0\}$ are two independent standard Brownian motions. Now, let

$$B_t = \int_0^t X_u\mathrm{d}W_u^x + Y_u\mathrm{d}W_u^y. \tag{A.4}$$

B_t is a stochastic integral with respect to a Brownian motion with quadratic variation given by

$$\langle B\rangle_t = \int_0^t \left[(X_u)^2 + (Y_u)^2\right] \mathrm{d}u = \int_0^t Z_u \mathrm{d}u. \tag{A.5}$$

Consequently, by Levy's characterization theorem (Theorem 8.6.1 in [79]), the stochastic process

$$W_t = \int_0^t \frac{1}{\sqrt{Z_u}} \left(X_u \mathrm{d}W_u^x + Y_u \mathrm{d}W_u^y\right) \tag{A.6}$$

is a standard Brownian motion. This enables one to write the SDE of Z_t as

$$\mathrm{d}Z_t = p\left(\theta - Z_t\right)\mathrm{d}t + \sigma\sqrt{Z_t}\mathrm{d}W_t, \quad Z_0 = z_0, \tag{A.7}$$

where $p = 2/\tau$, $\theta = 2D\tau$, $\sigma = 2\sqrt{2D}$, and Z_0 is the starting point of the process. To solve the SDE, we multiply both sides of (A.7) by e^{pt} and obtain

$$e^{pt}\mathrm{d}Z_t + pe^{pt}Z_t\mathrm{d}t = p\theta e^{pt}\mathrm{d}t + \sigma e^{pt}\sqrt{Z_t}\mathrm{d}W_t. \tag{A.8}$$

Applying the chain rule, $\mathrm{d}\left(Z_t e^{pt}\right) = e^{pt}\mathrm{d}Z_t + pe^{pt}Z_t\mathrm{d}t$, we can rewrite (A.8) as

$$\mathrm{d}\left(Z_t e^{pt}\right) = p\theta e^{pt}\mathrm{d}t + \sigma e^{pt}\sqrt{Z_t}\mathrm{d}W_t. \tag{A.9}$$

Integrating both sides over time interval $[0, t]$, and multiplying by e^{-pt}, the solution of the SDE is equal to

$$Z_t = z_0 e^{-pt} + \theta\left(1 - e^{-pt}\right) + \sigma\int_0^t \sqrt{Z_u}e^{p(u-t)}\mathrm{d}W_u. \tag{A.10}$$

A.2 Proof of the density function of the squared distance process

Here, we provide a brief outline for the derivation of the pdf expression in (3.22). Beginning with (3.21) and averaging over Z_0, we can write the density function as follows

$$f_{Z_t}(z_t) = \int_0^\infty f_{Z_t|Z_0}(z_t|z_0)\, f_{Z_0}(z_0)\, \mathrm{d}z_0. \tag{A.11}$$

Then, letting $Z_0 \sim Exp(\theta)$, i.e., the initial condition of the process is drawn according to the limiting distribution, we obtain

$$f_{Z_t}(z_t) = \int_0^\infty c_0 e^{-(z_t c_0 + z_0 u_0)} \mathrm{I}_0\left(2\sqrt{z_t u_0 z_0 c_0}\right) \frac{1}{\theta} e^{-z_0/\theta} \mathrm{d}z_0. \tag{A.12}$$

Now, $\mathrm{I}_0\left(2\sqrt{z_t u_0 z_0 c_0}\right)$ is the modified Bessel function of the first kind with order zero, and it is defined as

$$\mathrm{I}_0\left(2\sqrt{z_t u_0 z_0 c_0}\right) = \sum_{j=0}^{\infty} \frac{(z_t u_0 z_0 c_0)^j}{j!\Gamma(j+1)}. \tag{A.13}$$

Substituting (A.13) in (A.12) we obtain

$$\begin{aligned}
f_{Z_t}(z_t) =& c_0 e^{-z_t c_0} \frac{1}{\theta} \sum_{j=0}^{\infty} \frac{(z_t u_0 c_0)^j}{j!\Gamma(j+1)} \int_0^\infty e^{-z_0 u_0} z_0^j e^{-z_0/\theta} \mathrm{d}z_0 \\
=& \frac{c_0 e^{-z_t c_0}}{u_0\theta + 1} \sum_{j=0}^{\infty} \left(\frac{z_t u_0 c_0 \theta}{u_0\theta + 1}\right)^j \frac{1}{j!} \\
=& \frac{c_0}{u_0\theta + 1} e^{-\frac{z_t c_0}{u_0\theta + 1}} \\
=& \frac{1}{\theta} e^{-z_t/\theta},
\end{aligned} \tag{A.14}$$

where $c_0 = \frac{1}{\theta(1-e^{-pt})}$, $u_0 = ce^{-pt}$, and $\Gamma(\cdot)$ is the gamma function.

A.3 Proof of the autocovariance function of the squared distance process

In the following, we calculate the stationary autocovariance function of the process $\{Z_t, t \geq 0\}$. In this case, the autocorrelation function depends only on the time shift $s - t = \Delta t$, i.e.,

$$K_Z(\Delta t) = \mathbb{E}\{Z_s Z_t\} - \mu_Z^2, \tag{A.15}$$

where $\mu_Z = \theta$ is the stationary mean. Substituting (A.10) in (A.15), we obtain

$$K_Z(\Delta t) = \sigma^2 e^{-p(t+s)} \mathbb{E}\left\{\left(\int_0^t \sqrt{Z_u} e^{pu} \mathrm{d}W_u\right)^2\right\}. \tag{A.16}$$

Using the Itô isometry (Lemma 3.1.5 in [79]), the integral simplifies to

$$\mathbb{E}\left\{\left(\int_0^t \sqrt{Z_u} e^{pu} \mathrm{d}W_u\right)^2\right\} = \mathbb{E}\left\{\int_0^t Z_u e^{2pu} \mathrm{d}u\right\}. \tag{A.17}$$

As $t, s \to \infty$, the stationary autocovariance function simplifies to

$$K_z(\Delta t) = \theta^2 e^{-p\Delta t},$$

which has been shown in Proposition 3.

A.4 Proof of the stochastic differential equation of the link SNR

The squared distance process Z_t is an Itô process with stochastic differential equation given by (3.19). Now, let $N_t = g(t, Z_t) = Z_t^{-\eta/2}$. From Itô's formula (Theorem 4.1.2 in [79]), N_t is again an Itô process with SDE

$$\mathrm{d}N_t = \frac{\delta g}{\delta t}(t, Z_t)\,\mathrm{d}t + \frac{\delta g}{\delta z}(t, Z_t)\,\mathrm{d}Z_t + \frac{1}{2}\frac{\delta^2 g}{\delta z^2}(t, Z_t)\,(\mathrm{d}Z_t)^2,$$

where

$$\frac{\delta g}{\delta t}(t, Z_t) = 0, \quad \frac{\delta g}{\delta z}(t, Z_t) = -\frac{\eta}{2} Z_t^{-(\eta/2+1)}, \quad \frac{\delta^2 g}{\delta z^2}(t, Z_t) = \frac{\eta}{2}\left(\frac{\eta}{2}+1\right) Z_t^{-(\eta/2+2)},$$

and

$$(\mathrm{d}Z_t)^2 = \sigma^2 Z_t \mathrm{d}t.$$

A.5 Proof of the bivariate distribution of the link SNR

Here, we provide a brief outline for the derivation of the bivariate cumulative distribution function in (3.30).

$$\begin{aligned} F_{N_s,N_t}(\rho_s, \rho_t) &= \mathbb{P}(N_s \le \rho_s, N_t \le \rho_t) = \mathbb{P}\left(Z_s \ge \rho_s^{-2/\eta}, Z_t \ge \rho_t^{-2/\eta}\right) \\ &= \int_{z_t=\rho_t^{-2/\eta}}^{\infty} f_{Z_t} \int_{z_s=\rho_s^{-2/\eta}}^{\infty} f_{Z_s|Z_t} \mathrm{d}z_s \mathrm{d}z_t. \end{aligned} \tag{A.18}$$

Substituting (3.21) and (3.22) in (A.18), we obtain

$$\begin{aligned}
F_{N_s,N_t}\left(\rho_s,\rho_t\right) =& \int_{z_t=\rho_t^{-2/\eta}}^{\infty} \frac{1}{\theta} e^{-z_t/\theta} \int_{z_s=\rho_s^{-2/\eta}}^{\infty} c e^{-uz_t} e^{-cz_s} \sum_{j=0}^{\infty} \frac{u^j c^j z_t^j z_s^j}{j!\Gamma\left(j+1\right)} \mathrm{d}z_s \mathrm{d}z_t \\
=& \int_{z_t=\rho_t^{-2/\eta}}^{\infty} \frac{1}{\theta} e^{-z_t/\theta} e^{-uz_t} \sum_{j=0}^{\infty} \frac{u^j c^{j+1} z_t^j}{j!\Gamma\left(j+1\right)} \int_{z_s=\rho_s^{-2/\eta}}^{\infty} e^{-cz_s} z_s^j \mathrm{d}z_s \mathrm{d}z_t \\
=& \int_{z_t=\rho_t^{-2/\eta}}^{\infty} \frac{1}{\theta} e^{-z_t/\theta} e^{-uz_t} \sum_{j=0}^{\infty} \frac{u^j z_t^j}{j!\Gamma\left(j+1\right)} \gamma\left(j+1, c\rho_s^{-2/\eta}\right) \mathrm{d}z_t \\
=& \frac{1}{\theta} \sum_{j=0}^{\infty} \frac{u^j \gamma\left(j+1, c\rho_s^{-2/\eta}\right) \gamma\left(j+1, c\rho_t^{-2/\eta}\right)}{j! c^{j+1} \Gamma\left(j+1\right)},
\end{aligned}$$

where the first equality follows from the definition of $\mathrm{I}_0\left(2\sqrt{z_s u z_t c}\right)$, i.e., $\mathrm{I}_0\left(2\sqrt{z_s u z_t c}\right) = \sum_{j=0}^{\infty} \frac{(z_s u z_t c)^j}{j!\Gamma(j+1)}$.

A.6 Proof of the density function of the link SNR

Here, we provide a brief outline for the derivation of the pdf expression in (3.32). The conditional density function of N_t, given $\Upsilon_t = \upsilon$, is equal to

$$f_{N_t|\Upsilon_t}\left(\rho|\upsilon\right) = \upsilon e^{-\rho\upsilon}. \tag{A.19}$$

The unconditional distribution of the SNR results from marginalizing (A.19) over the random variable Υ_t, i.e.,

$$f_{N_t}\left(\rho\right) = \int_0^{\infty} f_{N_t|\Upsilon_t}\left(\rho|\upsilon\right) f_{\Upsilon_t}(\upsilon)\, \mathrm{d}\upsilon. \tag{A.20}$$

By the change-of-variables formula, the density function of Υ_t is given by

$$f_{\Upsilon}\left(\upsilon\right) = \frac{2}{\eta\theta} \upsilon^{2/\eta - 1} e^{-\frac{\upsilon^{2/\eta}}{\theta}}. \tag{A.21}$$

It follows that the stationary probability density of the process $\{N_t, t \geq 0\}$ is equal to

$$f_{N_t}(\rho) = \frac{2}{\eta\theta} \int_0^\infty \upsilon^{\frac{2}{\eta}} e^{-\rho\upsilon} e^{-\frac{\upsilon^{2/\eta}}{\theta}} \mathrm{d}\upsilon. \tag{A.22}$$

Given $\eta = p/q$ with p and q integers, we define

$$I(x) = \int_0^\infty t^{2q/p} e^{-xt} e^{-\frac{t^{2q/p}}{\theta}} \mathrm{d}t. \tag{A.23}$$

We use the Mellin-transform (MT) method for the exact calculation of the integral $I(x)$. We can get the Mellin transform as

$$\mathcal{M}\{I(x); s\} = \int_0^\infty t^{2q/p} e^{-\frac{t^{2q/p}}{\theta}} \left(\int_0^\infty x^{s-1} e^{-xt} \mathrm{d}x \right) \mathrm{d}t. \tag{A.24}$$

Next, we make the substitution $u = xt$ in the internal integral and obtain

$$\mathcal{M}\{I(x); s\} = \frac{p}{2q} \theta^{\frac{2q+p-ps}{2q}} \Gamma(s) \Gamma\left(\frac{2q+p-ps}{2q} \right), \tag{A.25}$$

for $0 < Re(s) < \frac{2q+p}{p}$. Then the inverse transform can be written as

$$I(x) = \frac{\theta^{\frac{2q+p}{2q}}}{2\pi i} \frac{p}{2q} \int_{\delta'-i\infty}^{\delta'+i\infty} \left(x\theta^{\frac{p}{2q}} \right)^{-s} \Gamma(s) \Gamma\left(1 + \frac{p}{2q} - \frac{ps}{2q} \right) \mathrm{d}s. \tag{A.26}$$

Given $p, q \in \mathbb{N}$, we make the substitution $s = 2qu$ and write

$$
\begin{aligned}
I(x) &= \frac{1}{2\pi i} \frac{p^{\frac{3}{2}+\frac{p}{2q}}}{\sqrt{2q}} (2\pi)^{1-q-\frac{p}{2}} \theta^{1+\frac{p}{2q}} \\
&\quad \times \int_{\delta'-i\infty}^{\delta'+i\infty} \left(\left(\frac{x}{2q} \right)^{2q} (p\theta)^p \right)^{-u} \prod_{n=0}^{2q-1} \Gamma\left(u + \frac{n}{2q} \right) \prod_{n=0}^{p-1} \Gamma\left(\frac{n+1}{p} + \frac{1}{2q} - u \right) \, \mathrm{d}u \\
&= \frac{p^{\frac{3}{2}+\frac{p}{2q}}}{\sqrt{2q}} (2\pi)^{1-q-\frac{p}{2}} \theta^{1+\frac{p}{2q}} G_{p,2q}^{2q,p}\left(\left(\frac{x}{2q} \right)^{2q} \left(\frac{p}{c_0} \right)^p \middle| \begin{matrix} \frac{2pq-2q-p}{2pq}, \ldots, \frac{-p}{2pq} \\ 0, \ldots, \frac{2q-1}{2q} \end{matrix} \right),
\end{aligned}
$$

where $G_{s,t}^{m,n}(z| \begin{smallmatrix} u_1,\ldots,u_s \\ v_1,\ldots,v_t \end{smallmatrix})$ denotes Meijer-G function, $0 < \delta' < \frac{2q+p}{p}$, and the first equality holds from the Gauss's multiplication formula for the gamma function.

Chapter 4

Entropy as a Measure of Topological Uncertainty

In this chapter, we propose an entropy-based metric that quantifies link uncertainty by taking full advantage of the correlation between the link current and future state. We exploit the statistics of the distance and the SNR processes presented in chapter 3 for the evaluation of this metric. Our formulation is based on a stationary Markov chain representation of link connectivity, enabling memory effects in network dynamics. The existence of a link between two nodes depends on their distance, which is governed by the mobility model, and the environmental factors controlling the radio channel between devices. We show that the stochastic process describing the state of the dynamic system is stationary. This result then enables us to derive simple bounds on the network entropy metric. Numerical results show that the proposed approach can accurately reflect the random variations in the network and fully captures the link dynamics. Thus, it may be considered a valuable performance metric for quantifying the topological uncertainty and connectivity in these networks.

4.1 Introduction

In this chapter, we present a detailed framework to analyze the evolution of the random topology of a time-varying wireless network via the information-theoretic notion of entropy rate. As discussed in section 2.6.3, the typical approach used in the literature to characterize the entropy of the mobile networks has been limited to the study of static network topologies. This approach has a fundamental limitation in the analysis of the evolution of the interactions, as it neglects the network's temporal properties. Hence, we believe the entropy rate can represent a more accurate stability metric in dynamic networks, considering its ability to measure the uncertainty of the future state of the link given its current state.

This chapter is divided into two main sections. In the first one, we analyze the impact of the small-scale fading on the link connectivity. We consider a static wireless network with Rayleigh fading affecting the connections between nodes. In this scenario, two important parameters affect link connectivity: the path-loss exponent and the maximum Doppler frequency. In the second section, we consider wireless mobile networks without Rayleigh fading. In the absence of small-scale fading, the only source of randomness in the link state is provided by the separation distance between nodes. In our analysis, nodes move randomly according to an Ornstein-Uhlenbeck process using one tuning parameter to obtain different levels of randomness in the mobility pattern. In both scenarios, we present conditions under which the link state can be approximated as a first-order Markov chain. We then model the network state as a stationary stochastic process, analyze its evolution via entropy rate, and finally, derive lower and upper bounds on the entropy rate of the wireless network.

4.2 System Model

We consider a wireless network of n nodes $\mathcal{V} = \{1, \ldots, n\}$ representing wireless devices located randomly in a a two-dimensional space $\mathcal{K}$ with finite volume and diameter D. We assume that the wireless devices are identical, have the same typical connection range r_0, and that these devices are present throughout the system's lifetime. Instead of observing the locations of the nodes continuously, we monitor them at regular time steps $t_k = t_0 + k\ \Delta t$, $k \in \mathbb{N}$ and $\Delta t > 0$. These time steps are finite and with an equal duration. The locations of the nodes at any time step t_k, $\mathbf{A}_k = (A_{i,k})_{i \in \mathcal{V}}$, are given by $A_{i,k} = (X_{i,k}; Y_{i,k})$. The random vector $\mathbf{R}_k = (R_{ij,k})_{i<j}$ collects the pair distances $R_{ij,k} = \|A_{j,t} - A_{i,k}\|$, at any time step t_k. Next, let $L_{ij,k}$ be a Bernoulli random variable that models the existence of the link (edge) between nodes i and j at any time step t_k. Then $\mathbf{L}_k = (L_{ij,k})_{i<j}$ captures the topological state of the wireless system at any time step t_k. In modeling the mobile radio channel, we refer to section 2.2. We assume that large-scale fading is only caused by the path-loss, neglecting the shadowing effect. We assume either that there is no small-scale fading or the small-scale fading is Rayleigh. We refer to section 3.2.2 to model the movement of the nodes. Each device movement is assumed to be independent from the others.

4.3 Static Wireless Networks Subject to Rayleigh Fading

In this section, we quantify the topological uncertainty in wireless networks due to the variations in the propagation channel via an entropy-based metric. Our model considers static nodes located randomly in $\mathcal{K}$, different bounding geometries (square, circle, triangle), Rayleigh fading affecting link connectivity, and moving scatterers.

In this scenario, the locations of the nodes are static, i.e., $\mathbf{A}_k = \mathbf{A}$, but they are independently and uniformly distributed in $\mathcal{K}$. The probability density function of the random vector $\mathbf{R} = (R_{ij})_{i<j}$ is given by $f_{\mathbf{R}}(\mathbf{r}) : [0, D]^{n(n-1)/2} \rightarrow [0, \infty)$. The geometry of the domain $\mathcal{K}$ defines the density $f_{R_{ij}}(r_{ij})$.

In such environments, a scatterer's movement will lead to perturbations of the static wireless channel. This is quite a general situation in outdoor settings with moving traffic or indoor environments with people walking, doors opening, etc [92]. Indoor radio propagation has been studied extensively to evaluate different transmission systems for application in wireless local area networks.

4.3.1 Wireless Local Area Network

A Wireless Local Area Network (WLAN) is a network that links two or more devices using wireless communication within a limited area such as a home, school, computer laboratory, campus, or office building. A typical WLAN consists of an Access Point (AP) and Several Stations (STAs) connected to this central AP. The IEEE 802.11 is the primary standard in use for WLAN in current real world implementation. It has two basic modes of operation: infrastructure and ad hoc mode. In infrastructure mode, communication to/from nodes is always carried over the APs. In ad hoc mode, the communication between two STAs can take place directly without the requirement of an AP. WLANs provide coverage up to an area of $50 - 100$ meters. The IEEE 802.11 uses a variety of physical layers to increase the aggregate throughput of the network. For instance, IEEE 802.11a and 802.11g are based on OFDM (Orthogonal Frequency Division Multiplexing), which significantly increases the AP's overall throughput.

4.3.2 Markov Model of Link Connectivity

The purpose of this section is to model the existence of a communication link between two nodes i and j at given locations as a two-state Markov chain. The transmission range of each node and the quality of the propagation channel jointly affect link connectivity. The key departure point is to treat the link state as a random process that exhibits random changes due to variations in the propagation channel. A transmission from node i to node j is successful if the received instantaneous SNR, $N_{ij,k}$, is greater than the SNR threshold $\rho_{th} = \psi/r_0^{\eta}$, where r_0 is the typical connection range. Given the pair distance $R_{ij} = r_{ij}$, the Bernoulli random variable $L_{ij,k}$ is equal to

$$L_{ij,k} = \begin{cases} 1, & \text{if } N_{ij,k} \geq \rho_{th}, \\ 0, & \text{otherwise}, \end{cases} \tag{4.1}$$

at any time step t_k. As described in section 2.4, in static wireless networks subject to Rayleigh fading the received instantaneous SNR follows an exponential distribution with time-invariant mean $\rho_0 = \psi r_{ij}^{-\eta}$, with ψ normalized to 1 for analysis simplification. Its pdf is given by

$$f_{N_{ij,k}}(\rho_{ij}) = \frac{1}{\rho_0} e^{-\rho_{ij}/\rho_0}, \quad \rho_{ij} \geq 0. \tag{4.2}$$

Then, the connectivity probability is obtained by integrating (4.2). Given the pair distance, it is equal to

$$\mathbb{P}\left(L_{ij,k} = 1 | R_{ij} = r_{ij}\right) = \mathbb{P}\left(N_{ij,k} \geq \rho_{th} | R_{ij} = r_{ij}\right) = e^{-\rho_{th}/\rho_0} = e^{-(r_{ij}/r_0)^{\eta}}. \tag{4.3}$$

Commonly, equation (4.3) is referred to as the pair connection function for nodes i and j [53].

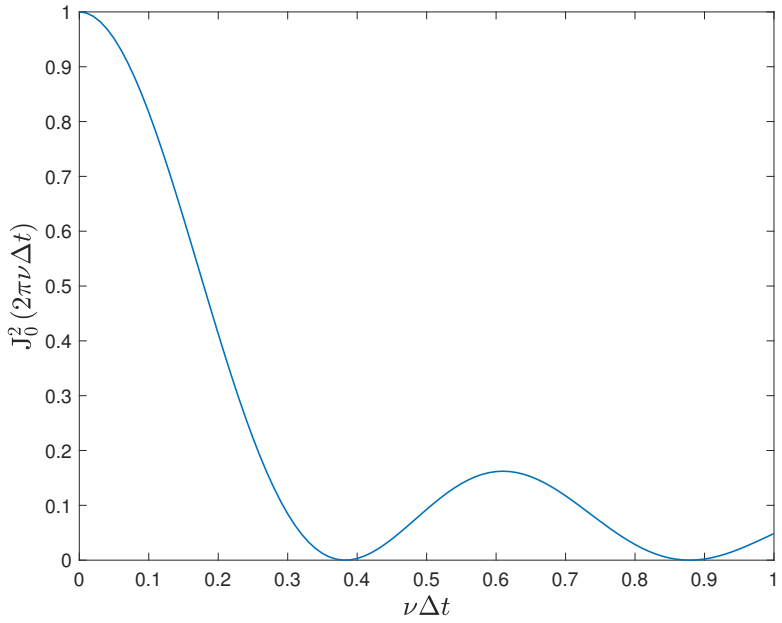

Figure 4.1: The normalized autocovariance function of the channel gain G_t.

The first-order Markov assumption implies that the conditional distribution of the link state $L_{ij,k}$ depends only on $L_{ij,k-1}$ and is independent of any other previous state. The sampling interval Δt controls the degree of memory in the channel gain stochastic process $\{G_{ij,k}, k \in \mathbb{N}\}$, and consequently in the link state evolution $\{L_{ij,k}, k \in \mathbb{N}\}$. In Fig. 4.1, we plot the correlation of $G_{ij,k}$ as a function of the product between the maximum Doppler shift ν_{ij} and the sampling interval Δt. There are several interesting observations from this plot. First we see that the autocorrelation function is equal to zero for $\nu_{ij}\Delta t \sim 0.4$. Next, we notice that the signal recorrelates after it becomes uncorrelated. Thus, we cannot assume that the signal remains independent from its initial value if $\nu_{ij}\Delta t > 0.4$. As a result, a Markov model is not completely accurate for Rayleigh fading because of this recorrelation property. However, in many systems, a correlation coefficient below 0.5 does not significantly degrade performance relative to uncorrelated fading [20, 21]. Consequently, we can

model the link process as Markov by assuming that once the fading correlation function falls below 0.5, the link state has become decorrelated with any other previous state. To that end, the sampling interval Δt must satisfy the following condition

$$\Delta t \geq \frac{0.18}{\nu_{ij}}. \tag{4.4}$$

Under this formalism, we can write

$$\mathbb{P}\left(L_{ij,k} = a | L_{ij,k-1} = b, L_{ij,k-2} = c, R_{ij} = r_{ij}\right) \simeq \mathbb{P}\left(L_{ij,k} = a | L_{ij,k-1} = b, R_{ij} = r_{ij}\right), \tag{4.5}$$

for all $a, b, c \in \{0, 1\}$ and any time step t_k.

As described in section 2.2.5, the transmitted wave is subject to the Doppler effect, i.e., a shift in the received frequency due to the movements of either the transmitter, the receiver, and/or external scatterers. In this section, we consider stationary terminals and moving scatterers. In such environments, a scatterer's movement will lead to perturbations of the static wireless channel. This is quite a general situation in outdoor settings with moving traffic or indoor environments with people walking, doors opening, etc. [92]. The maximum Doppler shift ν_{ij} typically lies between 1 Hz and 1 kHz [20]. In outdoor environments, vehicles' velocities range from 5 to 40 m/s [93]. Given a carrier frequency $f_c = 2.4$ GHz, then typical values of the maximum Doppler shift in outdoor settings lie between 40 Hz and 320 Hz. For indoor settings in presence of moving people, it was shown in [94] that the maximum Doppler shifts achievable in such environments is 40 Hz.

The fading characteristics of the channel are determined by the maximum Doppler frequency, ν_{ij}. The level crossing rate of the instantaneous received SNR is a mea-

sure of the rapidity of the fading. It quantifies how often the signal level crosses the threshold ρ_{th}, usually in the positive-going direction, and is defined as [95]

$$\mathrm{LCR}\left(\rho_{th}\right) = \sqrt{2\pi}\left(\frac{\rho_{th}}{\rho_0}\right)^{1/2} \nu_{ij}\ \mathrm{e}^{-\rho_{th}/\rho_0}. \tag{4.6}$$

Expressing the level crossing rate as a function of pair distance $R_{ij} = r_{ij}$, we obtain

$$\mathrm{LCR}\left(r_{ij}\right) = \sqrt{2\pi}\left(\frac{r_{ij}}{r_0}\right)^{\eta/2} \nu_{ij}\ \mathrm{e}^{-(r_{ij}/r_0)^{\eta}}. \tag{4.7}$$

The slow fading assumption, i.e., the Rayleigh fading channel is slow enough that the received SNR remains at a certain level for the time duration of a channel symbol, is crucial in our analysis. Under this assumption, the level crossing rate at ρ_{th} is much lower than the average number of symbols per second transmitted when the channel is in state "on" (a link exists) or "off" (a link does not exist). Hence, in a communication system with a transmission rate of B symbols per second, the state transition probability, conditioned on the pair distance R_{ij}, can be approximated as [95]

$$\mathbb{P}\left(L_{ij,k} = 1 - a | L_{ij,k-1} = a, R_{ij} = r_{ij}\right) \approx \frac{\mathrm{LCR}(r_{ij})}{\mathbb{P}\left(L_{ij,k-1} = a | R_{ij}\right) \times B} \tag{4.8}$$

for each $a \in \{0, 1\}$. To that end, conditioned on the pair distance, we can approximate the stochastic process $\{L_{ij,k}, k \in \mathbb{N}\}$ capturing the time evolution of the link between nodes i and j as a stationary Discrete Time Markov Chain (DTMC) with transition probabilities given by (4.8) and steady state probability by (4.3).

4.3.3 Link Entropy

Here, we introduce a metric based on the information-theoretic notion of entropy rate to evaluate the link uncertainty in static wireless ad hoc networks. The vari-

ations in the propagation channel due to moving scatterers produce a sequence of on-off links leading to frequently changing network connectivity. In our analysis, the link state evolution $\{L_{ij,k}, k \in \mathbb{N}\}$ is modeled as a stationary Markov chain, and from section 2.6.2 we know that its entropy rate is equal to the conditional entropy

$$H\left(L_{ij,2}|L_{ij,1}\right) = -\sum_{a\in\{0,1\}} \mathbb{P}\left(L_{ij,1}=a\right) \times \sum_{b\in\{0,1\}} \mathbb{P}\left(L_{ij,2}=b|L_{ij,1}=a\right) \log \mathbb{P}\left(L_{ij,2}=b|L_{ij,1}=a\right). \quad (4.9)$$

$\mathbb{P}\left(L_{ij}=a\right)$ is simply the probability that edge $i \leftrightarrow j$ exists ($a=1$) or not ($a=0$), averaged over the pair distance R_{ij}. More accurately, we can write

$$\mathbb{P}\left(L_{ij}=a\right) = \int_0^D \mathbb{P}\left(L_{ij}=a|R_{ij}=r_{ij}\right) f_{R_{ij}}\left(r_{ij}\right) \mathrm{d}r_{ij}, \quad (4.10)$$

where D is the diameter of the two-dimensional space $\mathcal{K}$. The geometry of the domain $\mathcal{K}$ defines the density $f_{R_{ij}}\left(r_{ij}\right)$. In the same fashion, $\mathbb{P}\left(L_{ij,2}=b|L_{ij,1}=a\right)$ is the link transition probability averaged over the pair distance, and is given by

$$\mathbb{P}\left(L_{ij,2}=b|L_{ij,1}=a\right) = \int_0^D \mathbb{P}\left(L_{ij,2}=b|L_{ij,1}=a, R_{ij}=r_{ij}\right) f_{R_{ij}}\left(r_{ij}\right) \mathrm{d}r_{ij}. \quad (4.11)$$

We can interpret the conditional entropy given in (4.9) as a measure of the uncertainty of the link's future state, given its current state. The transition probability, $\mathbb{P}\left(L_{ij,2}=a|L_{ij,1}=b\right)$, reflects the random changes in the propagation environment and fully captures the link dynamics. There are three important parameters in our model that affect link connectivity: the typical connection range r_0, the path-loss exponent η and the maximum Doppler frequency ν_{ij}. The level crossing rate $\mathrm{LCR}\left(r_{ij}\right)$ changes when at least one of these parameters changes influencing the value of ran-

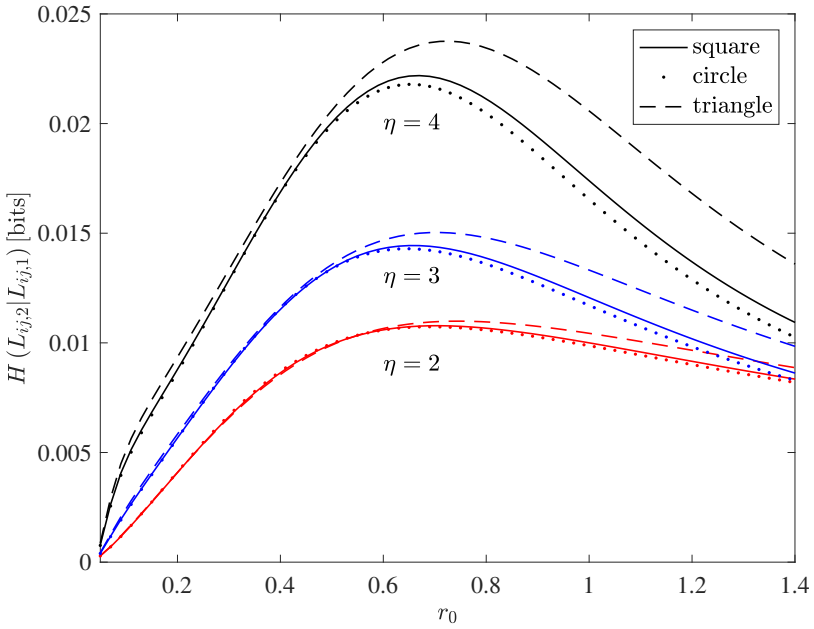

Figure 4.2: Numerical evaluation for the entropy rate $H\,(L_{ij,2}|L_{ij,1})$ versus the typical connection range ν_{ij}; bounding geometries: square of unit side length, circle of radius $1/\sqrt{\pi}$, and equilateral triangle of side length $2/\sqrt[4]{3}$; path-loss exponent values are $\eta = 2, 3, 4$; maximum Doppler frequency $\nu_{ij} = 200$ Hz.

dom variable $L_{ij,n}$, and therefore of $H\,(L_{ij,2}|L_{ij,1})$. Thus, the metric $H\,(L_{ij,2}|L_{ij,1})$ is a good approach to characterize the uncertainty due to the random variations in the propagation channel.

It is of fundamental interest to understand the impact of these variables on the uncertainty metric. Without a closed-form solution for the transition and steady state probabilities, we calculate the conditional entropy by numerically evaluating (4.10) and (4.11). We consider two nodes i and j embedded in unit area geometries, specifically, a square of unit side length, circle of radius $1/\sqrt{\pi}$, and equilateral triangle of side length $2/\sqrt[4]{3}$. The geometry of the domain $\mathcal{K}$ defines $f_{R_{ij}}\,(r_{ij})$. Analytic expressions for $f_{R_{ij}}\,(r_{ij})$ are known for simple, convex geometries [96, 97]. Before presenting the numerical results, we need to guarantee the assumptions of our model as stated in section 4.3.2. As noted before, we approximate the transition

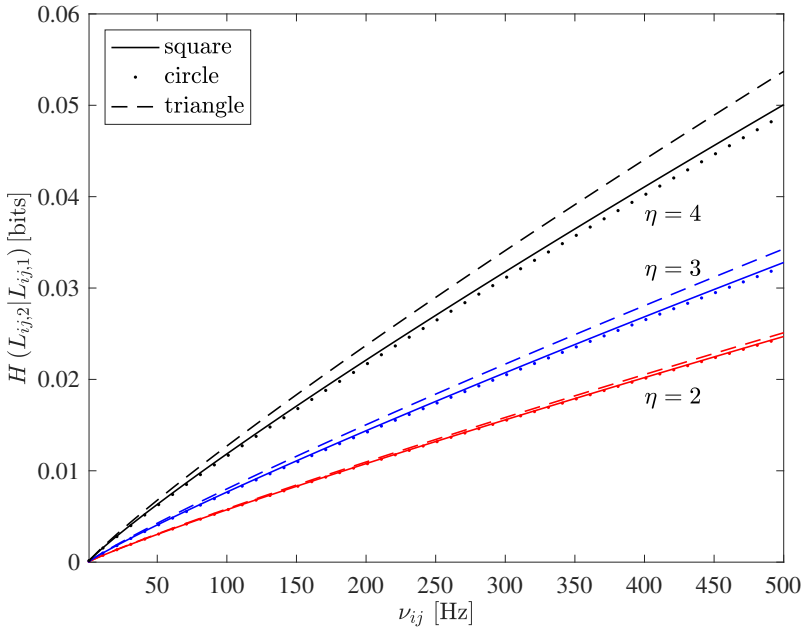

Figure 4.3: Numerical evaluation for the entropy rate $H\left(L_{ij,2}|L_{ij,1}\right)$ versus the maximum Doppler frequency ν_{ij}; bounding geometries: square of unit side length, circle of radius $1/\sqrt{\pi}$, and equilateral triangle of side length $2/\sqrt[4]{3}$; path-loss exponent values are $\eta = 2, 3, 4$; typical connection range $r_0 = 0.7$.

probabilities given in (4.11) under the slow fading assumption. If we take, for instance, a communication system using 802.11a protocols, the symbol rate is $B = 12$ MBd. This constraint restricts the values of the maximum Doppler frequency, path-loss exponent, and the typical connection range. These values should be carefully chosen to guarantee that (4.8) represents a valid probability distribution.

In Fig. 4.2 and in Fig. 4.3 we analyze the conditional entropy $H\left(L_{ij,2}|L_{ij,1}\right)$ for different bounding geometries. A few important things can be noted from these figures. First, we notice that for practical values of the Doppler frequency the link's dynamics can be quantified by very few bits. From section 2.6, we have that the maximum value for the conditional entropy of a Bernoulli random variable $L_{ij,k}$ is equal to one bit, i.e., $H\left(L_{ij,2}|L_{ij,1}\right) = H\left(L_{ij,2}\right) = 1$ bit. As expected, if the maximum Doppler frequency increases, the uncertainty in the link state slightly

increases. Doppler frequency is a measure for the rate of change of the channel. Second, the entropy decreases as $r_0 \to 0$ and $r_0 \to \infty$. Intuitively, one can recognize that when $r_0 \to \infty$ the probability that the communication link $i \leftrightarrow j$ is active tends to 1. On the contrary, when $r_0 \to 0$ this probability tends to 0. Next, we notice that impact of the path-loss exponent on the conditional entropy. The parameter η indicates how quickly a transmission is attenuated as it propagates through the wireless medium. It is usually taken to be $\eta = 2$ in free space and $\eta > 2$ in cluttered urban environments. As the path-loss exponent increases, the correlation between $L_{ij,2}$ and $L_{ij,1}$ gradually decreases, leading to higher conditional entropy. Fourth, it can be observed that when the nodes are randomly located inside a square or a circle, the geometry of the domain does not significantly affect the entropy rate. Whereas, choosing a triangle as the confining geometry has a non-negligible effect on it. Finally, for very soft connection functions (e.g., $\eta = 2$), there is little dependence upon the spatial embedding.

In conclusion, the transition probability, $\mathbb{P}\left(L_{ij,2} = a | L_{ij,1} = b\right)$, reflects the random changes in the propagation environment and fully captures the link dynamics. The entropy rate quantifies how quickly the link state is varying with time. So, a high entropy rate indicates that the link is frequently changing over time. Thus, the metric $H\left(L_{ij,2} | L_{ij,1}\right)$ can be considered a good approach to characterize the uncertainty in the link state due to the random variations in the propagation channel.

4.3.4 Network Entropy

In this section, we develop further our analysis to evaluate the topological unceratinty of a network composed of $\mathcal{V} = \{1, \ldots, n\}$, $n > 2$ nodes. We model a wireless ad hoc network at any time step t_k as an instance of a soft undirected random geometric graph $\mathcal{G}_k = (\mathcal{V}, \mathbf{L}_k)$, where $\mathbf{L}_k = (L_{ij,k})_{i<j}$. Soft random geo-

metric graphs (RGGs) are network structures consisting of a set of nodes placed according to a point process where the probability of two nodes being connected decays as a function of their Euclidean distance in order to consider signal fading [98, 99]. Examples of soft RGGs application include modeling the collective behavior of multi-robot swarms [100], electrical smart grid engineering [101] and ad hoc wireless networks [102, 103]. Consequently, a time-ordered sequence of RGGs, $\{\mathcal{G}_k, k \in \mathbb{N}\}$, represents the time-varying evolution of the wireless system with each graph corresponding to a snapshot of the network at any time step t_k. It is assumed that nodes are present throughout the lifetime of the system; that is, each graph has the same node set $\mathcal{V}$. Hence, the scope of this section is to analyze the evolution of the random topology of the time-varying wireless ad hoc network $\{\mathcal{G}_k, k \in \mathbb{N}\}$ via the information-theoretic notion of entropy rate.

We start from the assumption that the edge trajectories, $L_{ij,1}, \ldots, L_{ij,k}$, $\forall i < j$, conditioned on the pair distances, are independent. Then, we represent the evolution of each link $i \leftrightarrow j$, for $i, j \in \mathcal{V}$, as a stationary Markov chain, following the model explained in section 4.3.2. This enables us to write

$$\begin{aligned}\mathbb{P}\left(\mathbf{L}_1 = \mathbf{l}_1, \ldots, \mathbf{L}_k = \mathbf{l}_k | \mathbf{R} = \mathbf{r}\right) \\ = \prod_{i<j} \left[\prod_{u=2}^{k} \mathbb{P}\left(L_{ij,u} = l_{ij,u} | L_{ij,u-1} = l_{ij,u-1}, R_{ij} = r_{ij}\right) \right. \\ \left. \times \mathbb{P}\left(L_{ij,1} = l_{ij,1} | R_{ij} = r_{ij}\right) \right] \quad (4.12)\end{aligned}$$

for each $\mathbf{l}_u \in \{0,1\}^{n(n-1)/2}, u = 1, \ldots, k$ and $\mathbf{r} \in [0, D]^{n(n-1)/2}$. The equality follows from the chain rule. Therefore, the joint pdf of the network state variables is

obtained by averaging eq. (4.12) over the pair distances, i.e.,

$$\mathbb{P}\left(\mathbf{L}_1 = \mathbf{l}_1, \ldots, \mathbf{L}_k = \mathbf{l}_k\right) = \int_{\mathcal{R}} \mathbb{P}\left(\mathbf{L}_1 = \mathbf{l}_1, \ldots, \mathbf{L}_k = \mathbf{l}_k | \mathbf{R} = \mathbf{r}\right) f_{\mathbf{R}}(\mathbf{r}) \mathrm{d}\mathbf{r}, \tag{4.13}$$

where the integration domain is $\mathcal{R} = [0, D]^{n(n-1)/2}$. After averaging, the resulting stochastic process $\mathbf{L}_k$ does not possess the Markov property. On the contrary, $\mathbf{L}_k$ inherits the stationary property, i.e., the joint distribution of any subset of the sequence of the random variables is invariant to shifts in the time index [51].

From section 2.6.2 we have that the entropy rate of the stationary stochastic process $\mathbf{L}_k = (L_{ij,k})_{i<j}$ is equal to

$$H\left(\mathcal{L}\right) = \lim_{k \to \infty} \frac{H\left(\mathbf{L}_1, \ldots, \mathbf{L}_k\right)}{k}. \tag{4.14}$$

In the next section, we analyze the maximum and minimum value that the network entropy can take.

4.3.4.1 Minimum and Maximum Value of Network Entropy

Evaluation of the joint entropy in equation (4.14) requires the joint probability distribution function $f_{\mathbf{R}}(\mathbf{r})$ of pair distances. However, expressions are not available for $v > 2$ when nodes are confined inside a triangle/square. For $v = 3$ expressions are available if nodes are confined in a circle [104]. For these reasons, we resort to bounding the entropy rate of the random geometric graph $\mathcal{G}_k = (\mathcal{V}, \mathbf{L}_k)$.

What are the minimum and maximum value that the network entropy can attain? Coon derived an upper bound on the graph entropy in [53] for a static network. The author used the fact that the distribution of the graph is equivalent to the distribution of the edge set. Let $L_{ij,k}$ denote a Bernoulli random variable that

models the existence (or not) of edge $i \leftrightarrow j$. Formally,

$$L_{ij,k} = \begin{cases} 1, & \text{with probability } p \\ 0, & \text{with probability } 1-p. \end{cases} \tag{4.15}$$

Using Coon's result in [53], we can write

$$H\left(\mathbf{L}_1, \ldots, \mathbf{L}_k\right) \leq \sum_{i<j} kH\left(L_{ij,1}\right), \tag{4.16}$$

which leads to

$$H\left(\mathcal{L}\right) \leq \binom{n}{2} H\left(L_{ij,1}\right), \tag{4.17}$$

where the equality holds only if $\left(L_{ij,1}\right)_{i<j}$ are independent. From an information-theoretic perspective, the entropy measures the average number of bits required to describe the random variable $L_{ij,k}$. The link entropy is defined as

$$H(L_{ij,1}) = -p \log p - (1-p) \log(1-p) = H(p), \tag{4.18}$$

where

$$p = \mathbb{P}\left(L_{ij} = 1\right) = \int_0^D \mathbb{P}\left(L_{ij} = 1 | R_{ij} = r_{ij}\right) f_{R_{ij}}\left(r_{ij}\right) \mathrm{d}r_{ij} \tag{4.19}$$

In Fig. 4.4 we plot the graph of the function $H(p)$. This figures illustrates some of the basic properties of the entropy such as entropy is greater or equal to zero, and the entropy is at most one bit. For instance, it reaches its highest value $H(p) = 1$ bit when $p = 1/2$, and equals 0 when $p = 0$ or 1. This makes sense because the uncertainty is maximum for $p = 1/2$, and there is no uncertainty when $p = 0$ or 1. Consequently, the minimum and maximum values that the network entropy can

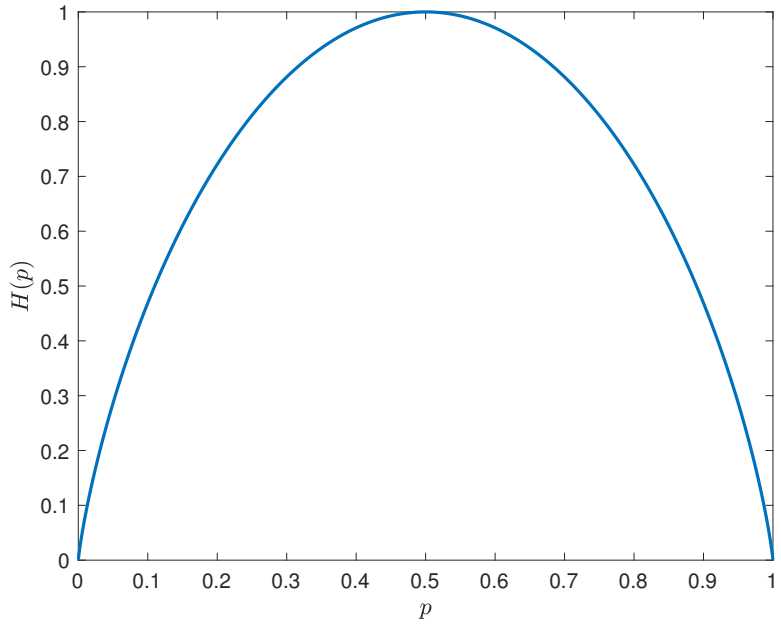

Figure 4.4: $H(p)$ versus p.

take are

$$0 \leq H\left(\mathcal{L}\right) \leq \binom{n}{2} H\left(L_{ij,1}\right) \leq \binom{n}{2}. \tag{4.20}$$

In the large n limit the upper bound on the entropy rate scales like $\mathcal{O}\left(n^2\right)$ for a network composed of n nodes.

Can we do better than this? In the next sections, we make progress by deriving a tighter lower and a tighter upper bound on the entropy rate of the dynamical system. This result is presented in equation (4.30). We will show how the value of the network entropy $H\left(\mathcal{L}\right)$ can actually be much less than this maximum $\binom{n}{2}$ bits because of the correlation in the link state from one time step to the next, which is induced by the Rayleigh fading.

4.3.4.2 Tighter Upper Bound on the Entropy Rate

In the following, we consider the trajectories of individual links, i.e., $L_{ij,1}, \ldots, L_{ij,k}$, $\forall i < j$. For any time step t_k, we can write

$$H\left(\mathbf{L}_1, \ldots, \mathbf{L}_k\right) \leq \sum_{i<j} H\left(L_{ij,1}, \ldots, L_{ij,k}\right), \tag{4.21}$$

where the inequality follows from the subadditivity property of the entropy, i.e., the joint entropy cannot be greater than the sum of the entropies of disjoint subsets of variables. Equality holds if and only if $\left(L_{ij,k}\right)_{i<j}$ are independent. Next, by the chain rule, it follows that

$$H\left(\mathbf{L}_1, \ldots, \mathbf{L}_k\right) \leq \sum_{i<j} \left[\sum_{u=2}^{k} H\left(L_{ij,u} | L_{ij,u-1}, \ldots, L_{ij,1}\right) + H\left(L_{ij,1}\right)\right]. \tag{4.22}$$

The link state evolution $\{L_{ij,k}, k \in \mathbb{N}\}$ forms a stationary Markov chain. Hence, we can write

$$\begin{aligned} H\left(\mathbf{L}_1, \ldots, \mathbf{L}_k\right) &\leq \sum_{i<j} \left[\sum_{u=2}^{k} H\left(L_{ij,u} | L_{ij,u-1}\right) + H\left(L_{ij,1}\right)\right] \\ &= \sum_{i<j} \left[(k-1) H\left(L_{ij,2} | L_{ij,1}\right) + H\left(L_{ij,1}\right)\right], \end{aligned} \tag{4.23}$$

where the second equality follows from the stationary property of the stochastic process $\mathbf{L}_k = (L_{ij,k})_{i<j}$. Dividing by k and taking the limit $k \to \infty$, and by using eqs. (4.14) and (4.23), we arrive at the entropy rate relation

$$H\left(\mathcal{L}\right) \leq \sum_{i<j} H\left(L_{ij,2} | L_{ij,1}\right). \tag{4.24}$$

It is straightforward to notice that the steady state probabilities given in (4.10) are equal for different links, i.e., $\mathbb{P}(L_{ij} = a) = \mathbb{P}(L_{kl} = a)$ for $(k, l) \neq (i, j)$. Similarly, it is clear from eqs. (4.8) and (4.11) that when different links have equal maximum Doppler frequencies they will also have equal transition probabilities. Assuming that the maximum Doppler frequencies of different links are equal, i.e., $\nu_{ij} = \nu_{kl} = \nu$, the upper bound on the entropy rate simplifies to

$$H(\mathcal{L}) \leq \binom{n}{2} H(L_{ij,2}|L_{ij,1}). \tag{4.25}$$

The conditional entropy satisfies the following property $H(L_{ij,2}|L_{ij,1}) \leq H(L_{ij,2})$. Equality holds if and only if the random variables $L_{ij,2}$ and $L_{ij,1}$ are independent. We then have

$$0 \leq H(\mathcal{L}) \leq \binom{n}{2} H(L_{ij,2}|L_{ij,1}) \leq \binom{n}{2} H(L_{ij,2}) \leq \binom{n}{2}. \tag{4.26}$$

In the large n limit, the upper bound on the entropy rate scales like $\mathcal{O}(n^2)$ for a network composed of n nodes. In our numerical results, we will show how the value of the network entropy $H(\mathcal{L})$ can be much less than this maximum $\binom{n}{2}$ bits because of the correlation in the link state from one time step to the next. This is because the Rayleigh fading channel is correlated, which induces the correlation of the link state.

4.3.4.3 Tighter Lower Bound on the Entropy Rate

To enable us to find a lower bound on the entropy rate of the soft undirected random geometric graph $\mathcal{G}_k = (\mathcal{V}, \mathbf{L}_k)$ evolving over time, we turn to the information-theoretic notion of conditional entropy, presented in section 2.6. Conditioning re-

duces entropy, hence, we can write

$$H\left(\mathbf{L}_1, \mathbf{L}_2, \ldots, \mathbf{L}_k\right) \geq H\left(\mathbf{L}_1, \mathbf{L}_2, \ldots, \mathbf{L}_k | \mathbf{R}\right). \tag{4.27}$$

Conditioned on pair distances, the link trajectories are independent, and each of them is a stationary Markov chain. This naturally leads to the following entropy relation

$$H\left(\mathbf{L}_1, \mathbf{L}_2, \ldots, \mathbf{L}_k\right) \geq \sum_{i<j} \left[(k-1) H\left(L_{ij,2} | L_{ij,1}, R_{ij}\right) + H\left(L_{ij,1} | R_{ij}\right)\right]. \tag{4.28}$$

Equivalently, combining the arguments employed in eq. (4.24) with the assumption made in eq. (4.44), we obtain

$$H(\mathcal{L}) \geq \binom{n}{2} H\left(L_{ij,2} | L_{ij,1}, R_{ij}\right), \tag{4.29}$$

where

$$H\left(L_{ij,2} | L_{ij,1}, R_{ij}\right) = -\int_0^D f_{R_{ij}}(r_{ij}) \sum_{a \in \{0,1\}} \mathbb{P}\left(L_{ij,1} = a | R_{ij} = r_{ij}\right)$$
$$\times \sum_{b \in \{0,1\}} \left[\mathbb{P}\left(L_{ij,2} = b | L_{ij,1} = a, R_{ij} = r_{ij}\right) \times \log \mathbb{P}\left(L_{ij,2} = b | L_{ij,1} = a, R_{ij} = r_{ij}\right)\right] \mathrm{d}r_{ij}.$$

Hence, to evaluate the lower bound, we assume prior knowledge of the node locations and average the entropy rate over the spatial distribution. Putting together eqs. (4.44), and (4.29) manifests in the relation

$$0 \leq \binom{n}{2} H\left(L_{ij,2} | L_{ij,1}, R_{ij}\right) \leq H(\mathcal{L}) \leq \binom{n}{2} H\left(L_{ij,2} | L_{ij,1}\right) \leq \binom{n}{2}. \tag{4.30}$$

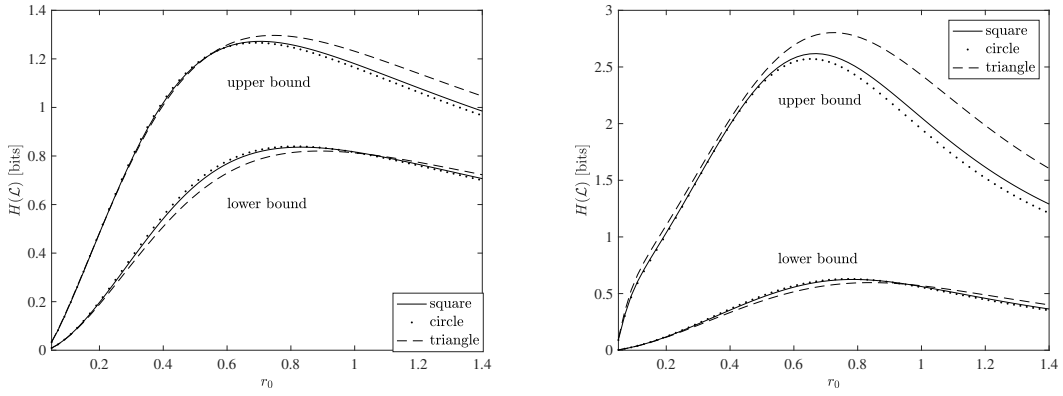

(a) $\eta = 2$ **(b)** $\eta = 4$

Figure 4.5: Numerical evaluation for the bounds on the entropy rate of a twenty-node RGG versus the typical connection range r_0; bounding geometries: square of unit side length, circle of radius $1/\sqrt{\pi}$, and equilateral triangle of side length $2/\sqrt[4]{3}$; maximum Doppler frequency $\nu = 200$ Hz.

Hence, in this section we calculated a tighter lower and upper bound on the entropy rate of the dynamical system.

We now study the entropy bounds derived in (4.30). To this end, in Fig. 4.5 and in Fig. 4.6, we investigate the impact of the path-loss exponent, the maximum Doppler frequency, and typical connection range on the entropy rate of a twenty-node random geometric graph, for different bounding geometries. The increase in the upper bound and the reduction in lower bound for increasing "hardness" in the connection function (4.3) is evident in these figures. Mathematically, the parameter η controls the stretch of the decaying exponential. For $\eta \to \infty$, we recover the hard connection model. In the case of the lower bound, as we increase η, the pairwise uncertainty (and consequently the conditional entropy) decreases [105]. Clearly, as $\eta \to \infty$ the lower bound tends to zero, but the upper bound on entropy rate $H(\mathcal{L})$ is still $\mathcal{O}(n^2)$.

In this scenario, the maximum value that the network entropy $H(\mathcal{L})$ can take is $\binom{20}{2} = 190$ bits. Instead, we notice from Fig. 4.5, and Fig. 4.6 that for practical

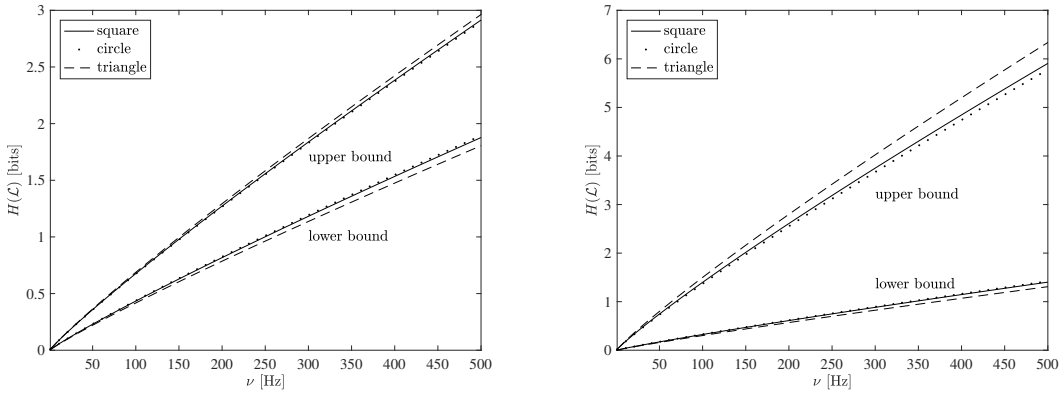

(a) $\eta = 2$ **(b)** $\eta = 4$

Figure 4.6: Numerical evaluation for the bounds on the entropy rate of a twenty-node RGG versus the path-loss exponent η; bounding geometries: square of unit side length, circle of radius $1/\sqrt{\pi}$, and equilateral triangle of side length $2/\sqrt[4]{3}$; typical connection range $r_0 = 0.7$.

values of the Doppler frequency the system's dynamics is quantified by less than 7 bits, $H(\mathcal{L}) < 7$ bits. This is due to the correlation in the link state from one time step to the next induced by the Rayleigh fading. Finally, as $r_0 \to \infty$ the network is completely connected (a complete graph), and as $r_0 \to 0$ the network is completely disconnected; hence the topological uncertainty tends to zero.

The entropy rate quantifies how quickly the underlying topology is varying with time. So, a high entropy rate indicates that the network topology is frequently changing over time. Thus, the metric $H(\mathcal{L})$ can be considered a good approach to quantitatively characterize the complexity and topological uncertainty of wireless ad hoc networks due to the random variations in the propagation channel.

4.3.5 A Note on Entropy Growth

Analytically, we can deduce from (4.46) that the upper bound grows like $\mathcal{O}(n^2)$ if all other system parameters are held constant. Intuitively, the addition of a node to the network increases the number of communication links (by one less than the

total number of nodes), which will in turn increase the uncertainty in the network topology. From a fundamental perspective, unbounded network uncertainty may be undesirable. To lend an operational interpretation for wireless networks, consider the unchecked evolution of the Internet of Things, where mesh topologies are employed for reliability and coverage purposes. With node densities set to exceed one connection per square meter in the not-too-distant future, it is easy to imagine the case where complexity even on a local scale becomes unmanageable. In this context, the entropy rate of the wireless network would define the number of bits needed to store the network topology (or a portion thereof) or indeed to convey this information to other nodes in the network. Without mitigating entropy growth in such evolving networks, huge operational problems would soon be encountered. This postulate motivates our investigation of the scaling behavior of entropy rate with respect to system properties such as typical connection range and path-loss exponent.

4.4 Mobile Networks Without Rayleigh Fading

In this section, we consider mobile terminals and no Rayleigh fading affecting the communication between two nodes i and j, i.e., $G_{ij,k} = 1$. In our analysis, nodes move randomly according to an Ornstein-Uhlenbeck (OU) process using one tuning parameter to obtain different levels of randomness in the mobility pattern. This process is particularly suited for modeling node mobility in robotic swarms or D2D UAV networks subject to positional perturbations. These types of networks are widely utilized in various rescues, disaster management and military operations nowadays [83]. As described in section 3.3, in mobile networks without Rayleigh fading the received instantaneous SNR at any time step t_k is given by $N_{ij,k} = \psi R_{ij,k}^{-\eta}$, with ψ normalized to 1 for analysis simplification.

In the previous section, we used the entropy rate to analyze the topological uncertainty due to the variations in the propagation channel, but we did not consider node mobility. The entropy rate gives a measure, in unit of bits, that describes the uncertainty in the link state evolution from one time step to the next one. If we consider one communication link, the entropy rate can reach its maximum value of one bit when the link state at time t_k is independent from the link state at time $tk-1$. We will show how the value of the entropy rate can actually be much less than this maximum because of the correlation in the link state from one time step to the next, which is induced by the node mobility. In this section, we exploit the statistics derived in section 3.3 to build an information-theoretic framework for characterizing the uncertainty of the link connectivity due to node mobility and model the on-off transition as a stationary discrete-time Markov Chain. The crux of the problem lies in justifying the use of the Markov model for the link state process.

4.4.1 Post-Disaster Emergency Networks

The OU process is suited for modeling node mobility in robotic swarms or D2D UAV networks subject to positional perturbations. These types of networks are widely utilized in various rescue, disaster management, and military operations [83]. During a disaster, the existing infrastructure collapses, and the affected areas are disconnected. Communication between survivor and rescue crew is crucial to alleviate post-disaster consequences and save lives. Therefore, it is indispensable to design a reliable, resilient, and quickly deployable emergency communication network for the post-disaster situation. Mobile wireless ad hoc network (MANET) is considered an appealing technology for a post-disaster communication system. Since there is no fixed infrastructure, a wireless ad hoc network can be quickly deployed independently from the underlying territory or pre-existing networking capabilities.

The basic idea behind ad hoc networks is to set up a temporary multi-hop communication link between two or several nodes where each node acts as a router and host at the same time.

Nowadays, the UAV's advent gives a new dimension for emergency network design [83]. A UAV, also known as a drone, is a flying aircraft without a human pilot aboard. Thus, for the UAV-assisted emergency network's successful operation, mobility model is essential for navigating the UAVs fleet.

4.4.2 Discretization of the OU process

We can write the discrete version of the continuous time OU process $\{S_t, t \geq 0\}$, described in section 3.2.2, as [84]

$$S_k = S_{k-1}e^{-\Delta t/\tau} + \mu\left(1 - e^{-\Delta t/\tau}\right) + \sqrt{\frac{D\tau\left(1 - e^{-2\Delta t/\tau}\right)}{2}}\epsilon_{k-1}, \tag{4.31}$$

where $\epsilon_k \sim \mathcal{N}(0,1)$ are independent and identically distributed Gaussian random variables. The positive parameters τ and D are the *relaxation time* and the *diffusion coefficient*, respectively; $\sqrt{D}$ controls the fluctuation in the position of the devices along each coordinate axis, and $1/\tau$ controls the rate of reversion of the device to the desired position (the initial position) μ. This discretization is valid for any positive value of the sampling interval Δt. Given the starting point $\{S_0 = s_0, k = 0\}$, the expectation m and variance α of the discrete-time process are equal to:

$$\begin{aligned} m &= \mu + (s_0 - \mu)e^{-\Delta t/\tau}, \\ \alpha &= \frac{D\tau}{2}\left(1 - e^{-2\Delta t/\tau}\right). \end{aligned} \tag{4.32}$$

From (4.31), we observe the linear relationship between input and output in the form

$$S_k = \phi S_{k-1} + \mu\,(1-\phi) + \sqrt{\frac{D\tau\,(1-\phi^2)}{2}}\epsilon_{k-1},\ k \in \mathbb{N}, \tag{4.33}$$

which corresponds to a first-order autoregressive process, AR(1), with parameter $\phi = e^{-\Delta t/\tau}$. It is important to note that in our model $\phi \in (0,1)$ since $\Delta t > 0$ and $\tau > 0$. Therefore, the AR(1) process given in (4.33) is stationary because the regression parameter ϕ satisfies the condition $|\phi| < 1$, for every Δt [106].

4.4.3 Markov Model of Link Connectivity

The purpose of this section is to obtain conditions under which the link state can be approximated as a first-order Markov chain. The key departure point is to treat the link state as a random process that exhibits random changes due to node mobility. Now, consider two arbitrary mobile wireless devices i and j moving randomly over a two-dimensional plane, with initial positions $A_{i,0} = (0,0)$ and $A_{j,0} = (\beta, 0)$, respectively. At any time step t_k, their locations are given by $A_{i,k} = (X_{i,k}, Y_{i,k})$ and $A_{j,k} = (X_{j,k}, Y_{j,k})$. Each coordinate $X_{i,k}, Y_{i,k}, X_{j,k}, Y_{j,k}$ is equal in distribution with S_k, where $\{S_k, k \in \mathbb{N}\}$ is a discrete-time OU process. From the mobility model described in section 3.2.2, the random variables $X_{i,k}, Y_{i,k}, Y_{j,k} \sim \mathcal{N}(0,\alpha)$ and $X_{j,k} \sim \mathcal{N}(\beta,\alpha)$ are independent. On that account, the separation distance between nodes at any time step t_k is equal to $R_{ij,k} = \sqrt{X_{ij,k}^2 + Y_{ij,k}^2}$, where $X_{ij,k} = X_{j,k} - X_{i,k} \sim \mathcal{N}(\beta, 2\alpha)$ and $Y_{ij,k} = Y_{j,k} - Y_{i,k} \sim \mathcal{N}(0, 2\alpha)$ are independent random variables.

As shown in section 3.3, in mobile networks where nodes experience an OU mobility model, the distance process $\{R_{ij,k}, k \in \mathbb{N}\}$ forms a stationary Markov

process with transient distribution equal to

$$f_{R_{ij,k}}(r;k) = \frac{r}{2\alpha} e^{\frac{-\left(r^2+\beta^2\right)}{4\alpha}} \mathrm{I}_0\left(\frac{\beta r}{2\alpha}\right), \tag{4.34}$$

and steady state distribution equal to

$$f_{R_{ij,k}}(r) = \frac{2r}{\theta} e^{-r^2/\theta}, \tag{4.35}$$

where $\theta = 2D\tau$, and I_0 is the modified Bessel function of the first kind with order zero.

In the absence of small-scale fading fading, at any time step t_k, the only source of randomness in the state of the link is provided by the separation distance. The random variable $L_{ij,k}$ denotes the link state between nodes at any time step t_k, where 1(0) defines whether the link exists (does not exist). Formally,

$$L_{ij,k} = \begin{cases} 1, & \text{if } R_{ij,k} \leq r_0, \\ 0, & \text{otherwise}, \end{cases} \tag{4.36}$$

where $r_0 = (1/\rho_{th})^{\frac{1}{\eta}}$ is the typical connection range. This model is also known as the hard connection model of link connectivity [85]. It states that nodes can communicate whenever they lie within some critical distance of each other. Hence, in this scenario, the statistical properties of the link SNR are completely determined by the pair distance $R_{ij,k}$.

The first-order Markov assumption implies that the conditional distribution of $L_{ij,k}$ depends only on $L_{ij,k-1}$ and is independent from any other previous state. In the following, we will show that, under a set of constraints, the reduction in the uncertainty of $L_{ij,k}$ due to knowledge of $L_{ij,k-2}$, given the previous link state

$L_{ij,k-1}$, can be considered negligible. To make progress, we need to evaluate the conditional probability $L_{ij,k}$, which requires the knowledge of the joint probability distribution of $R_{ij,k-2}$, $R_{ij,k-1}$, and $R_{ij,k}$. Now, consider the Gaussian vectors $\mathbf{X} = (X_{ij,1}\ X_{ij,2}\ X_{ij,3})^T$ and $\mathbf{Y} = (Y_{ij,1}\ Y_{ij,2}\ Y_{ij,3})^T$. The mth component of the vector $\mathbf{R}$, $R_{ij,m} = \sqrt{X_{ij,m}^2 + Y_{ij,m}^2}$ where $m = 1, 2, 3$, is a Rician random variable with probability density function given in (4.34). Furthermore, let $\mathbf{\Sigma}$ denote the covariance matrix of $\mathbf{X}$, and $\mathbf{W} = \mathbf{\Sigma}^{-1}$ its inverse with elements equal to w_{uv}, $1 \leq u, v \leq 3$. Then the trivariate distribution of the Rician random variables $R_{ij,1}$, $R_{ij,2}$, and $R_{ij,3}$ is given by [107]

$$\begin{aligned} f_{R_1,R_2,R_3}(r_1, r_2, r_3) &= \frac{r_1 r_2 r_3}{|\mathbf{\Sigma}|} \exp\left\{-\frac{1}{2}\left(\sum_{l=1}^{3} w_{ll} r_l^2 + \beta^2 w_4\right)\right\} \\ &\times \sum_{q=0}^{\infty} \sum_{p=-\infty}^{\infty} \varepsilon_k\, (-1)^{q+p}\, \mathrm{I}_q(w_3 \beta r_3) \mathrm{I}_q(w_{32} \beta r_2 r_3) \\ &\times \mathrm{I}_p(w_1 \beta r_1) \mathrm{I}_p(w_{12} r_1 r_2) \mathrm{I}_{q+p}(w_2 \beta r_2), \end{aligned} \tag{4.37}$$

where $w_1 = w_{11} + w_{12}$, $w_2 = w_{22} + w_{23} + w_{12}$, $w_3 = w_{33} + w_{23}$, $w_4 = w_1 + w_2 + w_3$, I_p is the modified Bessel function of the first kind and order p, $|\mathbf{\Sigma}|$ is the determinant of the covariance matrix, and ε_k is the Neumann factor ($\varepsilon_0 = 1, \varepsilon_n = 2$ for $n = 1, 2, \dots$). The joint probability distribution given in (4.37) is valid only when $\mathbf{X}$ and $\mathbf{Y}$ have identical covariance matrix $\mathbf{\Sigma}$, and if $\mathbf{W}$ is a *tridiagonal matrix* (i.e. $w_{13} = w_{31} = 0$). Indeed, in our mobility formulation both these conditions are satisfied. The covariance matrices of $\mathbf{X}$ and $\mathbf{Y}$ are identical and equal to

$$\mathbf{\Sigma} = D\tau \begin{bmatrix} 1 & \phi & \phi^2 \\ \phi & 1 & \phi \\ \phi^2 & \phi & 1 \end{bmatrix},$$

where $\phi = e^{-\Delta t/\tau}$ is the regression parameter in (4.33). The matrix $\mathbf{\Sigma}$ has a Toeplitz structure, i.e. the correlation coefficients decay exponentially as the time shift between the elements of $\mathbf{\Sigma}$ increase. The inverse covariance matrix $\mathbf{W}$ has the tridiagonal property ($w_{13} = w_{31} = 0$), hence (4.37) applies. To better understand the coefficients of the covariance matrix $\mathbf{\Sigma}$, we refer to (4.33). Clearly, as $\phi \to 0$ or $\Delta t \to \infty$ while fixing τ the process described by (4.33) represents a drifting random walk mobility pattern with mean μ and variance $D\tau/2$. We can consider the random walk as a specific random waypoint model with pause time set to zero. The random waypoint model is used in several simulation studies of ad hoc network protocols. For instance, it appears to create realistic mobility patterns for the way people might move in a conference setting or museum [6]. On the other hand, when $\phi \to 1$ or $\Delta t \to 0$ it degenerates into a constant mobility pattern with $S_k = S_0$ for all $k \in \mathbb{N}$. This pattern is used to model nodes' mobility in a Vehicular Ad hoc Network (VANET) in a highway where nodes move following a certain path in a certain direction. For $0 < \phi < 1$, the process described by (4.33) is particularly suited for modeling node mobility in robotic swarms or D2D UAV networks subject to positional perturbations. These types of networks are widely utilized in various rescues, disaster management and military operations nowadays [83]. Therefore, the OU model represents a wide range of patterns with various degrees of memory, where ϕ can be seen as a tuning parameter to obtain different levels of random movement between these two extremes.

For a fixed OU mobility model, the sampling interval Δt controls the degree of memory in the link state process $\{L_{ij,k}, k \in \mathbb{N}\}$. To assess the validity of the first-order Markov assumption we evaluate a mutual-information-based metric as a function of the sampling interval Δt. Given $L_{ij,k-1}$, the importance of $L_{ij,k-2}$ in providing information for $L_{ij,k}$ can be measured by the ratio of the *conditional*

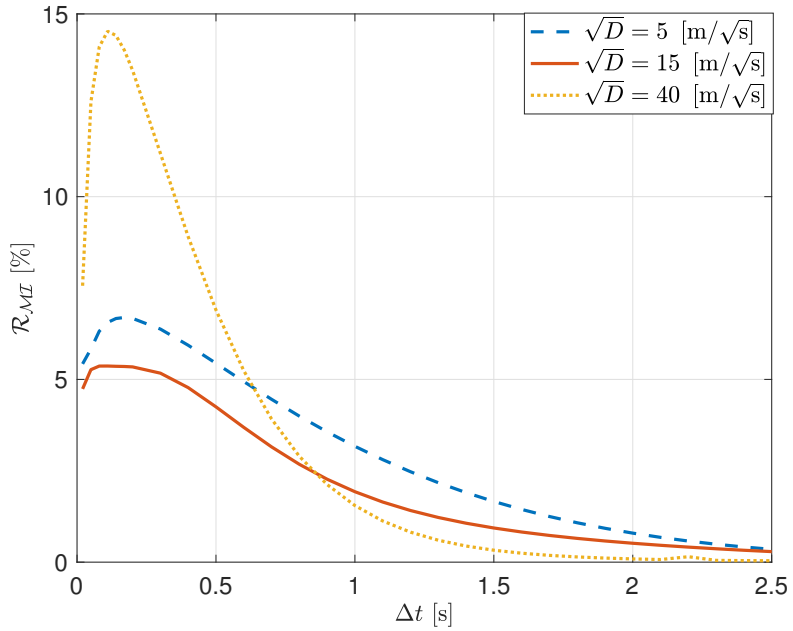

Figure 4.7: Numerical evaluation for the mutual information ratio $\mathcal{R}_{\mathcal{MI}}$ versus the sampling interval Δt; mobility parameters: $\tau = 1$ s, $\beta = 5$ m, and connection range $r_0 = 15$ m.

mutual information and the *mutual information* [108]

$$\mathcal{R}_{\mathcal{MI}} = \frac{I\left(L_{ij,k}; L_{ij,k-2} | L_{ij,k-1}\right)}{I\left(L_{ij,k}; L_{ij,k-1}, L_{ij,k-2}\right)}, \tag{4.38}$$

for $t_k = t_0 + k\Delta t$, $k \in \mathbb{N}$. Without a closed-form solution for the joint probability distribution of $L_{ij,1}$, $L_{ij,2}$, and $L_{ij,3}$, we numerically evaluate (4.38) for typical values of the tuning parameter $\phi \in (0, 1)$.

In Fig. 4.7 we plot the mutual information ratio $\mathcal{R}_{\mathcal{MI}}$ versus the sampling interval Δt, for a given correlation time $\tau = 1s$ and for different values of the parameter $\sqrt{D}$. The diffusion coefficient D in (4.31) expresses the mean square distance traveled per unit of time [76]. A few important things can be noted from the figure. First, as the sampling interval increases, the correlation between $L_{ij,k-2}$ and $L_{ij,k}$ gradually decreases leading to $\mathcal{R}_{\mathcal{MI}} \to 0$. The opposite behavior is evident for small

values of Δt, where the mutual information between $L_{ij,k-2}$ and $L_{ij,k}$ increases. However, for very small values of Δt we notice a decrease in the value of the ratio $\mathcal{R}_{\mathcal{MI}}$, particularly for low/high values of $\sqrt{D}$. The reason behind this behavior is that, fixing τ, as $\sqrt{D}$ decreases or increases the node's movement becomes more or less restricted, respectively, causing less variations in the link state. This, in turn, reduces $I\left(L_{ij,k}; L_{ij,k-2}|L_{ij,k-1}\right)$, which measures the reduction in the uncertainty of $L_{ij,k}$ due to knowledge of $L_{ij,k-2}$ given $L_{ij,k-1}$.

Second, the importance of $L_{ij,k-2}$ given $L_{ij,k-1}$ can be considered negligible (less than 15 %) for all values of Δt. Specifically, when $\Delta t \geq \tau$, we observe a clear decline in the value of $\mathcal{R}_{\mathcal{MI}}$ (less than 4 %) given that τ indicates how strong the current node's location is correlated to its past ones. This behavior is verified for different values of the diffusion coefficient, as illustrated in Fig 4.7. Consequently, the first-order Markovian assumption is approximately verified $\forall\ \Delta t > 0$.

From a practical point of view, Fig. 4.7 provides important information for network design. In a mobile ad hoc network, it is vital to monitor routing paths between nodes continuously. Self-organization in an ad hoc network consists of the following steps: when a node fails, or a new node is added, its neighbors find out about the available nodes through the route discovery protocol. As part of the protocol, all nodes send hello messages containing a unique identifier and position information to their neighbors at regular intervals Δt. Several ad hoc routing protocols make use of periodic broadcast messages to determine local connectivity [109, 110]. Failure to receive any hello message from a neighbor for several time intervals indicates that the neighbor is no longer within transmission range and connectivity has been lost. Two variables control the determination of connectivity using hello messages; the first variable specifies the maximum time interval between the transmission of hello messages. The second variable specifies the maximum number of periods to

wait without receiving a hello message before declaring a connectivity loss. From this plot, we can see that the maximum time interval between the transmission of hello messages could take any value $\Delta t > 0$. However, we would recommend a value $\Delta t > 0.5$ s because for such a value the importance of $L_{ij,k-2}$ given $L_{ij,k-1}$ is negligible.

Now, under the first-order Markovian assumption, we can write

$$\mathbb{P}\left(L_{ij,k} = a | L_{ij,k-1} = b, L_{ij,k-2} = c\right) \simeq \mathbb{P}\left(L_{ij,k} = a | L_{ij,k-1} = b\right), \tag{4.39}$$

for all $a, b, c \in \{0, 1\}$ and any time step t_k. To that end, we can approximate the stochastic process $\{L_{ij,k}, k \in \mathbb{N}\}$ capturing the time evolution of the link between nodes as a stationary DTMC with transition probabilities

$$\mathbb{P}\left(L_{ij,2} = a | L_{ij,1} = b\right) = \frac{\int_{r_3 \in \mathbb{R}^+} \int_{r_2 \in \mathcal{I}_a} \int_{r_1 \in \mathcal{I}_b} f_{R_1,R_2,R3}\left(r_1, r_2, r_3\right) \mathrm{d}r_1 \mathrm{d}r_2 \mathrm{d}r_3}{\int_{r \in \mathcal{I}_b} f_R(r) \mathrm{d}r}. \tag{4.40}$$

The steady state probability is derived by integrating (4.35), i.e,

$$\mathbb{P}\left(L_{ij,1} = b\right) = \int_{r \in \mathcal{I}_b} f_R(r) \mathrm{d}r, \tag{4.41}$$

where the state variables $a, b \in \{0, 1\}$ determine the integration intervals $\mathcal{I}_a$ and $\mathcal{I}_b$, respectively. For instance, $\mathcal{I}_a = (r_0, \infty)$ corresponds to $a = 0$ and $\mathcal{I}_a = (0, r_0)$ to $a = 1$.

4.4.4 Link Entropy

The random movements of the nodes produce a sequence of on-off links leading to frequently changing network connectivity. In our analysis, the link state evolution $\{L_{ij,k}, k \in \mathbb{N}\}$ is modeled as a stationary Markov chain, and its entropy rate is equal

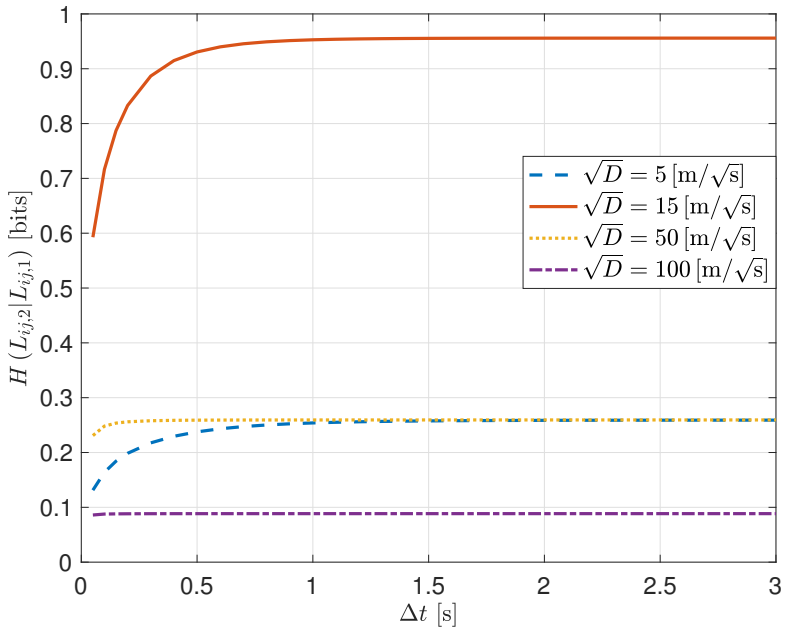

Figure 4.8: Numerical evaluation for the conditional entropy $H\,(L_{ij,2}|L_{ij,1})$ versus the sampling interval Δt; mobility parameters: $\tau = 1$ s, $\beta = 5$ m, connection range $r_0 = 15$ m.

to the transition entropy

$$H\,(L_{ij,2}|L_{ij,1}) = -\sum_{b\in\{0,1\}} \mathbb{P}\,(L_{ij,1} = b) \times \sum_{a\in\{0,1\}} \mathbb{P}\,(L_{ij,2} = a|L_{ij,1} = b) \log_2 \mathbb{P}\,(L_{ij,2} = a|L_{ij,1} = b)\,. \quad (4.42)$$

It is important to note that the OU model is not strictly stationary since its statistics in (4.32) depend on time step t_k. However, for the entropy rate, the transient behavior is suppressed when we take the limit $H\,(L_{ij,2}|L_{ij,1}) = \lim_{k\to\infty} H\,(L_{ij,k}|L_{ij,k-1}, \ldots, L_{ij,1})$, and $t_k = t_0 + k\Delta t$, $k \in \mathbb{N}$.

There are three important parameters in our model that affect the movement of nodes i and j, and therefore their separation distance: $\Delta t, \tau$, and $\sqrt{D}$. It is of fundamental interest to understand the impact of these parameters on the entropy

metric. Without a closed-form solution for the joint probability density of $L_{ij,1}$, $L_{ij,2}$, and $L_{ij,3}$, we calculate the entropy rate by numerically evaluating (4.40). This evaluation is performed for typical values of the tuning parameter $\phi \in (0, 1)$ which determines the intervals of Δt and τ.

In Fig. 4.8 we analyze the behavior of the entropy rate $H\left(L_{ij,2}|L_{ij,1}\right)$ versus the sampling interval Δt, for a given correlation time τ. As the sampling interval increases the correlation between $L_{ij,2}$ and $L_{ij,1}$ gradually decreases. Consequently, the transition entropy asymptotically converges to its maximum value $H\left(L_{ij,2}\right)$. Here, we also explore the impact of the parameter $\sqrt{D}$ on the location uncertainty metric. It is clear from the figure that when $\sqrt{D}$, which controls the fluctuation in the position of the devices, is very close in value to the connection range, there is maximum uncertainty in the link state. This makes perfect sense, as in this scenario the separation distance oscillates around r_0. In the hard connection model nodes are connected whenever they lie within some critical distance of each other. Therefore, the link state between two nodes lying at the border of each other's radio range is characterized by maximum uncertainty. Instead, when $\sqrt{D}$ increases or decreases with respect to r_0, the link uncertainty decreases and for very high values, $\sqrt{D} = 100$ $[\mathrm{m}/\sqrt{\mathrm{s}}]$, the transition entropy is the same for any Δt.

The impact of the square root of the mean square distance traveled per unit of time on the entropy rate is shown in Fig. 4.9. Note that the transition entropy approaches its maximum value of 1 bit as $\sqrt{D} \approx r_0$. In contrast, the transition entropy decreases as $\sqrt{D} \to 0$ and $\sqrt{D} \to \infty$. This behavior verifies the observations made previously. Intuitively, one can recognize that, fixing τ, a node's instantaneous displacement becomes more unrestricted with the increase of $\sqrt{D}$. Two nodes initially connected/disconnected will continue to remain so, introducing memory in the system. Hence, the uncertainty of the future state of the link given its current

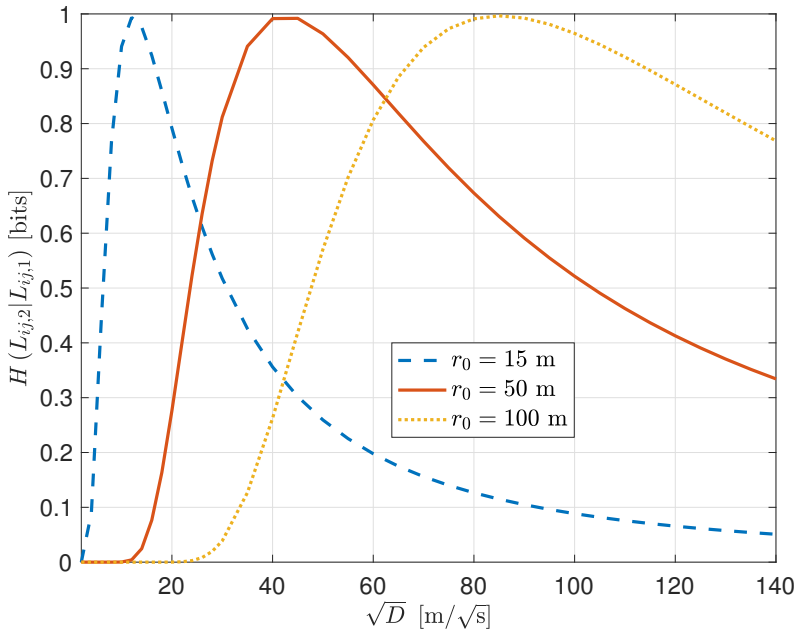

Figure 4.9: Numerical evaluation for the entropy rate $H\,(L_{ij,2}|L_{ij,1})$ versus the square root of the diffusion coefficient $\sqrt{D}$; mobility parameters: $\tau = 1$ s, $\Delta t = 1$ s, and $\beta = 5$ m.

state decreases.

Finally, in Fig. 4.10 we investigate the effect of the relaxation time on the entropy rate. Fixing Δt, as τ increases the randomness in the link state decreases. This is straightforward from the fact that an increase in τ suggests that the node's current and past displacements are becoming more correlated, decreasing the uncertainty of the link future state given its current one. On the contrary, as τ decreases the opposite behavior is observed, where the uncertainty of the future state of the link given its current state increases. However, for small values of τ it is shown in Fig. 4.10 that with the decrease of τ the entropy rate is actually decreasing. The reason behind this initial decay on the entropy rate, which may seem counterintuitive, is related to the stationary variance of node's displacement along the x-axis and y-axis. From (4.33) we have

$$\alpha_\infty = \frac{D\tau}{2}. \tag{4.43}$$

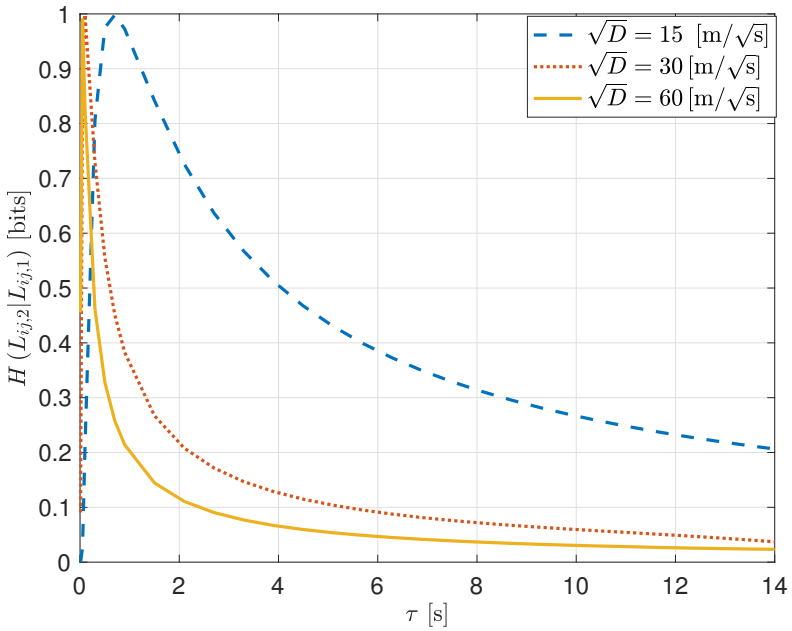

Figure 4.10: Numerical evaluation for the entropy rate $H(L_{ij,2}|L_{ij,1})$ versus the correlation time τ; mobility parameters: $\Delta t = 1$ s, $\beta = 5$ m, and connection range $= 15$ m.

The variance of an OU process is controlled by τ and D. For small values of τ while fixing D the node's displacement can become very restricted. Therefore, their separation distance will vary less, reducing the uncertainty in the link state.

The simulation results demonstrate that the metric $H(L_{ij,2}|L_{ij,1})$ can be considered a good approach to characterize the uncertainty due to the random mobility. The transition probability, $\mathbb{P}(L_{ij,2} = a|L_{ij,1} = b)$, reflects the random mobility in the network and fully captures the link dynamics. The distance $R_{ij,k}$ changes due to the movement of nodes influencing the value of random variable $L_{ij,k}$, and therefore of $H(L_{ij,2}|L_{ij,1})$. The entropy rate quantifies how quickly the link state is varying with time. So, a high entropy rate indicates that the link is frequently changing over time.

4.4.5 Network Entropy

The purpose of this section is to characterize the topological uncertainty of mobile ad hoc networks caused by node mobility. Similarly as in section 4.3.4, we consider a mobile ad hoc network composed of $\mathcal{V} = \{1, \ldots, n\}$, $n > 2$ nodes. We model this network as a time-ordered sequence of graphs, i.e., $\mathcal{G}_k = (\mathcal{V}, \mathbf{L}_k)$, where $\mathbf{L}_k = (L_{ij,k})_{i<j}$. Each graph corresponds to a snapshot of the wireless network at a particular time instance t_k. We assume that nodes are present throughout the lifetime of the system; that is, each graph has the same node set $\mathcal{V}$.

Now, under the assumption that the link trajectories, $L_{ij,1}, \ldots, L_{ij,n}$, $\forall i < j$, are independent, the evolution of each link $i \leftrightarrow j$, for $i, j \in \mathcal{V}$ can be modeled as a stationary Markov chain, following the model explained in section 4.4.3.

From section 4.3.4.1 we have that the minimum and maximum values that the network entropy can take are

$$0 \leq H(\mathcal{L}) \leq \binom{n}{2} H(L_{ij,1}) \leq \binom{n}{2}. \tag{4.44}$$

By using a similar argument to that employed in section 4.3.4.2, we derive a tighter lower and a tighter upper bound on the entropy rate of the dynamical system

$$\sum_{i<j} H(L_{ij,2}|L_{ij,1}, R_{ij}) \leq H(\mathcal{L}) \leq \sum_{i<j} H(L_{ij,2}|L_{ij,1}). \tag{4.45}$$

In the hard connection model nodes are connected whenever they lie within some critical distance of each other. In this scenario, the probability that two nodes are connected is completely determined when the pair distance $R_{ij,k}$ is given. Conse-

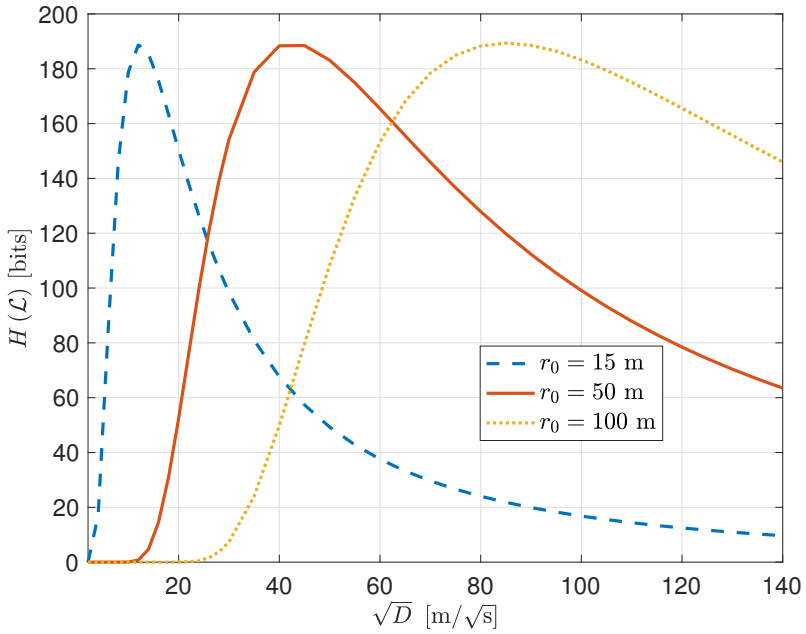

Figure 4.11: Numerical evaluation for the upper bound on the entropy rate of a twenty-node mobile ad hoc network versus the square root of the diffusion coefficient $\sqrt{D}$; mobility parameters: $\tau = 1$ s, $\Delta t = 1$ s, and $\beta = 5$ m.

quently, the lower bound is equal to zero. Hence, we can write

$$0 \leq H(\mathcal{L}) \leq \sum_{i<j} H\left(L_{ij,2}|L_{ij,1}\right). \tag{4.46}$$

It is obvious from (4.40) that when different nodes follow the same mobility model with similar parameters, e.g. τ and D, they will have equal transition and steady state probabilities. In this regard, the bounds on the entropy rate simplifies to

$$0 \leq H\left(\mathcal{L}\right) \leq \binom{n}{2} H\left(L_{ij,2}|L_{ij,1}\right) \leq \binom{n}{2} H\left(L_{ij,1}\right) \leq \binom{n}{2}. \tag{4.47}$$

To be thorough, we investigate the impact of the mobility parameters τ, and $\sqrt{D}$ on the network entropy metric. To that end, in Fig. 4.11 we plot the upper bound on the entropy rate of a twenty-node mobile ad hoc network versus the square

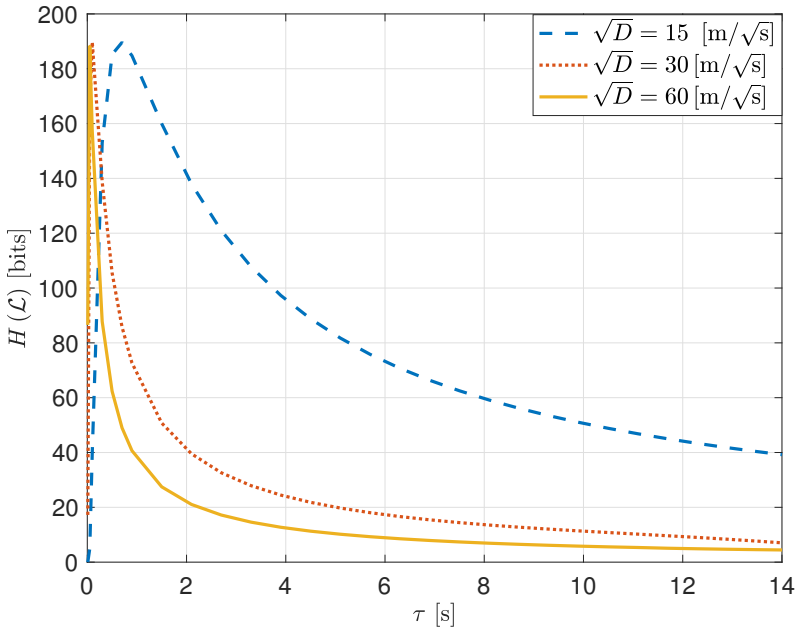

Figure 4.12: Numerical evaluation for the upper bound on the entropy rate of a twenty-node mobile ad hoc network versus the correlation time τ; mobility parameters: $\Delta t = 1$ s, $\beta = 5$ m, and connection range $= 15$ m.

root of the diffusion D, and in Fig. 4.12 we illustrate the upper bound versus the correlation time τ. There are several interesting observations from these two plots. First, as expected, the upper bound on the entropy rate scales like $\mathcal{O}(n^2)$ for a network composed of n nodes. Second, as shown in Fig. 4.6 for practical values of the Doppler frequency, fewer bits are necessary to quantify the dynamics of static wireless networks. This does not hold for mobile ad hoc networks, where the upper bound can reach its maximum value of $\frac{n(n-1)}{2}$ bits, for similar system parameters encapsulated in the typical connection range r_0. The entropy rate quantifies how quickly the underlying topology is varying with time. A higher entropy rate indicates that the topology is frequently changing over time, increasing the uncertainty in the system. Consequently, nodes need to constantly send updated information about their state to the neighbors, leading to an increase in overhead throughout the

network.

4.5 Summary

In this chapter, we developed a framework based on the entropy rate measure for evaluating network complexity and topological uncertainty in mobile ad hoc networks. Due to node mobility and wireless channel randomness, the topological structure shows a time-dependent evolution. In this regard, we took into account both the temporal and spatial properties of the system. We started our analysis by modeling the existence of an edge between two nodes as a stationary Markov chain whose source of randomness is the separation distance between the nodes or the variations in the propagation channel. Using this model, we formulated an entropy-based metric that quantifies link uncertainty. The presented metric takes full advantage of the correlation between the link's current and future state. We then showed that the stochastic process describing the state of the dynamic system is stationary. This result enabled us to derive simple bounds on the network entropy. These bounds are obtained under the assumption that the maximum Doppler frequencies of different links are equal and that nodes' movements are identical. We applied our calculations to nodes experiencing an OU mobility model and Rayleigh fading and investigated the impact of the mobility and channel parameters on the entropy metric. Finally, through numerical results, we demonstrated that the proposed scheme thoroughly captures the link dynamics and accurately reflects changes in the state of a wireless connection.

From an information-theoretic perspective, the entropy rate measures the average minimum description length of the stochastic process, capturing the network dynamics. A broader analysis of the beneficial effects of the entropy rate on routing algorithms will be presented in the next chapter. The entropy-based metric pre-

sented here will be used as a source of information to quantify path uncertainty and select the route with the longest expected lifetime between two nodes.

Chapter 5

Quantifying Topological Uncertainty in MANETs

Node mobility and Rayleigh fading channel are the main factors impacting the network stability and connectivity, and consequently, the performance of MANETs' protocols. In this chapter, we extend the theoretical analysis carried out in chapter 4 and quantify the uncertainty of the link connectivity when both random mobility and Rayleigh fading affect the wireless communication between nodes. Then, we investigate the main source of uncertainty in the link state. Finally, we lend an operational interpretation of the entropy-based metric and propose a new routing decision strategy for MANETs. The key idea of this strategy is to identify and select the route with the longest lifetime between a source and a destination in an environment where different paths are available.

5.1 Introduction

In chapter 4, we analyzed static wireless networks subject to Rayleigh fading and mobile networks without Rayleigh fading. In both cases, we investigated the impact of the channel parameters, η and ν_{ij}, and mobility parameters, τ and $\sqrt{D}$, on the uncertainty metric, respectively. In Figs. 4.3, 4.9, and 4.10 we plotted the conditional entropy versus these parameters. There are several interesting observations from these plots. First, we observe that in static wireless networks subject to Rayleigh fading the transition entropy never approaches its maximum value of 1 bit. In contrast, in mobile networks without Rayleigh, the transition entropy reaches its maximum value. These observations lead to the question: Which is the primary source of uncertainty in the link state in MANETs, the node mobility, or the small-scale fading? The focus of the first part of this chapter is to provide answer to this question.

In the second part, we present an operational interpretation of the conditional entropy. We propose a routing decision strategy for MANETs, where we consider the conditional entropy $H\left(L_{ij,2}|L_{ij,1}\right)$ as the main indicator of link dynamics. This metric effectively identifies and selects the route with longest expected lifetime between a source and a destination in an environment where different paths are available. Several works, e.g., [10, 111, 112], proposed an entropy-based model for supporting and evaluating route stability in MANETs. However, we believe conditional entropy can represent a more accurate metric of link uncertainty in dynamic networks because of its ability to capture the uncertainty in the link state evolution from one time step to the next one. The performance evaluation of the strategy is performed via simulation and analysis.

5.2 Mobile Networks With Rayleigh Fading

This section's main goal is to quantify the topological uncertainty via the conditional entropy metric when both mobility and Rayleigh fading affect the communication between nodes i and j. Our model consists of mobile wireless devices moving randomly over a two-dimensional plane using the radio channel to communicate with each other, path-loss large-scale fading, Rayleigh small-scale fading, and static scatterers. In our analysis, nodes move randomly according to an Ornstein-Uhlenbeck (OU) process using one tuning parameter to obtain different randomness levels in the mobility pattern. Each device movement is assumed to be independent of the others.

5.2.1 Markov Model of Link Connectivity

Consider two arbitrary mobile wireless devices i and j moving randomly over a two-dimensional plane, with same initial positions $A_{i,0} = (0,0)$ and $A_{j,0} = (0,0)$, respectively. At any time step $t_k = t_0 + k\Delta t$, $k \in \mathbb{N}$, their locations are given by $A_{i,k} = (X_{i,k}, Y_{i,k})$ and $A_{j,k} = (X_{j,k}, Y_{j,k})$. Each coordinate $X_{i,k}, Y_{i,k}, X_{j,k}, Y_{j,k}$ is equal in distribution with S_k, where $\{S_k, k \in \mathbb{N}\}$ is a discrete-time OU process. From the mobility model described in section 3.2.2, the random variables $X_{i,k}, Y_{i,k}, Y_{j,k}, X_{j,k} \sim \mathcal{N}(0, \alpha)$ are independent, with $\alpha = \frac{D\tau}{2}\left(1 - e^{-2\Delta t/\tau}\right)$. On that account, the separation distance between nodes at any time step t_k is equal to $R_{ij,k} = \sqrt{X_{ij,k}^2 + Y_{ij,k}^2}$, where $X_{ij,k} = X_{j,k} - X_{i,k} \sim \mathcal{N}(0, 2\alpha)$ and $Y_{ij,k} = Y_{j,k} - Y_{i,k} \sim \mathcal{N}(0, 2\alpha)$ are independent random variables.

As described in section 3.4, in mobile networks subject to Rayleigh fading the received instantaneous SNR at any time step t_k is given by

$$N_{ij,k} = \psi R_{ij,k}^{-\eta} G_{ij,k}, \tag{5.1}$$

where η is the path-loss exponent (typically $2 \leq \eta \leq 6$), $G_{ij,k}$ is the channel gain with $\mathbb{E}[G_{ij,k}] = 1$, and ψ is normalized to 1 for analysis simplification. In this scenario, the distribution of the link SNR depends both on the pair distance, which is governed by the mobility model, and the environmental factors controlling the channel between devices. In section 3.4, we showed that the link SNR $\{N_{ij,k}, k \in \mathbb{N}\}$ is a first-order stationary stochastic process with steady state distribution given by (3.32) for rational path-loss exponents η. For the special cases $\eta = 2$ and $\eta = 4$, the pdf simplifies to the expressions given in (3.33) and (3.34), respectively.

The random variable $L_{ij,k}$ denotes the link state between nodes at any time step t_k, where 1(0) defines whether the link exists (does not exist). Formally,

$$L_{ij,k} = \begin{cases} 1, & \text{if } N_{ij,k} \geq \rho_{th}, \\ 0, & \text{otherwise,} \end{cases} \tag{5.2}$$

where $\rho_{th} = 1/r_0^{\eta}$ is the SNR threshold and r_0 is the typical connection range. The first-order Markov assumption implies that the conditional distribution of $L_{ij,k}$ depends only on $L_{ij,k-1}$, and is independent of any other previous state. The sampling interval Δt controls the degree of memory in the link state evolution $\{L_{ij,k}, k \in \mathbb{N}\}$. In this scenario, Δt must satisfy simultaneously both conditions derived in chapter 4, i.e.,

$$\Delta t \geq \begin{cases} 0.18/\nu_{ij}, & \text{in static wireless networks subject to Rayleigh fading,} \\ 0, & \text{in mobile networks without Rayleigh fading.} \end{cases} \tag{5.3}$$

Hence, we can model the link process as Markov when the sampling interval Δt

satisfies the following condition

$$\Delta t \geq \frac{0.18}{\nu_{ij}}. \tag{5.4}$$

Under this formalism, we can approximate the stochastic process $\{L_{ij,k}, k \in \mathbb{N}\}$ capturing the time evolution of the link between nodes as a stationary discrete-time Markov chain with transition probabilities

$$\mathbb{P}\left(L_{ij,k} = a | L_{ij,k-1} = b, \ldots, L_{ij,1} = c\right) \simeq \mathbb{P}\left(L_{ij,2} = a | L_{ij,1} = b\right), \tag{5.5}$$

and steady state probability

$$\mathbb{P}\left(L_{ij,1} = b\right) = \int_{\rho \in \mathcal{I}_b} f_N\left(\rho\right) \mathrm{d}\rho, \tag{5.6}$$

for all $a, b, c \in \{0, 1\}$ and any time step t_k. The function $f_N\left(\rho\right)$ represents the steady state pdf given by (3.32) for rational path-loss exponents η, and the state variable b determines the integration interval $\mathcal{I}_b$.

5.2.2 Link Entropy

The random movements of the nodes and the quality of the propagation channel jointly affect link connectivity. They are the main factors impacting the network stability and connectivity, and consequently, the performance of MANETs' protocols. Similarly as in chapter 4, we use an entropy-based metric to measure the topological uncertainty of the mobile networks subject to Rayleigh fading and quantify how quickly the underlying topology is varying over time. In our analysis, the link state evolution $\{L_{ij,k}, k \in \mathbb{N}\}$ is modeled as a stationary discrete-time Markov chain, and

its entropy rate is equal to the conditional entropy

$$H\left(L_{ij,2}|L_{ij,1}\right) = -\sum_{b\in\{0,1\}} \mathbb{P}\left(L_{ij,1}=b\right) \times \sum_{a\in\{0,1\}} \mathbb{P}\left(L_{ij,2}=a|L_{ij,1}=b\right)\log_2 \mathbb{P}\left(L_{ij,2}=a|L_{ij,1}=b\right). \quad (5.7)$$

Evaluation of the conditional entropy, and particularly the evaluation of transition probabilities (5.5) requires the joint probability distribution function $f_{N_k,N_{k-1}}\left(\rho_k,\rho_{k-1}\right)$ of the link SNR. In section 3.3.5, we derived closed-form formulae for the bivariate distribution of the link SNR in mobile networks without Rayleigh fading. However, these expressions are not available for mobile networks subject to Rayleigh fading. Similarly, a closed-form expression for the steady state probability exists only when $\eta = 2$ (given in (3.36)). For these reasons, we resort to numerically simulating the transition and steady state probabilities given in (5.5) and (5.6), respectively, using a counting function.

There are five important parameters that affect the link state: sampling interval Δt, mobility parameters τ and D, and the radio channel parameters η and ν_{ij}. The mobility parameters affect the movement of nodes i and j, and therefore their separation distance $R_{ij,k}$. The parameter $\sqrt{D}$ controls the fluctuation in the position of the devices, and $1/\tau$ controls the rate of reversion of the device to the initial position. The channel parameter η indicates how quickly a transmission is attenuated as it propagates through the wireless medium. It is usually taken to be $\eta = 2$ in free space and $\eta > 2$ in cluttered urban environments. On the other hand, the parameter ν_{ij} represents the maximum Doppler shift, which is a measure for the rate of change of the Rayleigh fading channel.

As described in section 2.2.5, the maximum Doppler frequency ν_{ij} depends on

the nodes' velocities, which in turn depend on the mobility parameters τ and D. Let $V_{i,k}$ and $V_{j,k}$ be the velocity of nodes i and j at time t_k, respectively. Then, the maximum Doppler shift is given by

$$\nu_{ij} = f_c \frac{\Delta V}{c}, \tag{5.8}$$

where f_c is the carrier frequency, c is the speed of light, and $\Delta V = |V_{i,k} - V_{j,k}|$ is the change in velocities. Given that nodes' movements are identical, the maximum Doppler frequencies of different links are equal, i.e., $\nu_{ij} = \nu_{kl} = \nu$. From section 3.2.2, we know $V_{i,k}$ and $V_{j,k}$ are independent and identically distributed Rayleigh random variables with parameter $\sqrt{D\tau}/\Delta t$, i.e., $V_{i,k}, V_{j,k} \sim \text{Rayleigh}\left(\sqrt{D\tau}/\Delta t\right)$. Hence, the Doppler frequency is a function of the mobility parameters, i.e., $\nu = f(\tau, D)$. Therefore, we have three degrees of freedom (τ, D, η) that affect the quality of the communication links in mobile networks subject to Rayleigh fading. In the next section, we make progress by analyzing the impact of these parameters on the entropy metric.

5.3 Numerical Results and Discussions

Before presenting the numerical results, we need to guarantee the assumptions of our model defined in section 5.2.1. As aforesaid, the sampling interval Δt must satisfy the condition $\Delta t \geq 0.18/\nu$. If we consider a communication system using 802.11a protocols, the carrier frequency is $f_c = 5$ GHz. When simulating MANETs, the maximum node velocity is usually set to $V_{\max} = 30$ m/s [113, 114]. We then enforce the condition that the expectation of the Rayleigh random variable $V_{i,k}$ is lower or equal to $V_{\max}$, i.e., $\mathbb{E}\{V_{i,k}\} = \sqrt{D\tau}/\Delta t \times \sqrt{\pi/2} \leq V_{\max}$. All these constraints will set restrictions on both values of τ, D and Δt and determine their range of possible values.

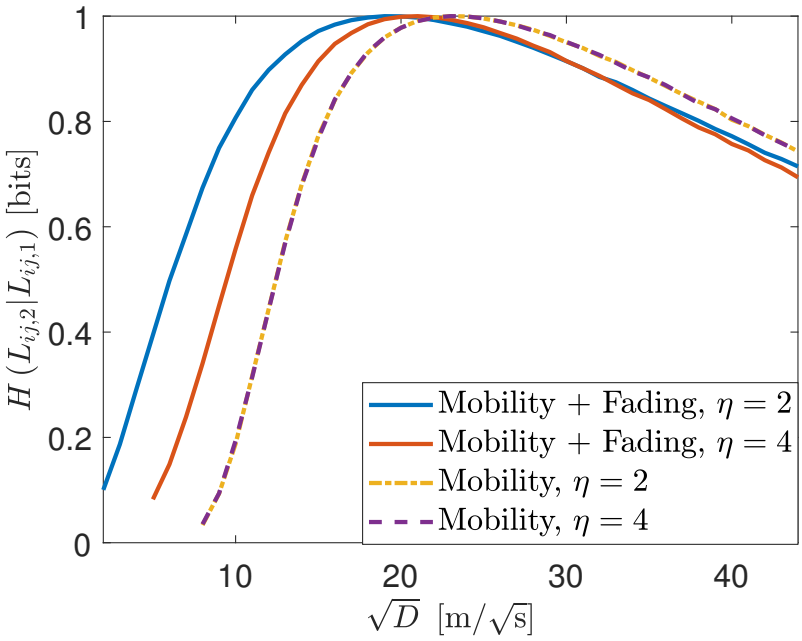

Figure 5.1: Numerical estimation for the conditional entropy $H\left(L_{ij,2}|L_{ij,1}\right)$ versus the square root of the diffusion coefficient $\sqrt{D}$; parameters $\tau = 0.3$ s, $\Delta t = 1$ s, and $r_0 = 15$ m.

In the following we perform numerical simulations with the following parameters: nodes' initial positions $X_{i,0}, Y_{i,0}, Y_{j,0}, X_{j,0} \sim \mathcal{N}(0, \alpha)$, $\alpha = \frac{D\tau}{2}$, number of trials $N_{\text{trials}} = 10^5$, speed of light $c = 3 * 10^8$ m/s, and typical connection range $r_0 = 15$ m. The maximum Doppler frequency is obtained from the formula $\nu = f_c \frac{\Delta V}{c}$ where $\Delta V = |V_{i,k} - V_{j,k}|$ is the change in velocities. Hence, we simulate two Rayleigh random variables, i.e, $V_{i,k}, V_{j,k} \sim \text{Rayleigh}\left(\sqrt{D\tau}/\Delta t\right)$, take their difference and then compute the Doppler frequency.

5.3.1 Impact of the Diffusion Coefficient D

In Fig. 5.1, we plot the conditional entropy $H\left(L_{ij,2}|L_{ij,1}\right)$, in the presence and absence of Rayleigh fading, versus the square root of the diffusion coefficient $\sqrt{D}$, for different values of path-loss exponent η. To gain further insight, we also analyze the marginal and transition probabilities. In Figure 5.2 we plot the marginal

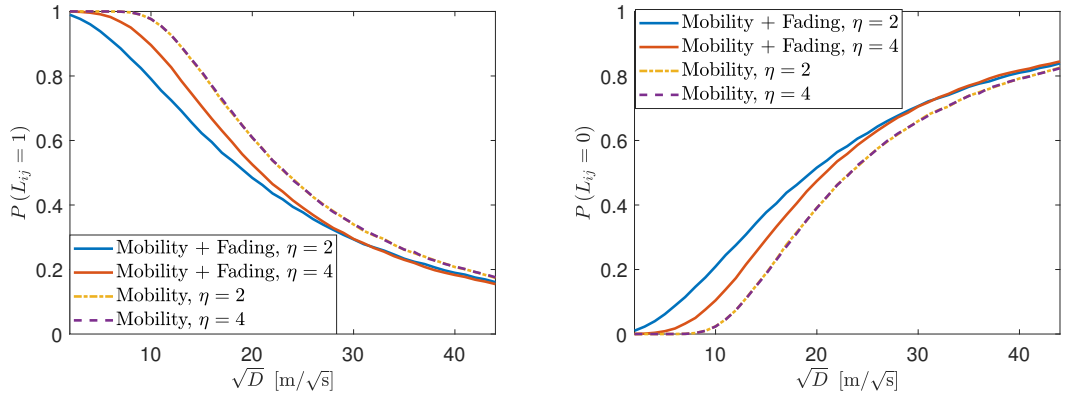

(a) $\mathbb{P}(L_{ij} = 1)$ **(b)** $\mathbb{P}(L_{ij} = 0)$

Figure 5.2: Numerical estimation for the marginal probabilities $\mathbb{P}(L_{ij} = 1)$ and $\mathbb{P}(L_{ij} = 0)$ versus the square root of the diffusion coefficient $\sqrt{D}$; parameters $\tau = 0.3$ s, $\Delta t = 1$ s, and $r_0 = 15$ m.

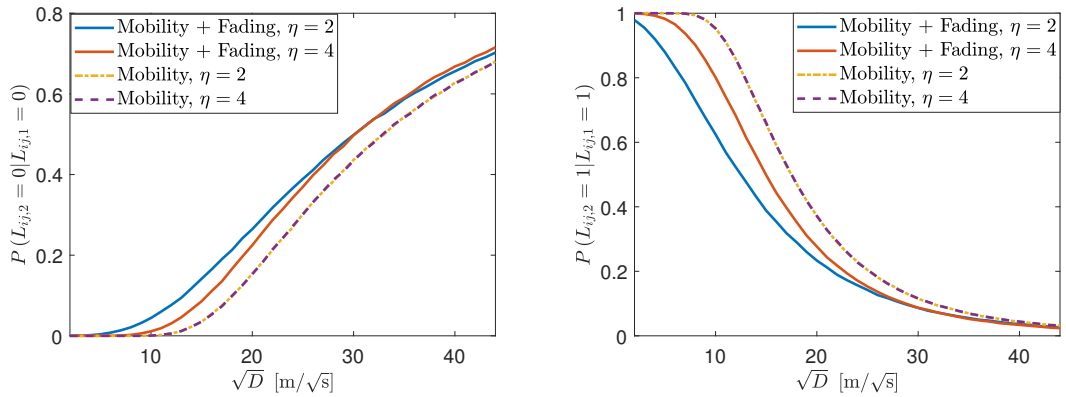

(a) $\mathbb{P}(L_{ij,2} = 0|L_{ij,1} = 0)$ **(b)** $\mathbb{P}(L_{ij,2} = 1|L_{ij,1} = 1)$

Figure 5.3: Numerical estimation for the transition probabilities $\mathbb{P}(L_{ij,2} = 0|L_{ij,1} = 0)$ and $\mathbb{P}(L_{ij,2} = 1|L_{ij,1} = 1)$ versus the square root of the diffusion coefficient $\sqrt{D}$; parameters $\tau = 0.3$ s, $\Delta t = 1$ s, and $r_0 = 15$ m.

probabilities $\mathbb{P}(L_{ij} = 1)$ and $\mathbb{P}(L_{ij} = 0)$. In Fig. 5.3 we plot the transition probabilities $\mathbb{P}(L_{ij,2} = 0|L_{ij,1} = 0)$ and $\mathbb{P}(L_{ij,2} = 1|L_{ij,1} = 1)$ and in Fig. 5.4 we plot $\mathbb{P}(L_{ij,2} = 1|L_{ij,1} = 0)$ and $\mathbb{P}(L_{ij,2} = 0|L_{ij,1} = 1)$. The parameter $\sqrt{D}$ controls the fluctuation in the position of the devices. That is, fixing τ, the variance of node's displacement along the x-axis and y-axis is controlled by $\sqrt{D}$, given that the station-

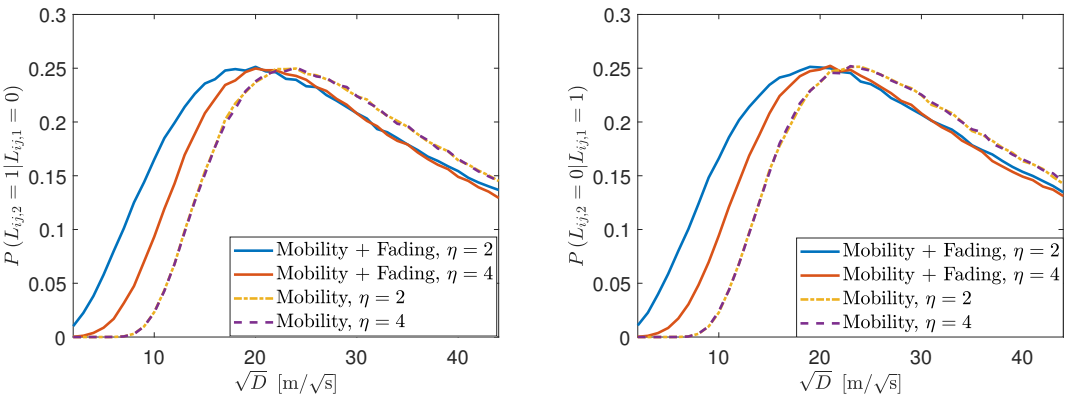

(a) $\mathbb{P}\,(L_{ij,2}=1|L_{ij,1}=0)$ **(b)** $\mathbb{P}\,(L_{ij,2}=0|L_{ij,1}=1)$

Figure 5.4: Numerical estimation for the transition probabilities $\mathbb{P}\,(L_{ij,2}=1|L_{ij,1}=0)$ and $\mathbb{P}\,(L_{ij,2}=0|L_{ij,1}=1)$ versus the square root of the diffusion coefficient $\sqrt{D}$; parameters $\tau=0.3$ s, $\Delta t=1$ s, and $r_0=15$ m.

ary variance is equal to $\alpha_\infty=\frac{D\tau}{2}$. A few important things can be noted from these figures. First, we can identify three regions: $\sqrt{D}\ll r_0$, $\sqrt{D}\approx r_0$, and $\sqrt{D}\gg r_0$. It is clear from the figure that when $\sqrt{D}$ is very close in value to the connection range, i.e., $\sqrt{D}\approx r_0$, there is maximum uncertainty in the link state as the transition entropy approaches its maximum value of 1 bit. In contrast, the conditional entropy decreases in the regions $\sqrt{D}\ll r_0$ and $\sqrt{D}\gg r_0$. The reason behind this behavior is that, fixing τ, as $\sqrt{D}$ decreases or increases the node's movement becomes more or less restricted, respectively, causing fewer variations in the link state. This, in turn, reduces the value of the transition probabilities $\mathbb{P}\,(L_{ij,2}=a|L_{ij,1}=b)$ for $a\neq b$. These observations are true for both fading and non-fading scenarios.

Next, it is clear that when $\sqrt{D}\gg r_0$, the primary source of the uncertainty in the link state in mobile networks subject to Rayleigh fading is node mobility. Indeed, the conditional entropy attains more or less similar values in the presence or absence of Rayleigh fading. Hence, we can argue that the impact of the fading channel on the link state, and consequently, on the link stability metric is negligible when $\sqrt{D}\gg r_0$.

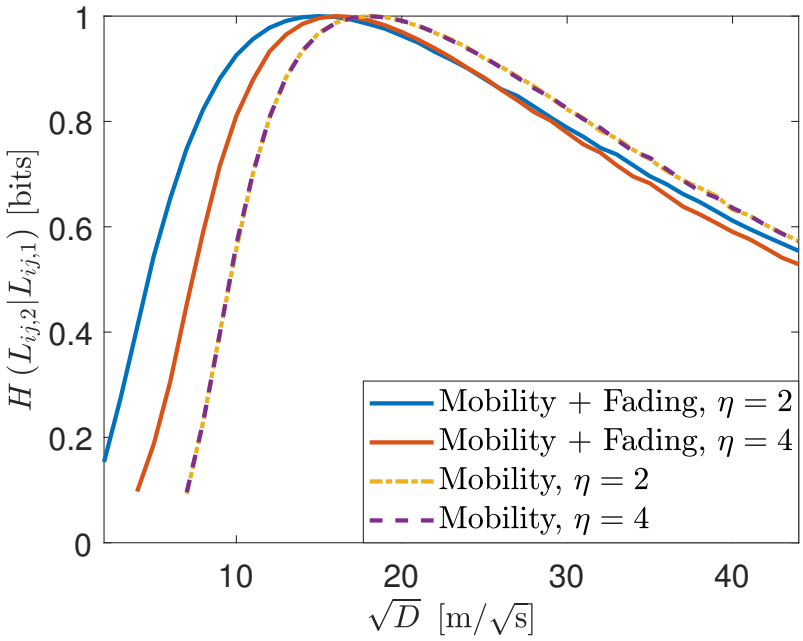

Figure 5.5: Numerical estimation for the conditional entropy $H\left(L_{ij,2}|L_{ij,1}\right)$ versus the square root of the diffusion coefficient $\sqrt{D}$; parameters $\tau = 0.5$ s, $\Delta t = 2$ s, and $r_0 = 15$ m.

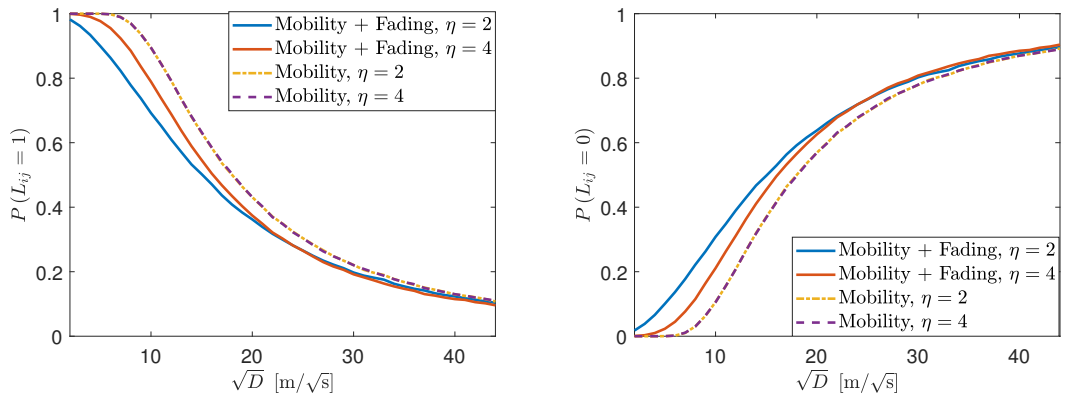

(a) $\mathbb{P}\left(L_{ij}=1\right)$ **(b)** $\mathbb{P}\left(L_{ij}=0\right)$

Figure 5.6: Numerical estimation for the marginal probabilities $\mathbb{P}\left(L_{ij}=1\right)$ and $\mathbb{P}\left(L_{ij}=0\right)$ versus the square root of the diffusion coefficient $\sqrt{D}$; parameters $\tau = 0.5$ s, $\Delta t = 2$ s, and $r_0 = 15$ m.

In this regard, at any time step t_k, the primary source of randomness in the link state is provided by the separation distance $R_{ij,k}$.

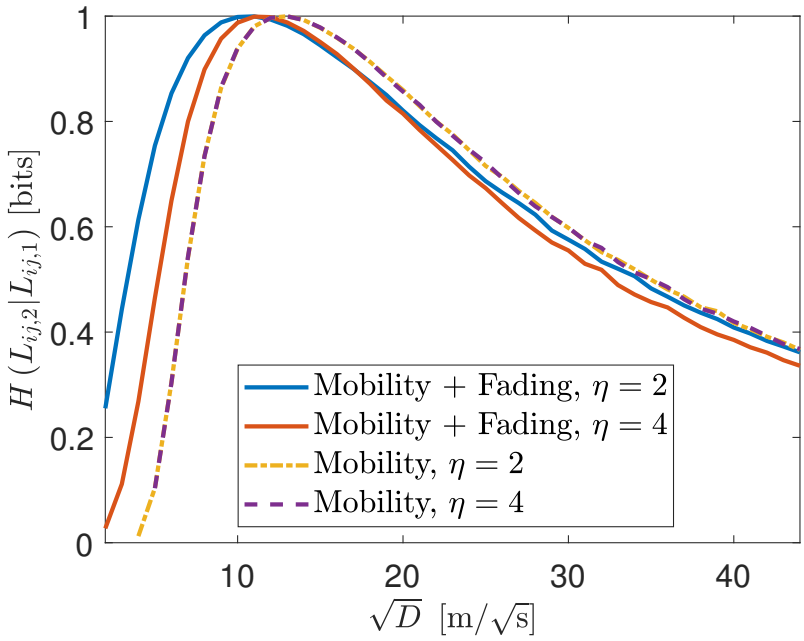

Figure 5.7: Numerical estimation for the conditional entropy $H\left(L_{ij,2}|L_{ij,1}\right)$ versus the square root of the diffusion coefficient $\sqrt{D}$; parameters $\tau = 1$ s, $\Delta t = 2$ s, and $r_0 = 15$ m.

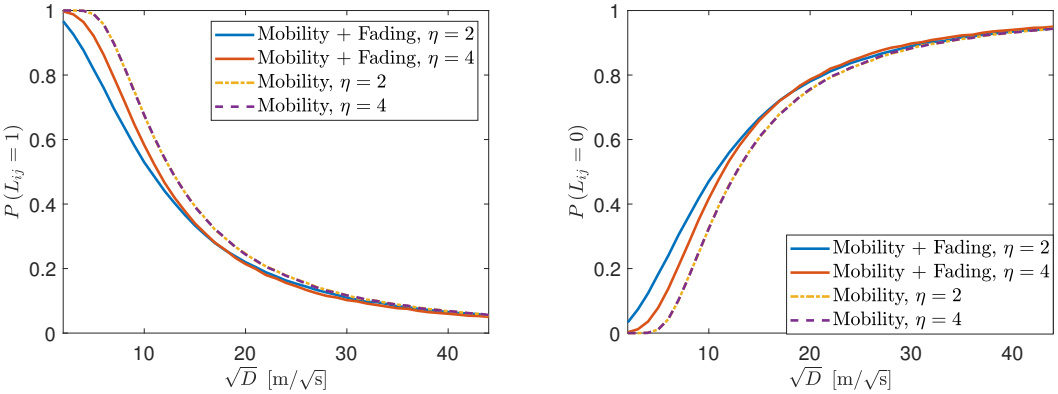

(a) $\mathbb{P}\left(L_{ij}=1\right)$ **(b)** $\mathbb{P}\left(L_{ij}=0\right)$

Figure 5.8: Numerical estimation for the marginal probabilities $\mathbb{P}\left(L_{ij}=1\right)$ and $\mathbb{P}\left(L_{ij}=0\right)$ versus the square root of the diffusion coefficient $\sqrt{D}$; parameters $\tau = 1$ s, $\Delta t = 2$ s, and $r_0 = 15$ m.

On the contrary, when $\sqrt{D} < r_0$, the channel fading causes higher variations in the link state, leading to a higher transition entropy. As the node's movements become more restricted, the small-scale fading has a more significant impact on link

connectivity. In the absence of small-scale fading nodes are connected whenever they lie within some critical distance. Two nodes initially connected/disconnected will continue to remain so, introducing memory in the system. Whereas, in the presence of small-scale fading, the probability that two nodes are connected decays exponentially with the pair distance. This influence the value of random variable $L_{ij,k}$, and therefore of $H\left(L_{ij,2}|L_{ij,1}\right)$.

As expected, in the "on" region, the dominant probability term is $\mathbb{P}\left(L_{ij,2}=1|L_{ij,1}=1\right)$, whereas, in the "off" region, the dominant term is $\mathbb{P}\left(L_{ij,2}=0|L_{ij,1}=0\right)$. In the high entropy region, we obtain "almost" a uniform probability distribution, i.e., $\mathbb{P}\left(L_{ij,2}=0|L_{ij,1}=0\right)=\mathbb{P}\left(L_{ij,2}=1|L_{ij,1}=1\right)\approx 0.25$, and $\mathbb{P}\left(L_{ij,2}=1|L_{ij,1}=0\right)=\mathbb{P}\left(L_{ij,2}=0|L_{ij,1}=1\right)\approx 0.25$. This confirms the observations made previously. The uncertainty in the link state is maximum when transition probabilities are equal.

In Fig. 5.5 and in Fig. 5.7 we plot the conditional entropy for different values of the sampling interval and correlation time, whereas in Fig. 5.6 and in Fig. 5.8 we show the marginal probabilities. The behavior of the conditional entropy is the same. After these observations, we can conclude that the region $\sqrt{D}\ll r_0$ represent an "on" state, i.e., link is active, the region $\sqrt{D}\gg r_0$ an "off" state, and $\sqrt{D}\approx r_0$ is the region with maximum uncertainty where the link state flips between "on" and "off".

5.3.2 Impact of the Path-Loss Exponent η

In Fig. 5.1, we also explore the impact of the path-loss exponent η on the link stability metric. First, we notice that in the absence of Rayleigh fading, the parameter η does not affect the conditional entropy. We then observe that, in presence of fading, when $\sqrt{D}\ll r_0$ and $\sqrt{D}\gg r_0$, as η increases the randomness in the link state decreases. This behavior, which may seem counterintuitive, is related to the

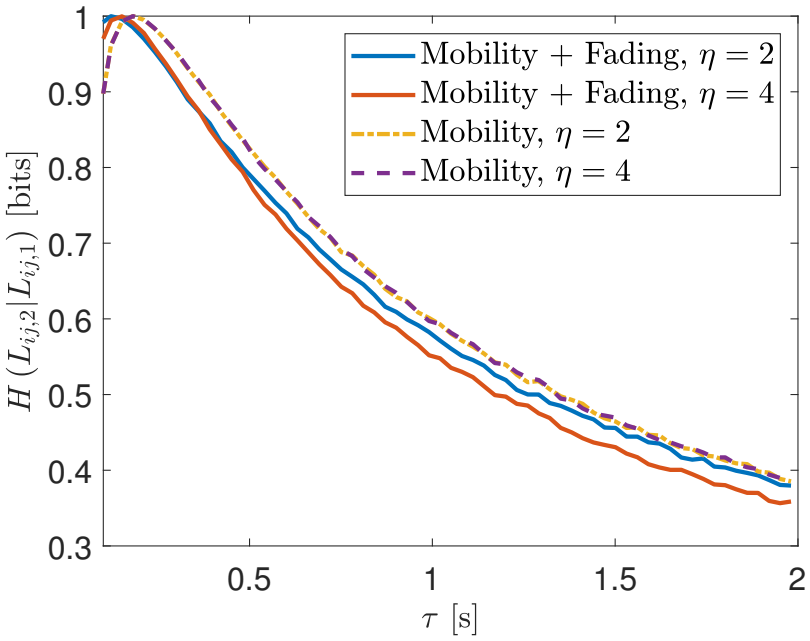

Figure 5.9: Numerical estimation for the conditional entropy $H\left(L_{ij,2}|L_{ij,1}\right)$ versus the correlation time τ; parameters $\sqrt{D} = 30$ m, $\Delta t = 1.8$ s, and $r_0 = 15$ m.

observations made previously. Intuitively, one can recognize that, fixing τ, a node's instantaneous displacement becomes less restricted with the increase of $\sqrt{D}$. Additionally, as η increases, transmissions are attenuated more quickly as they propagate through the wireless medium. Hence, it will be less likely for two nodes initially disconnected to establish successful communication in the future, introducing memory in the system. In the same fashion, for small values of $\sqrt{D}$, as η increases, the conditional entropy decreases. Mathematically, the parameter η controls the stretch of the decaying exponential function in the soft connection model. For $\eta \to \infty$, we recover the hard connection model.

5.3.3 Impact of the Correlation Time τ

The impact of the correlation time on the link stability metric is shown in Fig. 5.9, when $\sqrt{D} \gg r_0$. In Fig. 5.10 we plot the marginal probabilities, whereas in Fig. 5.11 and in Fig. 5.12 we plot the transition probabilities. In these figures, we can also

identify the "on", "off", and "flip" regions where the link is connected, disconnected, and flips between connected and disconnected, respectively. The parameter τ measures the correlation of node's current and past displacements. Furthermore, fixing $\sqrt{D}$, the variance of node's displacement along the x-axis and y-axis is controlled by τ.

As expected, we can notice from these figures the primary source of the uncertainty in the link state is node mobility, given that $\sqrt{D} \gg r_0$. Hence, the absence or presence of Rayleigh fading does not have any impact on the conditional entropy. To that end, the conclusions drawn from this plot are similar to those in Fig. 4.10. For instance, for a fixed Δt, as τ increases, the randomness in the link state decreases. The reason is that an increase in τ suggests that the node's current and past displacements are becoming more correlated, reducing the uncertainty of the future link state given its current one. On the contrary, as τ decreases, the opposite behavior is observed, where the uncertainty of the future link state given its current state increases.

In Fig. 5.13 and in Fig. 5.14 we plot the conditional entropy and the marginal probabilities versus τ when $\sqrt{D} \leq r_0$. In Fig. 5.15 and in Fig. 5.16 we plot the conditional entropy and the marginal probabilities versus τ when $\sqrt{D} \ll r_0$. In these simulations we only modify the $\sqrt{D}$; the rest of the parameters is unchanged. In these figures, we can observe that the small-scale fading has a non-negligible effect on the conditional entropy. Specifically, for small values of τ, fading is the main source of uncertainty in the link state. However, as τ increases, the conditional entropy attains similar values in the presence or absence of Rayleigh fading.

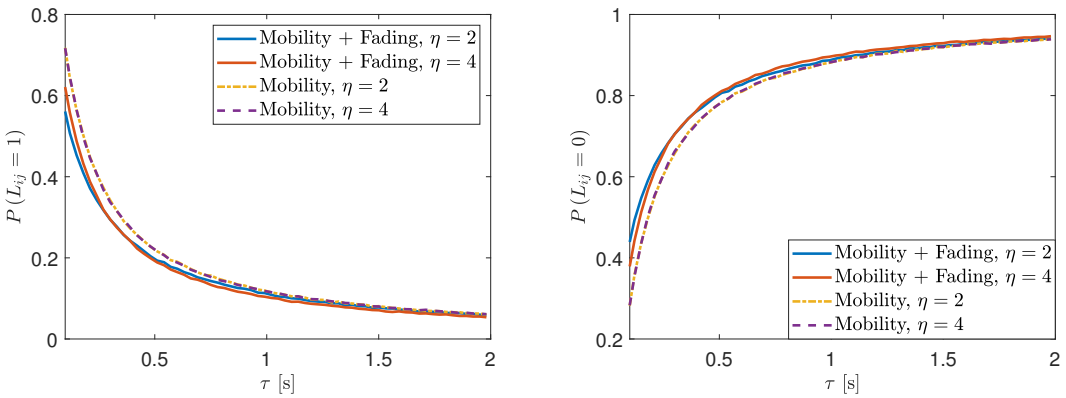

(a) $\mathbb{P}(L_{ij} = 1)$ **(b)** $\mathbb{P}(L_{ij} = 0)$

Figure 5.10: Numerical estimation for the marginal probabilities $\mathbb{P}(L_{ij} = 1)$ and $\mathbb{P}(L_{ij} = 0)$ versus the correlation time τ; parameters $\sqrt{D} = 30$ m, $\Delta t = 1.8$ s, and $r_0 = 15$ m.

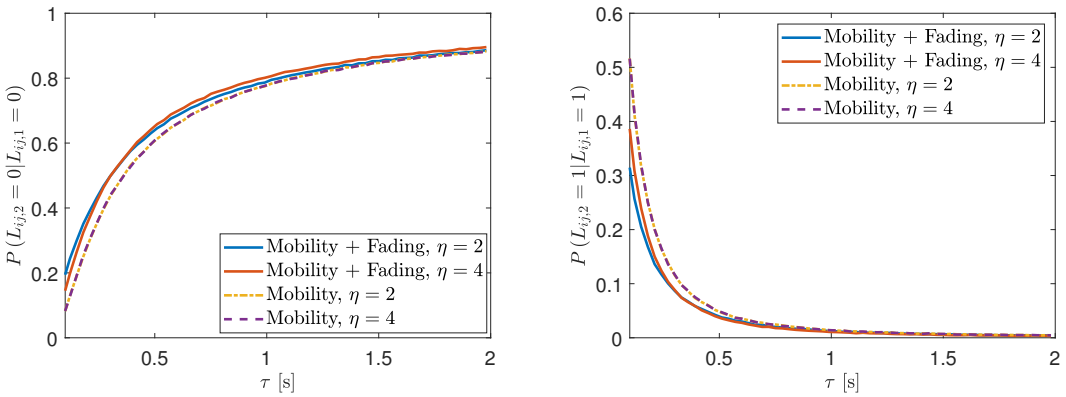

(a) $\mathbb{P}(L_{ij,2} = 0|L_{ij,1} = 0)$ **(b)** $\mathbb{P}(L_{ij,2} = 1|L_{ij,1} = 1)$

Figure 5.11: Numerical estimation for the transition probabilities $\mathbb{P}(L_{ij,2} = 0|L_{ij,1} = 0)$ and $\mathbb{P}(L_{ij,2} = 1|L_{ij,1} = 1)$ versus the correlation time τ; parameters $\sqrt{D} = 30$ m, $\Delta t = 1.8$ s, and $r_0 = 15$ m.

5.4 Operational Interpretation of Entropy-Based Metric

This section presents an operational interpretation of the entropy-based metric and proposes a new routing decision strategy for MANETs. The key idea of this

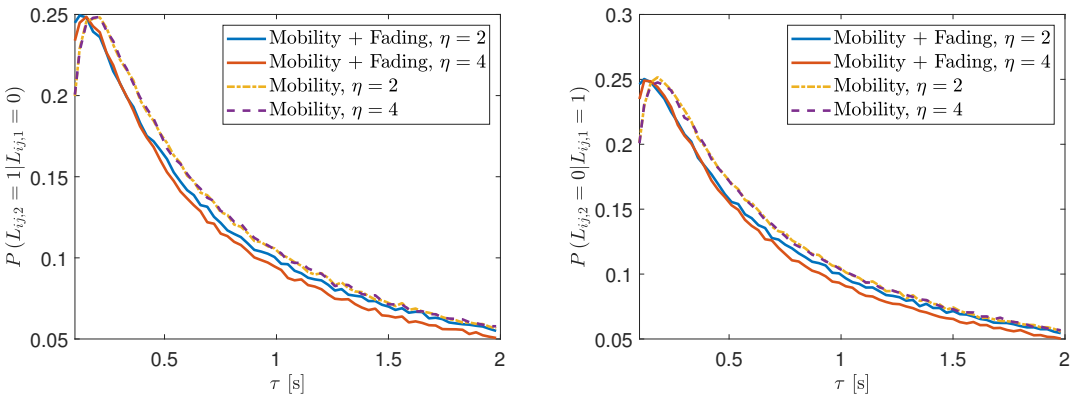

(a) $\mathbb{P}\left(L_{ij,2} = 1 | L_{ij,1} = 0\right)$ **(b)** $\mathbb{P}\left(L_{ij,2} = 0 | L_{ij,1} = 1\right)$

Figure 5.12: Numerical estimation for the transition probabilities $\mathbb{P}\left(L_{ij,2} = 1 | L_{ij,1} = 0\right)$ and $\mathbb{P}\left(L_{ij,2} = 0 | L_{ij,1} = 1\right)$ versus the correlation time τ; parameters $\sqrt{D} = 30$ m, $\Delta t = 1.8$ s, and $r_0 = 15$ m.

strategy is to identify and select the route with the longest lifetime between a source and a destination in an environment where different paths are available. In traditional routing protocols, e.g., DSDV and AODV, paths are generally established according to a minimum hop-count metric. Specifically, the number of intermediary links is the critical metric rather than the quality of links. In this section, we propose a routing decision strategy based on the characteristics of the links. In particular, we rely on the entropy-based metric to quantify the uncertainty of the link connectivity. This framework is similar to the one presented in [10], where the authors introduced an entropy-based model for evaluating route stability. However, we believe that using the conditional entropy as a metric to evaluate route stability represents a more accurate metric of topological uncertainty because of its ability to measure the uncertainty of the future state of the link given its current state.

Multi-path routing requires the availability of alternative paths between start and destination to prevent node failures from affecting the communication. However, available alternative paths are inherently unreliable, leading to an increase in

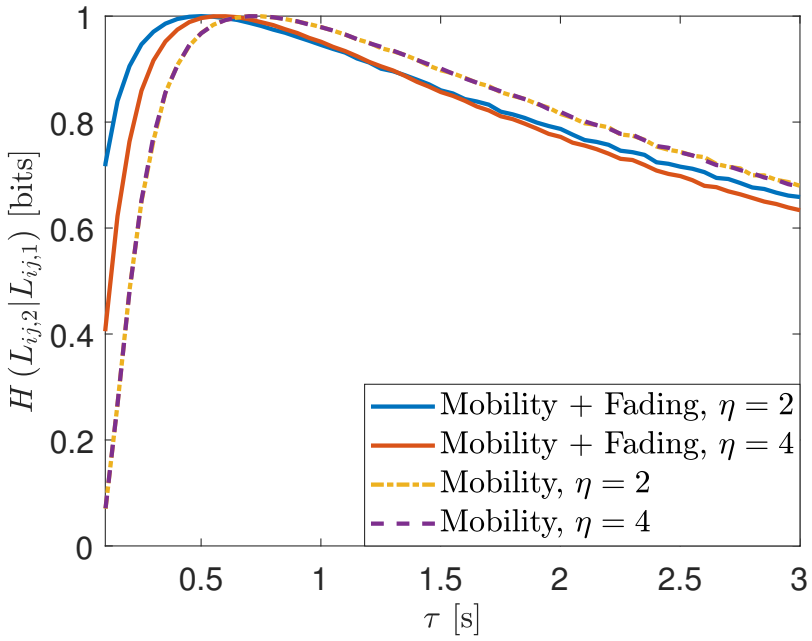

Figure 5.13: Numerical estimation for the conditional entropy $H\left(L_{ij,2}|L_{ij,1}\right)$ versus the correlation time τ; parameters $\sqrt{D} = 15$ m, $\Delta t = 1.8$ s, and $r_0 = 15$ m.

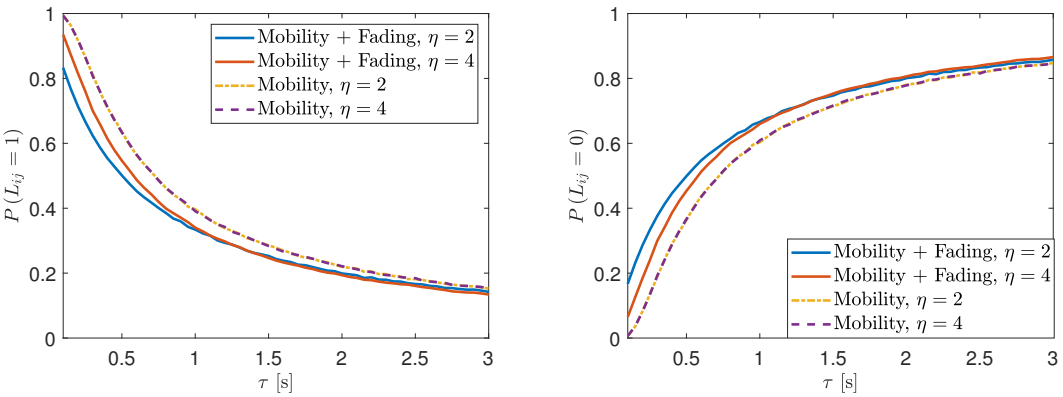

(a) $\mathbb{P}\left(L_{ij} = 1\right)$ **(b)** $\mathbb{P}\left(L_{ij} = 0\right)$

Figure 5.14: Numerical estimation for the marginal probabilities $\mathbb{P}\left(L_{ij} = 1\right)$ and $\mathbb{P}\left(L_{ij} = 0\right)$ versus the correlation time τ; parameters $\sqrt{D} = 15$ m, $\Delta t = 1.8$ s, and $r_0 = 15$ m.

overhead throughout the network due to frequent route discoveries control packets. We reduce the number of route reconstruction between two nodes k and l by selecting those links that, once activated, are expected to be active for a longer time. In our

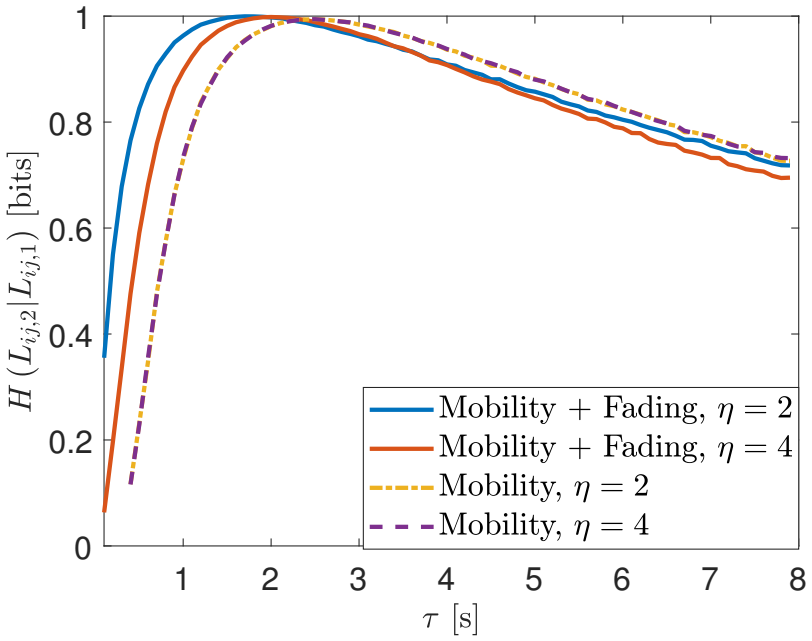

Figure 5.15: Numerical estimation for the conditional entropy $H\left(L_{ij,2}|L_{ij,1}\right)$ versus the correlation time τ; parameters $\sqrt{D} = 8$ m, $\Delta t = 1.8$ s, and $r_0 = 15$ m.

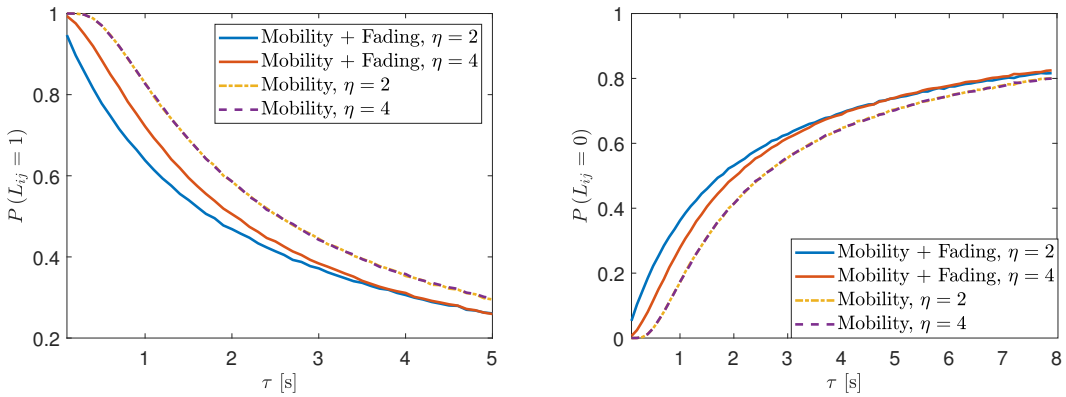

(a) $\mathbb{P}\left(L_{ij} = 1\right)$ **(b)** $\mathbb{P}\left(L_{ij} = 0\right)$

Figure 5.16: Numerical estimation for the marginal probabilities $\mathbb{P}\left(L_{ij} = 1\right)$ and $\mathbb{P}\left(L_{ij} = 0\right)$ versus the correlation time τ; parameters $\sqrt{D} = 8$ m, $\Delta t = 1.8$ s, and $r_0 = 15$ m.

framework, the uncertainty in the local link state $i \leftrightarrow j$ is low if $H\left(L_{ij,2}|L_{ij,1} = 1\right)$ is small, and vice-versa when the conditional entropy is large. We measure the lifetime

of a route between two nodes k and l as L_{kl}, i.e.,

$$L_{kl} = 1 - \max_{i,j \in \mathcal{N}} \left(H \left(L_{ij,2} | L_{ij,1} = 1 \right) \right), \tag{5.9}$$

where

$$H \left(L_{ij,2} | L_{ij,1} = 1 \right) = - \sum_{a \in \{0,1\}} \mathbb{P} \left(L_{ij,2} = a | L_{ij,1} = 1 \right) \log_2 \mathbb{P} \left(L_{ij,2} = a | L_{ij,1} = 1 \right), \tag{5.10}$$

and $\mathcal{N}$ denotes the set of intermediate mobile nodes over a route between the two end nodes (k, l). For any given route we can identify the bottleneck as the link with the highest conditional entropy. This is because the link with highest conditional entropy is expected to have the shortest lifetime. The goal of the next sections is to prove this hypothesis.

5.4.1 Numerical Results and Discussions

To evaluate the proposed modeling framework, we consider a D2D UAV network of 8 nodes $\mathcal{V} = \{1, \ldots, 8\}$ placed randomly within a rectangular region. It is assumed that nodes are present throughout the lifetime of the system. Each node is assumed to have a constant radio range of $r_0 = 40$ m. We consider a communication system using 802.11a protocols with carrier frequency $f_c = 5$ GHz, and an OFDM based physical layer. Two nodes can establish a successful communication, at any time step t_k, whenever their instantaneous SNR is greater than a certain threshold, $N_{ij,k} \geq \rho_{th}$, where $\rho_{th} = 1/r_0^{\eta}$. Connections between nodes are established and broken intermittently due to the nodes' mobility and large-scale fading.

A UAV, also known as drone, is a flying aircraft without a human pilot aboard. Thus, for the successful operation of UAV-assisted networks a mobility model is essential for navigating a fleet of UAVs. These types of networks are widely utilized

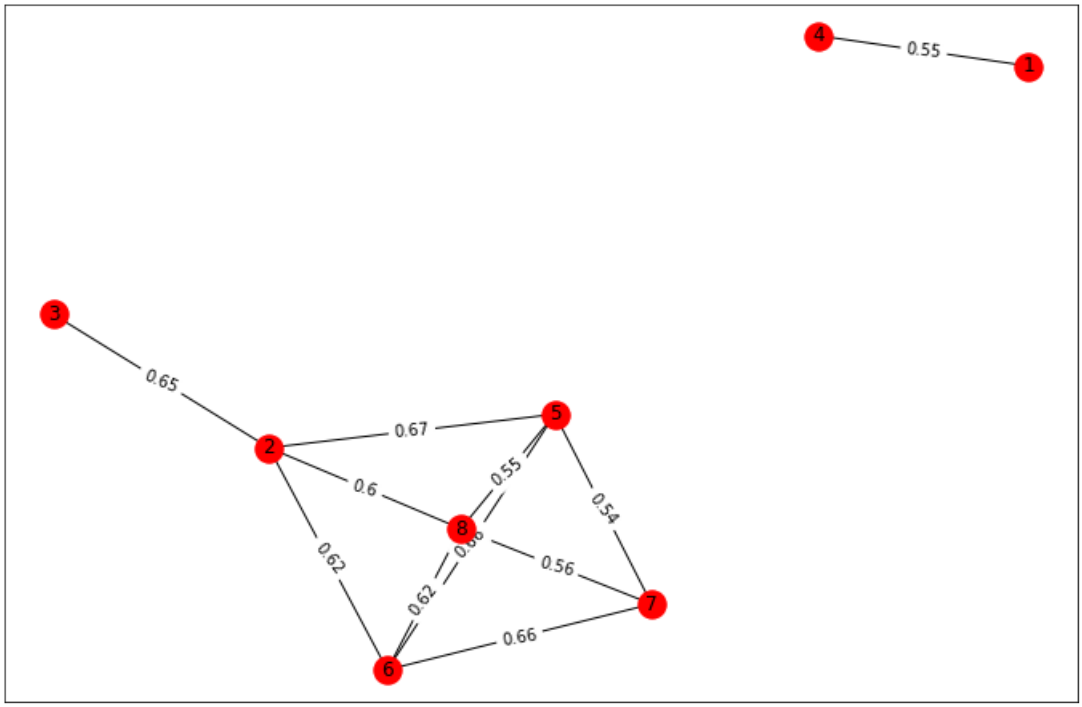

Figure 5.17: A snapshot of network at time $t_k = 5$ s, $n = 8$ nodes, typical connection range $r_0 = 40$ m, path-loss exponent $\eta = 2$; mobility parameters: $\tau = 1$ s, $\Delta t = 0.02$ s, and $\sqrt{D} = 40$ m/$\sqrt{\text{s}}$.

in various rescues, disaster management and military operations [83]. In our model, nodes move randomly according to an Ornstein-Uhlenbeck (OU) process. Each device movement is assumed independent of the others. The initial position, which is also the desired position, is different for each node. Specifically, the random variables $X_{i,k}, Y_{i,k}$ model the node displacements along the x and y coordinates for node $i \in \mathcal{V}$ at any time step $t_k = t_0 + k\,\Delta t$, $k \in \mathbb{N}$. From 3.2.2, we have that the random variables X_i and Y_i are normally distributed, i.e., $X_i \sim \mathcal{N}\left(m_x^i, \alpha\right), Y_i \sim \mathcal{N}\left(m_y^i, \alpha\right)$. The mean m_x^i, m_y^i follows a uniform distribution, i.e., $m_x^i, m_y^i \sim \mathcal{U}\left(0, 150\right)$, $i \in \mathcal{V}$. The variance α is equal for all nodes. This causes different link state distributions for different pairs of nodes; hence, the conditional entropy will also be different.

We assume that the path-loss causes large-scale fading, and there is either no small-scale fading or the small-scale fading is mitigated by using the frequency diver-

Node	**1**	**2**	**3**	**4**	**5**	**6**	**7**	**8**
1	0	0	0	0.55	0	0	0	0
2	0	0	0.65	0	**0.67**	0.62	0	0.6
3	0	0.65	0	0	0	0	0	0
4	0.55	0	0	0	0	0	0	0
5	0	**0.67**	0	0	0	0.66	0.54	0.55
6	0	0.62	0	0	0.66	0	0.66	0.62
7	0	0	0	0	0.54	0.66	0	0.56
8	0	0.6	0	0	0.55	0.62	0.56	0

Table 5.1: Adjacency matrix of weighted undirected graph at time $t_k = 5$ s. Edge weights are equal to the conditional entropy between nodes.

sity technique explained in section 2.2.4. We assume the use of orthogonal frequency division multiple access (OFDMA) as an access technique, which offers frequency diversity by spreading the carriers all over the used spectrum, leading to reduced multi-path effects in reception and increased spectral efficiency. The implementation of OFDMA requires a resource negotiation phase, but once the resources are allocated, transmissions can be performed without contentions on the medium.

The goal of this section is to show that a link with lower conditional entropy, once activated, remains, on average, active for a longer time than a link with higher conditional entropy. To that end, we perform 100 different experiments. For each experiment, we numerically estimate the transition probabilities and the conditional entropy given in eq. (5.10). The simulations parameters are: number of trials $N_{\text{trials}} = 5 \times 10^4$, the simulation starts at $t_0 = 0$ and last for 10 s, $\Delta t = 0.02$ s, $\sqrt{D} = 40$ m/$\sqrt{\text{s}}$, and $\tau = 1$ s.

Now, for each experiment, at time $t_k = 5$ s, we calculate the weighted adjacency

matrix $A = [A_{ij}]_{i,j\in\mathcal{V}}$ where

$$A_{ij} = \begin{cases} H\left(L_{ij,2}|L_{ij,1}=1\right), & \text{if } N_{ij} \geq \rho_{th}, \\ 0, & \text{otherwise.} \end{cases} \tag{5.11}$$

Hence, we represent the network as a weighted undirected graph with edge weights equal to the conditional entropy between nodes at time step $t_k = 5$ s. In Fig. 5.17, we plot the topology of the network in experiment 1 as a weighted undirected graph. In Table 5.1, we show the adjacency matrix of the graph. Then, in Table 5.2, we measure the number of time steps each link remained in the "on" state after $t_k = 5$ s. Now, we want to test the validity of our hypothesis; that is, a link with higher conditional entropy has, on average, a shorter life than one with lower conditional entropy. For this reason, in Table 5.3, we order the links in decreasing order with respect to their weights, i.e., conditional entropy. Consequently, we expect the links' lifetime to be in ascending order, proving the relationship that higher entropy leads to shorter lifetime. We then compute the ratio R given by

$$R = \frac{\#\text{links in correct order}}{\text{total number of links}}. \tag{5.12}$$

The ratio $0 \leq R \leq 1$ is a measure of the accuracy of our experiment. If $R = 1$, it means that for all links, our hypothesis is correct. On the other hand, if $R = 0$, the hypothesis is false for all links. In the case of experiment 1, it is clear from Table 5.3 that the number of links out of order is 2; links $(6, 7)$ and $(2, 3)$, respectively. Hence, in this experiment, the ratio is equal to $R_1 = 9/11 = 0.8182$; that is, for 81% of the links our hypothesis is true.

We repeat the same process for all 100 experiments. In Table 5.4, we show the

Node	**1**	**2**	**3**	**4**	**5**	**6**	**7**	**8**
1	0	0	0	248	0	0	0	0
2	0	0	43	0	**3**	248	0	248
3	0	43	0	0	0	0	0	0
4	248	0	0	0	0	0	0	0
5	0	**3**	0	0	0	82	248	248
6	0	248	0	0	82	0	4	248
7	0	0	0	0	248	4	0	248
8	0	248	0	0	248	248	248	0

Table 5.2: Number of time steps links continued to be active after $t_k = 5$ s; $\Delta t = 0.02$ s.

Link	$\mathbf{H}\left(\mathbf{L_{ij,2}}|\mathbf{L_{ij,1}}=\mathbf{1}\right)$	**Lifetime** (in # of time steps)
$(2,5)$	0.67	3
$(5,6)$	0.66	82
$(6,7)$	0.66	4
$(2,3)$	0.65	43
$(2,6)$	0.62	248
$(6,8)$	0.62	248
$(2,8)$	0.6	248
$(7,8)$	0.56	248
$(1,4)$	0.55	248
$(5,8)$	0.55	248
$(5,7)$	0.54	248

Table 5.3: Links sorted in descending order of conditional entropy.

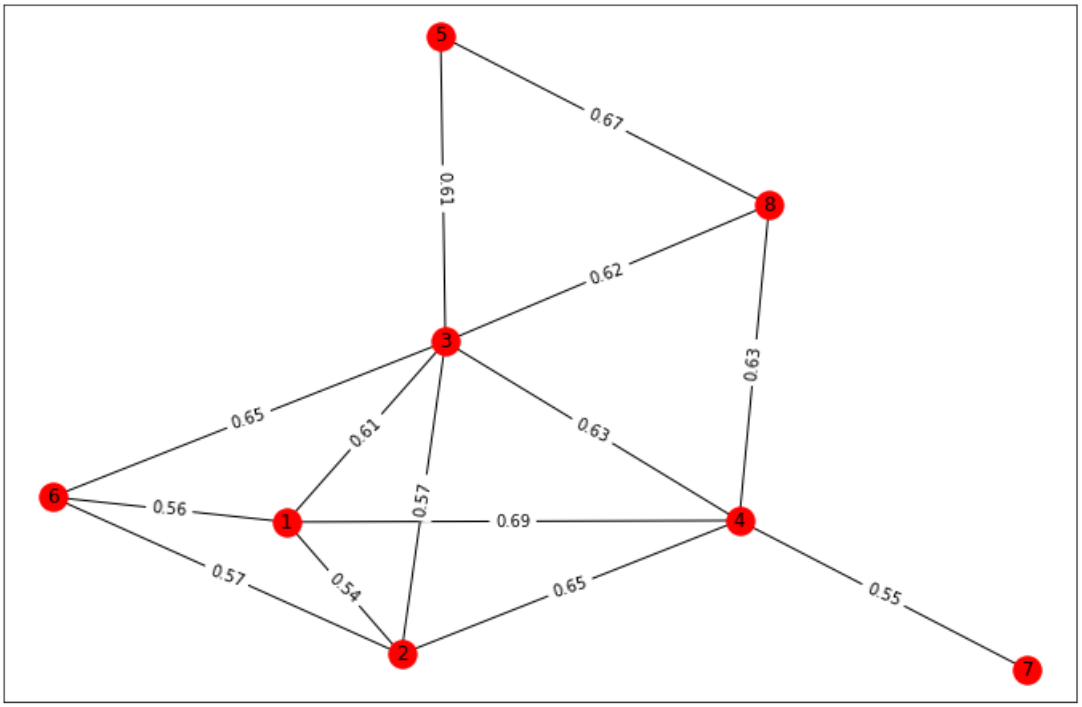

Figure 5.18: A snapshot of network at time $t_k = 5$ s, $n = 8$ nodes, typical connection range $r_0 = 40$ m, path-loss exponent $\eta = 2$; mobility parameters: $\tau = 1$ s, $\Delta t = 0.02$ s, and $\sqrt{D} = 40$ m/$\sqrt{\text{s}}$.

ratio R for each experiment, and in Table 5.5, we report the mean, median, and the standard deviation of the ratio R for all experiments. It is evident from these tables that, on average, 95% of the links in each experiment support our hypothesis. Hence, from the results presented in this section, we can conclude that the proposed mathematical framework and the conditional entropy metric $H\left(L_{ij,2}|L_{ij,1}=1\right)$ provide an excellent measure to estimate, quantify and evaluate the link uncertainty in mobile ad hoc wireless networks. Therefore, we can identify the links with the lowest expected lifetime via the conditional entropy and exclude them from route construction in routing algorithms.

Experiment	Ratio	Experiment	Ratio	Experiment	Ratio
2	1	3	1	4	1
5	0.77	6	1	7	1
8	0.91	9	0.92	10	1
11	1	12	1	13	1
14	0.93	15	0.91	16	0.93
17	0.87	18	1	19	0.94
20	1	21	0.83	22	0.92
23	0.93	24	1	25	0.93
26	1	27	1	28	0.87
29	0.93	30	0.95	31	1
32	1	33	1	34	1
35	0.95	36	0.94	37	1
38	0.93	39	0.89	40	1
41	1	42	0.94	43	1
44	0.92	45	0.82	46	1
47	1	48	1	49	0.89
50	1	51	0.94	52	0.94
53	1	54	1	55	1
56	1	57	0.89	58	1
59	0.95	60	0.87	61	0.8
62	1	63	0.86	64	0.83
65	0.93	66	0.94	67	1
68	0.92	69	0.94	70	1
71	0.94	72	0.82	73	0.86
74	0.78	75	0.89	76	1
77	1	78	1	79	0.87
80	0.94	81	1	82	1
83	1	84	1	85	0.92
86	1	87	1	88	1
89	0.86	90	0.94	91	1
92	1	93	0.91	94	1
95	0.88	96	1	97	0.93
98	1	99	0.85	100	0.9

Table 5.4: Ratio R for all 100 experiments.

Mean	Median	Standard Deviation
0.9476	0.9487	0.0618

Table 5.5: Analysis of the Ratio R for all experiments.

Node	**1**	**2**	**3**	**4**	**5**	**6**	**7**	**8**
1	0	0.54	0.61	**0.69**	0	0.56	0	0
2	0.54	0	0.57	0.65	0	0.57	0	0
3	0.61	0.57	0	0.63	0.61	0.65	0	0.62
4	**0.69**	0.65	0.63	0	0	0	0.55	0.63
5	0	0	0.61	0	0	0	0	0.67
6	0.56	0.57	0.65	0	0	0	0	0
7	0	0	0	0.55	0	0	0	0
8	0	0	0.62	0.63	0.67	0	0	0

Table 5.6: Adjacency matrix of weighted undirected graph at time $t_k = 5$ s. Edge weights are equal to the conditional entropy between nodes.

Node	**1**	**2**	**3**	**4**	**5**	**6**	**7**	**8**
1	0	248	248	**0**	0	248	0	0
2	248	0	248	147	0	248	0	0
3	248	248	0	248	248	1	0	248
4	**0**	147	248	0	0	0	0	248
5	0	0	248	0	0	0	248	0
6	248	248	1	0	0	0	0	0
7	0	0	0	248	0	0	0	0
8	0	0	248	248	0	0	0	0

Table 5.7: Number of time steps links continued to be active after $t_k = 5$ s; $\Delta t = 0.02$ s.

Path	$\mathbf{L_{27}}$	**Lifetime** (in # of time steps)
$(2, 1, 4, 7)$	0.31	0
$(2, 6, 1, 4, 7)$	0.31	0
$(2, 6, 3, 1, 4, 7)$	0.31	0
$(2, 3, 6, 1, 4, 7)$	0.31	0
$(2, 3, 1, 4, 7)$	0.31	0
$(2, 3, 5, 8, 4, 7)$	0.33	0
$(2, 1, 3, 5, 8, 4, 7)$	0.33	0
$(2, 6, 3, 5, 8, 4, 7)$	0.33	0
$(2, 1, 6, 3, 5, 8, 4, 7)$	0.33	0
$(2, 6, 1, 3, , 5, 8, 4, 7)$	0.33	0
$(2, 6, 3, 4, 7)$	0.35	1
$(2, 6, 3, 8, 4, 7)$	0.35	1
$(2, 4, 7)$	0.35	147
$(2, 6, 3, 1, 4, 7)$	0.35	1
$(2, 3, 6, 1, 4, 7)$	0.35	1
$(2, 3, 4, 7)$	0.37	248
$(2, 1, 3, 4, 7)$	0.37	248
$(2, 6, 1, 3, 4, 7)$	0.37	248
$(2, 3, 8, 4, 7)$	0.37	248
$(2, 1, 3, 8, 4, 7)$	0.37	248
$(2, 6, 1, 3, 8, 4, 7)$	0.37	248

Table 5.8: Links sorted in ascending order of entropy metric L_{27}.

5.4.2 Routing Decision Strategy Based on Entropy Metric

In this section, we propose a routing decision strategy using the metric L_{kl} in (5.9) as a measure of route uncertainty. To that end, we perform 100 different experiments with similar parameters as in the previous section. As an illustrative example, in Fig. 5.18, we plot the topology of the network in the first experiment as a weighted undirected graph. In Table 5.6, we show the adjacency matrix of the graph, and in Table 5.7, we measure the number of time steps each link stays in the "on" state after $t_k = 5$ s. This section aims to show that the route between two nodes k and l with higher metric L_{kl} has a longer lifetime. We pick two random nodes as source and destination, e.g., source = 2 and destination = 7. Then, in Table 5.8, we sort all the paths between $2 \leftrightarrow 7$ in ascending order according to the metric L_{27}. Consequently, we expect that the paths' lifetime to be in ascending order, proving the relationship that higher metric leads to a higher lifetime. We then compute the accuracy ratio R. If $R = 1$, it means that for all paths our hypothesis is true. On the other hand, if $R = 0$, the hypothesis is false for all paths. It is clear from Table 5.8 that the number of paths out of order is 2; paths $(2, 6, 3, 1, 4, 7)$ and $(2, 3, 6, 1, 4, 7)$, respectively. Hence, in this experiment, the ratio is equal to $R_1 = 19/21 = 0.9048$, that is, for 90% of the paths our hypothesis is true.

In classical routing protocols in MANETs, e.g., DSDV and AODV, paths are generally established according to the minimum hop-count metric. For instance, the minimum hop-count metric would have established path $(2, 4, 7)$ between nodes 2 and 7. Instead, the routing decision strategy based on the entropy metric proposed in this section would pick path $(2, 3, 4, 7)$, i.e., the path with the longest lifetime and the minimum number of intermediary links. In Table 5.9, we compare the proposed strategy with the one solely based on the minimum hop-count metric. It

is clear from this table that selecting the shortest path can lead to an increase in overhead due to frequent route reconstruction. We repeat the same process for all 100 experiments. In Table 5.10, we show the ratio R for each experiment, and in Table 5.11, we report the mean, median, and the standard deviation of the ratio R for all experiments. It is evident from these tables that, on average, 90% of the paths in each experiment support our hypothesis. Hence, the proposed routing strategy accurately identifies and selects the most stable route between a source and a destination in an environment where different paths are available.

5.4.2.1 Coding Aware Opportunistic Routing Based on Entropy Metric

In traditional routing schemes, the path between source and destination is established according to various metrics. Packets are forwarded from one node to the next following sequence of nodes in the pre-established path. Such traditional routing protocols do not utilize the broadcasting nature of the wireless medium [115]. Opportunistic routing [116, 117] has recently been proposed as an effective strategy to obtain high throughput in wireless networks with lossy links. In opportunistic routing, multiple neighbors can overhear a transmitting node. Upon receiving a packet, any selected set of a sender's neighbor can continue to forward the packet towards the destination. By exploiting the wireless medium's broadcast nature, opportunistic routing increases transmission reliability and ultimately improves the network throughput over that of conventional routing.

Network Coding (NC) [118, 119] has recently emerged as another promising approach for increasing network throughput. The benefit of network coding also comes from the inherent broadcast nature of the wireless medium. Previously, in conventional ad hoc networks, the only job of intermediate nodes within a network was to forward data packets towards the destination. The NC scheme proposes that, in addition to forwarding packets, a smart combination of data (from different sources

before forwarding) increases the network throughput. Therefore, in network coding, routers and switches have been replaced by coders that allow intermediate nodes to encode the incoming messages and then forward these messages to other nodes. This (encoding and forwarding) scheme increases networks' effective capacity by minimizing the number of bottlenecks.

Katti et al. in [120] proposed COPE, a new architecture for wireless mesh networks. COPE adds a coding layer between IP and MAC layers to detect coding opportunities and exploit them to forward multiple packets in a single transmission. It incorporates three techniques: opportunistic listening, opportunistic coding, and learning neighbor state. COPE uses the ETX (Expected Transmission Count) metric as its routing function. The ETX metric periodically assigns each link a weight proportional to the delivery probability. These weights are broadcast to all nodes in the network and used by a link-state routing protocol to compute the shortest paths. A possible improvement of COPE would be the use of the metric L_{kl} in (5.9) instead of ETX as a measure of route uncertainty, and the routing decision strategy proposed in section 5.4.2 as a routing function. We believe that using the conditional entropy as a metric to evaluate route stability represents a more accurate metric of topological uncertainty because of its ability to measure the uncertainty of the future state of the link given its current state.

5.4.2.2 Removal/Addition of a Node

In our analysis, we assume that nodes are present throughout the lifetime of the UAV system. However, there are times when some of the UAVs could go out of service due to power constraints. Failure of a single node causes the network to reorganize and maintain communication through other nodes. One reason why mesh networks are considered suitable for UAV based networks is that there is inherent fault tolerance in mesh networks. Once the nodes have been configured

Metric / Path	L_{74}	# of links	Lifetime [s]	Minimum hop	Our strategy
$(2, 4, 7)$	0.35	2	3	✓	
$(2, 3, 4, 7)$	0.37	3	5		✓

Table 5.9: Proposed strategy versus the minimum hop-count metric strategies.

and activated, they form a mesh structure automatically [121]. When this happens, the network becomes resilient to the failure of one or more nodes. Similarly, the addition of new nodes is easy and fast.

Self-organization in a UAV network consists of the following steps: When a node fails, or a new node is added, its neighbors find out about the available nodes through the route discovery protocol. As part of the protocol, all nodes send hello messages containing a unique identifier and position information to their neighbors at regular intervals. When a node receives a hello message, it creates or refreshes the routing table entry to the neighbor. Failure to receive any hello message from a neighbor for several time intervals indicates that the neighbor is no longer within transmission range and connectivity has been lost. For instance, in the scenario depicted in Fig. 5.18, let us assume that node 1 fails. Consequently, node 1 will not send the hello message at regular intervals to its neighbors. Topological changes in the network, such as removing or adding nodes, cause several nodes to exchange control messages for re-organization. This will lead to the removal of paths from the source 2 to destination 7 through node 1 from the routing table 5.8. After the route discovery process is completed, we would recalculate the uncertainty metric L_{kl} for every new route and repeat the procedure described in section 5.4.2.

5.5 Summary

In this chapter, we combine the theoretical modeling of the communication link developed in chapter 3 with the topological uncertainty analysis carried out in chap-

Experiment	Ratio	Experiment	Ratio	Experiment	Ratio
2	1	3	1	4	0.74
5	1	6	1	7	1
8	0.8	9	0.87	10	0.9
11	1	12	1	13	0.94
14	1	15	0.47	16	0.8
17	1	18	1	19	0.8
20	1	21	0.91	22	1
23	1	24	0.66	25	0.61
26	1	27	0.65	28	0.72
29	1	30	0.90	31	1
32	0.89	33	1	34	0.59
35	0.93	36	1	37	1
38	1	39	1	40	1
41	1	42	1	43	1
44	1	45	0.92	46	1
47	0.86	48	0.5	49	1
50	1	51	0.75	52	0.86
53	0.57	54	1	55	0.91
56	1	57	1	58	0.84
59	1	60	0.93	61	1
62	0.87	63	1	64	0.9
65	1	66	0.78	67	0.86
68	1	69	0.87	70	0.62
71	1	72	1	73	1
74	1	75	1	76	1
77	1	78	0.7	79	0.93
80	0.83	81	1	82	1
83	1	84	0.68	85	0.4
86	0.63	87	1	88	1
89	0.74	90	1	91	1
92	0.69	93	0.75	94	1
95	1	96	1	97	1
98	0.91	99	0.75	100	0.41

Table 5.10: Ratio R for all 100 experiments.

Mean	Median	Standard Deviation
0.8958	1	0.1529

Table 5.11: Analysis of the Ratio R for all experiments.

ter 4. Using these two tools, we investigate the main source of uncertainty in the link state, concluding that random mobility is the primary cause. Next, we give an operational interpretation of the entropy-based metric and propose a new routing decision strategy for MANETs. We consider the conditional entropy as the main indicator of link dynamics. The performance evaluation of the strategy is performed via simulation and analysis. The mathematical framework described in this chapter can be used by various routing protocols as a decision strategy for evaluation and selection of the route with the longest lifetime between a source and a destination wherever multiple routes are available, in order to enhance network connectivity and quality of service.

Chapter 6

Conclusion and Future Work

For a long time, ad hoc network research stayed in the realm of the military. In the middle of the 90s, with the advent of commercial radio technologies such as IEEE 802.11 and the proliferation of mobile computing devices, the research community became aware of the tremendous commercial potential and advantages of mobile ad hoc networks outside the military domain. The efforts of the research community, together with current and future MANET enabling radio technologies, will undoubtedly pave the way for a higher number of commercially viable solutions.

However, the dynamic nature of MANETs and the lack of a centralized structure pose several design issues to networking protocols able to provide efficient end-to-end communicatichapteron. Indeed, in this environment, communication links change over time due to node mobility and the variations in the propagation channel. Hence, connections between nodes are established and broken intermittently, leading to frequently-changing network topologies. For these reasons, the topology of any real-world MANET is not fixed. It exhibits a time-dependent evolution, i.e., a network snapshot represents a particular network evolution at a specific time. Understanding the evolution of the links and quantifying the topological uncertainty is

beneficial for network synchronization, routing protocols, and route stability evaluation. Therefore, it is imperative to take into account the random movements of nodes and the variations in the wireless medium when designing and implementing these networks. These are the main factors impacting the network stability and connectivity, and consequently, the performance of MANETs' protocols [14, 15].

This thesis examines the effects of node mobility and signal fading on the performance of mobile ad hoc networks.

In chapter 3, we derived closed-form expressions for the statistical properties of the link SNR and the separation distance in systems subject to Rayleigh Fading and Ornstein-Uhlenbeck Mobility. We started our analysis by first considering the case when there is no signal fading affecting the link between nodes. In this scenario, the statistical properties of the link SNR are entirely determined by the squared distance between the two nodes. We provided a full statistical description of the squared distance process, including its distribution and autocorrelation function, and showed that it forms a stationary Markov process. Then, we derived closed-form expressions for the pdf, the cdf, the bivariate pdf, and the bivariate cdf of the link SNR. Next, we extended our analysis to take into account variations in the propagation channel (e.g., fading), and calculated the pdf of the link SNR for rational path-loss exponents η.

In chapter 4, we exploited the statistics of the distance and the SNR processes presented in chapter 3 and evaluated an entropy-based metric that quantifies link uncertainty by taking full advantage of the correlation between the link current and future state. The motivations behind this work arose from the intrinsic location uncertainty of MANETs and the ability of the entropy to capture this randomness. Due to node mobility and wireless channel randomness, the topological structure shows a time-dependent evolution. In this regard, we took into account both the

temporal and spatial properties of the system. We started our analysis by modeling the existence of an edge between two nodes as a stationary Markov chain whose source of randomness is the separation distance between the nodes or the variations in the propagation channel. We applied our calculations to nodes experiencing an OU mobility model and Rayleigh fading and investigated the impact of the mobility and channel parameters on the entropy metric. Finally, through numerical results, we demonstrated that the proposed scheme thoroughly captures the link dynamics and accurately reflects changes in the state of a wireless connection.

Finally, in chapter 5, we investigated the main source of uncertainty in the link state in MANETs, concluding that random mobility is the primary cause. Then, we obtained conditions under which the impact of the small-scale fading can be neglected. Next, we presented an operational interpretation of the entropy-based metric and proposed a new routing decision strategy for MANETs. The key idea of this strategy is to identify and select the most stable route between a source and a destination in an environment where different paths are available rather than the shortest one. Identifying the set of most stable paths, i.e., those that are expected to be active for a longer time, can potentially reduce the number of route discoveries and overhead throughout the network.

This thesis provides a fundamental study of the SNR statistics in mobile environments; as it is the most complete such study, it forms the starting point for further work.

Future Work

Besides providing insights and solutions, the current thesis motivates several streams of potential future work that can be formalized into two categories, the first contains further investigation of the topics of this thesis, while the second consists

of other areas that are potentially beneficial to address. Potential ideas belonging to the first category are as follows:

- In chapter 3, we omit the slow fading caused by shadowing. Since fading (slow and fast) will affect whether a node can communicate with adjacent nodes, it can have a significant effect on network performance. Therefore, both slow and fast fading must be taken into consideration to simulate a real-world scenario. Omitting slow fading could lead to underestimating the degradation of the received SNR, thereby overestimating the performance of particular routing protocols. Hence, it would be beneficial to incorporate log-normal shadow fading into the analysis.

- Also, in chapter 3, we only focused on the Rayleigh fading. A natural step is to consider other small-scale fading models such as Nakagami or Rician fading.

- Throughout this thesis, we chose the OU process as a mobility model for the reasons explained in chapter 3. It would be interesting to analyze SNR statistics and the stochastic differential equation for other random mobility models applicable in mobile ad hoc wireless networks such as random walk model or random direction model.

- In chapter 4, a potential open problem is the study of non-Rayleigh pairwise connection models and their effect on topological uncertainty in wireless networks such as Nakagami or Rician models.

- Also, in chapter 4, future work may investigate the effect of imprecise path-loss exponents on network stability. The path-loss is typically an experimentally determined number that indicates how quickly a transmission is attenuated as it propagates through the wireless medium.

- In chapter 5, one could quantify how much uncertainty is left unexplained by neglecting the small-scale fading. Additionally, it would be interesting to verify the impact of log-normal shadow fading into the main source of uncertainty analysis. Is it still true that when $\sqrt{D} \gg r_0$ the main source of uncertainty in the link state is random mobility when log-normal shadow fading affects the link state?

- Due to the lack of experimental data, it was not possible to validate that the primary source of uncertainty in the link state is random mobility. A natural step is to try and obtain data from real mobile ad hoc networks and validate this result.

Potential ideas belonging to the second category are as follows:

- Mobile ad hoc networks are very likely to have multi-user interference. In our model, we assume that the communication link is affected by additive Gaussian noise, but we assume that multi-user interference is wholly mitigated through appropriate medium access control protocols [122]. For instance, the Hop-Reservation Multiple Access (HRMA) protocol [123], allows a pair of nodes in a MANET to reserve a frequency channel (through the use of Request-To-Send/Clear-To-Send (RTS/CTS) control packets exchange) for communication without interference from other nodes. These are the scenarios where our work could potentially be applied. One possible way to address the interference issue could be by following the analysis provided in [124]. In this paper, the author proposes to factorize the connectivity probability into the probability of a zero-noise network and the probability of a zero-interference network. This approach allows for an independent analysis of noise and interference. This is another topic that is worth investigating.

- Another beneficial study would be to conduct simulations on the NS-3 network simulator to analyze the performance improvement of the routing decision strategy proposed in this thesis. In the NS-3 simulator, real-world parameters can be set, such as channel capacity, traffic type, traffic sources, packet size, and MAC protocol. Several performance metrics could be considered to evaluate the new routing protocol's performance, such as packet delivery ratio, end-to-end delay, route discovery frequency, and routing overhead.

Bibliography

[1] R. R. Roy, *Handbook of Mobile Ad Hoc Networks for Mobility Models*. Springer Science & Business Media, 2010.

[2] J. P. Macker and M. S. Corson, "Mobile ad hoc networking and the ietf," *ACM SIGMOBILE Mobile Computing and Communications Review*, vol. 2, no. 1, pp. 9–14, 1998.

[3] M. Abolhasan, T. Wysocki, and E. Dutkiewicz, "A review of routing protocols for mobile ad hoc networks," *Ad hoc networks*, vol. 2, no. 1, pp. 1–22, 2004.

[4] Z. J. Haas, M. Gerla, D. B. Johnson, C. E. Perkins, M. B. Pursley, M. Steenstrup, C.-K. Toh, and J. F. Hayes, "Guest editorial wireless ad hoc networks," *IEEE Journal on Selected Areas in Communications*, vol. 17, no. 8, pp. 1329–1332, 1999.

[5] V. Lenders, J. Wagner, and M. May, "Analyzing the impact of mobility in ad hoc networks," in *Proceedings of the 2nd international workshop on Multi-hop ad hoc networks: from theory to reality*, pp. 39–46, 2006.

[6] T. Camp, J. Boleng, and V. Davies, "A survey of mobility models for ad hoc network research," *Wireless communications and mobile computing*, vol. 2, no. 5, pp. 483–502, 2002.

[7] F. Bai and A. Helmy, "A survey of mobility models in wireless ad hoc networks," in *Book chapter in Wireless Ad Hoc and Sensor Networks*, Kluwer academic Publishers, June 2004.

[8] D. Han and G. Chesi, "Robust synchronization via homogeneous parameter-dependent polynomial contraction matrix," *IEEE Transactions on Circuits and Systems I: Regular Papers*, vol. 61, no. 10, pp. 2931–2940, 2014.

[9] L. Pelusi, A. Passarella, and M. Conti, "Opportunistic networking: data forwarding in disconnected mobile ad hoc networks," *IEEE communications Magazine*, vol. 44, no. 11, 2006.

[10] B. An and S. Papavassiliou, "An entropy-based model for supporting and evaluating route stability in mobile ad hoc wireless networks," *IEEE Communications Letters*, vol. 6, no. 8, pp. 328–330, 2002.

[11] M. łgorzata Steinder and A. S. Sethi, "A survey of fault localization techniques in computer networks," *Science of computer programming*, vol. 53, no. 2, pp. 165–194, 2004.

[12] J. Hoebeke, I. Moerman, B. Dhoedt, and P. Demeester, "An overview of mobile ad hoc networks: applications and challenges," *Journal-Communications Network*, vol. 3, no. 3, pp. 60–66, 2004.

[13] A. Moussaoui and A. Boukeream, "A survey of routing protocols based on link-stability in mobile ad hoc networks," *Journal of Network and Computer Applications*, vol. 47, pp. 1–10, 2015.

[14] I. Chlamtac, M. Conti, and J. J.-N. Liu, "Mobile ad hoc networking: Imperatives and challenges," *Ad hoc networks*, vol. 1, no. 1, pp. 13–64, 2003.

[15] D. Miorandi, E. Altman, and G. Alfano, "The impact of channel randomness on coverage and connectivity of ad hoc and sensor networks," *IEEE Transactions on Wireless Communications*, vol. 7, no. 3, pp. 1062–1072, 2008.

[16] A. Cika, M.-A. Badiu, and J. P. Coon, "Statistical properties of transmissions subject to rayleigh fading and ornstein-uhlenbeck mobility," *IEEE Transactions on Mobile Computing*, 2020.

[17] A. Cika, M.-A. Badiu, J. P. Coon, and S. E. Tajbakhsh, "Entropy rate of time-varying wireless networks," in *IEEE Global Communications Conference (GLOBECOM)*, in press, 2018.

[18] A. Cika, M.-A. Badiu, and J. P. Coon, "Quantifying link stability in ad hoc wireless networks subject to ornstein-uhlenbeck mobility," in *IEEE International Conference on Communications (ICC)*, pp. 1–6, IEEE, 2019.

[19] M. Ilyas, *The handbook of ad hoc wireless networks*. CRC press, 2002.

[20] A. F. Molisch, *Wireless communications*, vol. 34. John Wiley & Sons, 2012.

[21] A. Goldsmith, *Wireless communications*. Cambridge university press, 2005.

[22] C. Perez-Vega, J. M. L. Higuera, *et al.*, "A simple and efficient model for indoor path-loss prediction," *Measurement science and technology*, vol. 8, no. 10, p. 1166, 1997.

[23] W. C. Jakes and D. C. Cox, *Microwave mobile communications*. Wiley-IEEE Press, 1994.

[24] T. Aulin, "A modified model for the fading signal at a mobile radio channel," *IEEE Transactions on Vehicular Technology*, vol. 28, no. 3, pp. 182–203, 1979.

[25] P. Santi, *Mobility models for next generation wireless networks: ad hoc, vehicular and mesh networks.* John Wiley & Sons, 2012.

[26] J. J. Garcia-Luna-Aceves and M. Spohn, "Source-tree routing in wireless networks," in *Proceedings. Seventh International Conference on Network Protocols*, pp. 273–282, IEEE, 1999.

[27] K. Govindan, K. Zeng, and P. Mohapatra, "Probability density of the received power in mobile networks," *IEEE transactions on Wireless communications*, vol. 10, no. 11, pp. 3613–3619, 2011.

[28] V. A. Aalo, C. Mukasa, and G. P. Efthymoglou, "Effect of mobility on the outage and ber performances of digital transmissions over nakagami-m fading channels," *IEEE Transactions on Vehicular Technology*, vol. 65, no. 4, pp. 2715–2721, 2015.

[29] D. B. Johnson and D. A. Maltz, "Dynamic source routing in ad hoc wireless networks," in *Mobile computing*, pp. 153–181, Springer, 1996.

[30] J. Garcia-Luna-Aceves and E. L. Madruga, "A multicast routing protocol for ad-hoc networks," in *IEEE INFOCOM'99. Conference on Computer Communications. Proceedings. Eighteenth Annual Joint Conference of the IEEE Computer and Communications Societies. The Future is Now (Cat. No. 99CH36320)*, vol. 2, pp. 784–792, IEEE, 1999.

[31] M. M. Zonoozi and P. Dassanayake, "User mobility modeling and characterization of mobility patterns," *IEEE Journal on selected areas in communications*, vol. 15, no. 7, pp. 1239–1252, 1997.

[32] C. Bettstetter, "Mobility modeling in wireless networks: categorization, smooth movement, and border effects," *ACM SIGMOBILE Mobile Computing and Communications Review*, vol. 5, no. 3, pp. 55–66, 2001.

[33] D. M. Blough, G. Resta, and P. Santi, "A statistical analysis of the long-run node spatial distribution in mobile ad hoc networks," *Wireless Networks*, vol. 10, no. 5, pp. 543–554, 2004.

[34] E. M. Royer, P. M. Melliar-Smith, and L. E. Moser, "An analysis of the optimum node density for ad hoc mobile networks," in *ICC 2001. IEEE International Conference on Communications. Conference Record (Cat. No. 01CH37240)*, vol. 3, pp. 857–861, IEEE, 2001.

[35] B. Liang and Z. J. Haas, "Predictive distance-based mobility management for pcs networks," in *IEEE INFOCOM'99. Conference on Computer Communications. Proceedings. Eighteenth Annual Joint Conference of the IEEE Computer and Communications Societies. The Future is Now (Cat. No. 99CH36320)*, vol. 3, pp. 1377–1384, IEEE, 1999.

[36] P. Smith and J. Coon, "Connectivity times for mobile d2d networks," in *2018 IEEE International Conference on Communications (ICC)*, pp. 1–6, IEEE, 2018.

[37] K. Farkas, T. Hossmann, F. Legendre, B. Plattner, and S. K. Das, "Link quality prediction in mesh networks," *Computer Communications*, vol. 31, no. 8, pp. 1497–1512, 2008.

[38] P. Madadi, F. Baccelli, and G. de Veciana, "Shared rate process for mobile users in poisson networks and applications," *IEEE Transactions on Information Theory*, vol. 64, no. 3, pp. 2121–2141, 2017.

[39] P. Madadi, F. Baccelli, and G. de Veciana, "On temporal variations in mobile user snr with applications to perceived qos," in *2016 14th International Symposium on Modeling and Optimization in Mobile, Ad Hoc, and Wireless Networks (WiOpt)*, pp. 1–8, IEEE, 2016.

[40] C. Bettstetter, "Topology properties of ad hoc networks with random waypoint mobility," *ACM SIGMOBILE Mobile Computing and Communications Review*, vol. 7, no. 3, pp. 50–52, 2003.

[41] C. Bettstetter, G. Resta, and P. Santi, "The node distribution of the random waypoint mobility model for wireless ad hoc networks," *IEEE Transactions on mobile computing*, vol. 2, no. 3, pp. 257–269, 2003.

[42] P. Santi, "The critical transmitting range for connectivity in mobile ad hoc networks," *ieee transactions on mobile computing*, vol. 4, no. 3, pp. 310–317, 2005.

[43] E. Salbaroli and A. Zanella, "A statistical model for the evaluation of the distribution of the received power in ad hoc and wireless sensor networks," in *2006 3rd Annual IEEE Communications Society on Sensor and Ad Hoc Communications and Networks*, vol. 3, pp. 756–760, IEEE, 2006.

[44] M. O. Hasna and M.-S. Alouini, "A performance study of dual-hop transmissions with fixed gain relays," *IEEE transactions on wireless communications*, vol. 3, no. 6, pp. 1963–1968, 2004.

[45] K. Kaemarungsi and P. Krishnamurthy, "Modeling of indoor positioning systems based on location fingerprinting," in *Ieee Infocom 2004*, vol. 2, pp. 1012–1022, IEEE, 2004.

[46] C. Mukasa, V. A. Aalo, and G. Efthymoglou, "On the performance of a dual-hop network with a mobile relay in a nakagami fading environment," in *2016 IEEE 21st International Workshop on Computer Aided Modelling and Design of Communication Links and Networks (CAMAD)*, pp. 43–47, IEEE, 2016.

[47] B. F. McGuffin, "Mobile radio power distribution in shadowing and variable range," *IEEE transactions on vehicular technology*, vol. 54, no. 1, pp. 404–408, 2005.

[48] M. L. Sim and H. T. Chuah, "Received signal statistics in ds-cdma channels with flat rayleigh fading and fast closed-loop power control," *IEEE transactions on communications*, vol. 51, no. 7, pp. 1040–1045, 2003.

[49] E. Biglieri, J. Proakis, and S. Shamai, "Fading channels: Information-theoretic and communications aspects," *IEEE transactions on information theory*, vol. 44, no. 6, pp. 2619–2692, 1998.

[50] C. E. Shannon, "A mathematical theory of communication," *Bell system technical journal*, vol. 27, no. 3, pp. 379–423, 1948.

[51] T. M. Cover and J. A. Thomas, *Elements of information theory*. John Wiley & Sons, 2012.

[52] M. Dehmer, "Information processing in complex networks: Graph entropy and information functionals," *Applied Mathematics and Computation*, vol. 201, no. 1-2, pp. 82–94, 2008.

[53] J. P. Coon, "Topological uncertainty in wireless networks," in *Global Communications Conference (GLOBECOM), 2016 IEEE*, pp. 1–6, IEEE, 2016.

[54] J. P. Coon and P. J. Smith, "Topological entropy in wireless networks subject to composite fading," in *Communications (ICC), 2017 IEEE International Conference on*, pp. 1–7, IEEE, 2017.

[55] A. Cika, J. P. Coon, and S. Kim, "Effects of directivity on wireless network complexity," in *Modeling and Optimization in Mobile, Ad Hoc, and Wireless Networks (WiOpt), 2017 15th International Symposium on*, pp. 1–7, IEEE, 2017.

[56] M. Badiu and J. P. Coon, "On the distribution of random geometric graphs," in *2018 IEEE International Symposium on Information Theory (ISIT)*, pp. 2137–2141, June 2018.

[57] J. P. Coon, M. A. Badiu, and D. Gündüz, "On the conditional entropy of wireless networks," in *2018 International Workshop on Spatial Stochastic Models for Wireless Networks (spaswin)-Invited Paper*, 2018.

[58] D. Wang and A. A. Abouzeid, "On the cost of knowledge of mobility in dynamic networks: An information-theoretic approach," *IEEE Transactions on Mobile Computing*, vol. 11, no. 6, pp. 995–1006, 2012.

[59] Q. Song, Z. Ning, S. Wang, and A. Jamalipour, "Link stability estimation based on link connectivity changes in mobile ad-hoc networks," *Journal of Network and Computer Applications*, vol. 35, no. 6, pp. 2051–2058, 2012.

[60] C. Yawut, B. Paillassa, and R. Dhaou, "Mobility metrics evaluation for self-adaptive protocols.," *JNW*, vol. 3, no. 1, pp. 53–64, 2008.

[61] M. Rosvall, A. V. Esquivel, A. Lancichinetti, J. D. West, and R. Lambiotte, "Memory in network flows and its effects on spreading dynamics and community detection," *Nature communications*, vol. 5, p. 4630, 2014.

[62] J. Saramäki and P. Holme, "Exploring temporal networks with greedy walks," *The European Physical Journal B*, vol. 88, no. 12, p. 334, 2015.

[63] R. Timo, K. Blackmore, and L. Hanlen, "On entropy measures for dynamic network topologies: Limits to manet," in *2005 Australian Communications Theory Workshop*, pp. 95–101, IEEE, 2005.

[64] Q.-M. Tran, A. Dadej, and S. Perreau, "Link change and generalized mobility metric for mobile ad-hoc networks," in *Military Communications Conference, 2006. MILCOM 2006. IEEE*, pp. 1–7, IEEE, 2006.

[65] E. M. Royer and C.-K. Toh, "A review of current routing protocols for ad hoc mobile wireless networks," *IEEE personal communications*, vol. 6, no. 2, pp. 46–55, 1999.

[66] A. Boukerche, B. Turgut, N. Aydin, M. Z. Ahmad, L. Bölöni, and D. Turgut, "Routing protocols in ad hoc networks: A survey," *Computer networks*, vol. 55, no. 13, pp. 3032–3080, 2011.

[67] C. E. Perkins and P. Bhagwat, "Highly dynamic destination-sequenced distance-vector routing (dsdv) for mobile computers," *ACM SIGCOMM computer communication review*, vol. 24, no. 4, pp. 234–244, 1994.

[68] T. Clausen, P. Jacquet, C. Adjih, A. Laouiti, P. Minet, P. Muhlethaler, A. Qayyum, and L. Viennot, "Optimized link state routing protocol (olsr)," 2003.

[69] D. Johnson, Y.-c. Hu, D. Maltz, *et al.*, "The dynamic source routing protocol (dsr) for mobile ad hoc networks for ipv4," tech. rep., RFC 4728, 2007.

[70] C. Perkins, E. Belding-Royer, and S. Das, "Rfc3561: Ad hoc on-demand distance vector (aodv) routing," 2003.

[71] A. Moussaoui, F. Semchedine, and A. Boukerram, "A link-state qos routing protocol based on link stability for mobile ad hoc networks," *Journal of Network and Computer Applications*, vol. 39, pp. 117–125, 2014.

[72] L. Chen and W. B. Heinzelman, "A survey of routing protocols that support qos in mobile ad hoc networks," *IEEE Network*, vol. 21, no. 6, pp. 30–38, 2007.

[73] W. Zhu, M. Song, and S. Olariu, "Integrating stability estimation into quality of service routing in mobile ad-hoc networks," in *200614th IEEE International Workshop on Quality of Service*, pp. 122–129, IEEE, 2006.

[74] N. Sarma and S. Nandi, "Route stability based qos routing in mobile ad hoc networks," *Wireless Personal Communications*, vol. 54, no. 1, pp. 203–224, 2010.

[75] J. L. Guo, W. Wu, and S. B. Xu, "Study on route stability based on the metrics of local topology transformation entropy in mobile ad hoc networks," in *Advanced Engineering Forum*, vol. 1, pp. 288–292, Trans Tech Publ, 2011.

[76] C. W. Gardiner, *Stochastic methods : A Handbook for the Natural and Social Sciences*. Springer series in synergetics, Berlin: Springer, 4th ed., 2009.

[77] G. E. Uhlenbeck and L. S. Ornstein, "On the theory of the brownian motion," *Physical review*, vol. 36, no. 5, p. 823, 1930.

[78] J. L. Doob, "The brownian movement and stochastic equations," *Annals of Mathematics*, pp. 351–369, 1942.

[79] B. Øksendal, *Stochastic Differential Equations*. Springer, 5 ed., 2003.

[80] B. Liang and Z. J. Haas, "Predictive distance-based mobility management for multidimensional pcs networks," *IEEE/ACM Transactions On Networking*, vol. 11, no. 5, pp. 718–732, 2003.

[81] S. Manvi and M. Kakkasageri, "Issues in mobile ad hoc networks for vehicular communication," *IETE Technical Review*, vol. 25, no. 2, pp. 59–72, 2008.

[82] H. Kim, J. Park, M. Bennis, and S.-L. Kim, "Massive uav-to-ground communication and its stable movement control: A mean-field approach," *arXiv preprint arXiv:1803.03285*, 2018.

[83] K. G. Panda, S. Das, D. Sen, and W. Arif, "Design and deployment of uav-aided post-disaster emergency network," *IEEE Access*, vol. 7, pp. 102985–102999, 2019.

[84] D. T. Gillespie, "Exact numerical simulation of the ornstein-uhlenbeck process and its integral," *Physical review E*, vol. 54, no. 2, p. 2084, 1996.

[85] M. Penrose, *Random Geometric Graphs*. Oxford University Press, 2003.

[86] J. C. Cox, J. E. Ingersoll Jr, and S. A. Ross, "A theory of the term structure of interest rates," *Econometrica*, vol. 53, no. 2, pp. 385–407, 1985.

[87] M. Jeanblanc, M. Yor, and M. Chesney, *Mathematical methods for financial markets*. Springer Science & Business Media, 2009.

[88] A. Göing-Jaeschke and M. Yor, "A survey and some generalizations of bessel processes," *Bernoulli*, pp. 313–349, 2003.

[89] W. Feller, "Two singular diffusion problems," *Annals of mathematics*, pp. 173–182, 1951.

[90] P. E. Kloeden and E. Platen, *Numerical solution of stochastic differential equations*, vol. 23. Springer Science & Business Media, 2013.

[91] M. C. Gursoy, "Secure communication in the low-snr regime," *IEEE transactions on communications*, vol. 60, no. 4, pp. 1114–1123, 2012.

[92] J. B. Andersen, J. O. Nielsen, G. F. Pedersen, G. Bauch, and G. Dietl, "Doppler spectrum from moving scatterers in a random environment," *IEEE Transactions on Wireless Communications*, vol. 8, no. 6, 2009.

[93] K. Bilstrup, E. Uhlemann, E. G. Strom, and U. Bilstrup, "Evaluation of the ieee 802.11 p mac method for vehicle-to-vehicle communication," in *2008 IEEE 68th Vehicular Technology Conference*, pp. 1–5, IEEE, 2008.

[94] B. Hanssens, E. Tanghe, L. Martens, C. Oestges, and W. Joseph, "Measurement-based analysis of delay-doppler characteristics in an indoor environment," *IEEE Transactions on Antennas and Propagation*, vol. 64, no. 1, pp. 370–374, 2015.

[95] H. S. Wang and N. Moayeri, "Finite-state markov channel-a useful model for radio communication channels," *IEEE transactions on vehicular technology*, vol. 44, no. 1, pp. 163–171, 1995.

[96] U. Bäsel, "Random chords and point distances in regular polygons," *Acta Mathematica Universitatis Comenianae*, vol. 83, no. 1, pp. 1–18, 2014.

[97] A. M. Mathai, *An introduction to geometrical probability: distributional aspects with applications*, vol. 1. CRC Press, 1999.

[98] J. Coon, C. P. Dettmann, and O. Georgiou, "Full connectivity: corners, edges and faces," *Journal of Statistical Physics*, vol. 147, no. 4, pp. 758–778, 2012.

[99] M. D. Penrose *et al.*, "Connectivity of soft random geometric graphs," *The Annals of Applied Probability*, vol. 26, no. 2, pp. 986–1028, 2016.

[100] J. von Brecht, T. Kolokolnikov, A. L. Bertozzi, and H. Sun, "Swarming on random graphs," *Journal of Statistical Physics*, vol. 151, no. 1-2, pp. 150–173, 2013.

[101] M. Amin, "Energy: The smart-grid solution," *Nature*, vol. 499, no. 7457, p. 145, 2013.

[102] O. Georgiou, C. P. Dettmann, and J. P. Coon, "Network connectivity: Stochastic vs. deterministic wireless channels," in *Communications (ICC), 2014 IEEE International Conference on*, pp. 77–82, IEEE, 2014.

[103] M. Haenggi, J. G. Andrews, F. Baccelli, O. Dousse, and M. Franceschetti, "Stochastic geometry and random graphs for the analysis and design of wireless networks," *IEEE Journal on Selected Areas in Communications*, vol. 27, no. 7, 2009.

[104] M.-A. Badiu and J. P. Coon, "On the distribution of random geometric graphs," in *2018 IEEE International Symposium on Information Theory (ISIT)*, pp. 2137–2141, IEEE, 2018.

[105] J. P. Coon, C. P. Dettmann, and O. Georgiou, "Entropy of spatial network ensembles," *arXiv preprint arXiv:1707.01901*, 2017.

[106] G. E. Box, G. M. Jenkins, G. C. Reinsel, and G. M. Ljung, *Time series analysis: forecasting and control.* John Wiley & Sons, 2015.

[107] P. Dharmawansa, N. Rajatheva, and C. Tellambura, "On the trivariate rician distribution," *IEEE Transactions on communications*, vol. 56, no. 12, pp. 1993–1997, 2008.

[108] H. S. Wang and P.-C. Chang, "On verifying the first-order markovian assumption for a rayleigh fading channel model," *IEEE Transactions on Vehicular Technology*, vol. 45, no. 2, pp. 353–357, 1996.

[109] M. Gerla, X. Hong, and G. Pei, "Landmark routing for large ad hoc wireless networks," in *Globecom'00-IEEE. Global Telecommunications Conference. Conference Record (Cat. No. 00CH37137)*, vol. 3, pp. 1702–1706, IEEE, 2000.

[110] J. Li, J. Jannotti, D. S. De Couto, D. R. Karger, and R. Morris, "A scalable location service for geographic ad hoc routing," in *Proceedings of the 6th annual international conference on Mobile computing and networking*, pp. 120–130, 2000.

[111] B. An, J. S. Lee, and N.-S. Kim, "An entropy-based routing protocol using mobility in mobile ad-hoc wireless sensor networks," in *2009 11th International Conference on Advanced Communication Technology*, vol. 2, pp. 949–952, IEEE, 2009.

[112] C. Gui, B. Sun, and C. Xia, "An entropy-based long-life multipath routing algorithm in manet," in *2008 Fourth International Conference on Natural Computation*, vol. 5, pp. 174–178, IEEE, 2008.

[113] W. A. Jabbar, M. Ismail, and R. Nordin, "On the performance of the current manet routing protocols for voip, http, and ftp applications," *Journal of Computer Networks and Communications*, vol. 2014, 2014.

[114] N.-U. Park, J.-C. Nam, and Y.-Z. Cho, "Impact of node speed and transmission range on the hello interval of manet routing protocols," in *2016 International Conference on Information and Communication Technology Convergence (ICTC)*, pp. 634–636, IEEE, 2016.

[115] M. A. Iqbal, B. Dai, B. Huang, A. Hassan, and S. Yu, "Survey of network coding-aware routing protocols in wireless networks," *Journal of Network and Computer Applications*, vol. 34, no. 6, pp. 1956–1970, 2011.

[116] S. Biswas and R. Morris, "Opportunistic routing in multi-hop wireless networks," *ACM SIGCOMM Computer Communication Review*, vol. 34, no. 1, pp. 69–74, 2004.

[117] E. Rozner, J. Seshadri, Y. Mebta, and L. Qiu, "Simple opportunistic routing protocol for wireless mesh networks," in *2006 2nd IEEE Workshop on Wireless Mesh Networks*, pp. 48–54, IEEE, 2006.

[118] R. Ahlswede, N. Cai, S.-Y. Li, and R. W. Yeung, "Network information flow," *IEEE Transactions on information theory*, vol. 46, no. 4, pp. 1204–1216, 2000.

[119] S.-Y. Li, R. W. Yeung, and N. Cai, "Linear network coding," *IEEE transactions on information theory*, vol. 49, no. 2, pp. 371–381, 2003.

[120] S. Katti, H. Rahul, W. Hu, D. Katabi, M. Médard, and J. Crowcroft, "Xors in the air: practical wireless network coding," *IEEE/ACM Transactions on networking*, vol. 16, no. 3, pp. 497–510, 2008.

[121] L. Gupta, R. Jain, and G. Vaszkun, "Survey of important issues in uav communication networks," *IEEE Communications Surveys & Tutorials*, vol. 18, no. 2, pp. 1123–1152, 2015.

[122] S. Kumar, V. S. Raghavan, and J. Deng, "Medium access control protocols for ad hoc wireless networks: A survey," *Ad hoc networks*, vol. 4, no. 3, pp. 326–358, 2006.

[123] Z. Yang and J. Garcia-Luna-Aceves, "Hop-reservation multiple access (hrma) for ad-hoc networks," in *IEEE INFOCOM'99. Conference on Computer Communications. Proceedings. Eighteenth Annual Joint Conference of the IEEE Computer and Communications Societies. The Future is Now (Cat. No. 99CH36320)*, vol. 1, pp. 194–201, IEEE, 1999.

[124] M. Haenggi, "On routing in random rayleigh fading networks," *IEEE Transactions on Wireless Communications*, vol. 4, no. 4, pp. 1553–1562, 2005.